Telematics
Computer Systems

Freie Universität Berlin

Properties and Topology of the DES-Testbed (2nd Extended Revision)

Bastian Blywis Mesut Günes Felix Juraschek
Oliver Hahm Nicolai Schmittberger

Computer Systems and Telematics
Institute of Computer Science
Freie Universität Berlin, Germany
{blywis, guenes, jurasch, oham, schmittb}@inf.fu-berlin.de

Technical Report
TR-NO: TR-B-11-04

July 4, 2011

Contents

1 Motivation **5**
- 1.1 Introduction . . . 5
- 1.2 Structure . . . 6

2 Experiment Setup **7**
- 2.1 DES-Testbed . . . 7
  - 2.1.1 Wireless Interfaces . . . 8
- 2.2 Experiment Parameters . . . 9

3 Evaluation **11**
- 3.1 Results from the 2.4 GHz Band . . . 12
  - 3.1.1 Packet Delivery Ratio . . . 12
  - 3.1.2 Link Asymmetry . . . 15
  - 3.1.3 Impact of the Packet Size . . . 17
  - 3.1.4 Node Degree . . . 18
  - 3.1.5 Distance . . . 19
  - 3.1.6 Number of Links . . . 24
  - 3.1.7 Diameter and Average Shortest Path . . . 25
  - 3.1.8 Unidirectional Links . . . 26
  - 3.1.9 Network Fragility . . . 27
  - 3.1.10 Topology . . . 29
- 3.2 Results from the 5 GHz Band . . . 32
  - 3.2.1 Packet Delivery Ratio . . . 32
  - 3.2.2 Link Asymmetry . . . 33
  - 3.2.3 Impact of the Packet Size . . . 34
  - 3.2.4 Node Degree . . . 35
  - 3.2.5 Distance . . . 35
  - 3.2.6 Number of Links . . . 44
  - 3.2.7 Diameter and Average Shortest Path . . . 44
  - 3.2.8 Unidirectional Links . . . 44
  - 3.2.9 Network Fragility . . . 45
  - 3.2.10 Topology . . . 47

4 Conclusion **49**

A Additional Figures and Discussion **51**
- A.1 Additional Figures for Channel 44 . . . 51
  - A.1.1 Impact of the Packet Size . . . 51

A.1.2 Node Degree . . . 52
A.1.3 Distance . . . 53
A.1.4 Number of Links . . . 56
A.1.5 Unidirectional Links . . . 56
A.1.6 Network Fragility . . . 57
A.2 ETX Metric and PDR Comparison . . . 58
A.3 Distribution of the Link Ranges . . . 59
A.4 Node Degree Distribution . . . 60
A.5 Asymmetry . . . 61

B Additional Results from the 2.4 GHz Band 69
B.1 Channel 1 . . . 69
B.1.1 Packet Delivery Ratio . . . 70
B.1.2 Link Asymmetry . . . 71
B.1.3 Node Degree . . . 72
B.1.4 Distance . . . 73
B.1.5 Number of Links . . . 76
B.1.6 Unidirectional Links . . . 76
B.1.7 Network Fragility . . . 77
B.2 Channel 7 . . . 78
B.2.1 Packet Delivery Ratio . . . 78
B.2.2 Link Asymmetry . . . 79
B.2.3 Node Degree . . . 80
B.2.4 Distance . . . 81
B.2.5 Number of Links . . . 83
B.2.6 Unidirectional Links . . . 83
B.2.7 Network Fragility . . . 84

List of Figures

2.1.1 Distance between the routers 8
2.1.2 Position of the nodes 9

3.1.1 Distribution of the packet delivery ratio on channel 13 14
3.1.2 Link asymmetry on channel 13 16
3.1.3 Absolute and relative PDR differences for channel 13 18
3.1.4 Distribution of the node degree measured on channel 13 19
3.1.5 Scatter plot of the PDR for each link over the distance on channel 13 22
3.1.6 Pseudo-color plot of the PDR for each link over the distance on channel 13 23
3.1.7 Number of links on channel 13 24
3.1.8 Network diameter and shortest paths on channel 13 27
3.1.9 Fraction of the unidirectional links on channel 13 28
3.1.10 Network fragility on channel 13 30
3.1.11 Topology of the DES-Testbed on channel 13 31
3.2.1 Distribution of the packet delivery ratio on channel 40 and 44 . . . 36
3.2.2 Quantile-Quantile plots of the PDR 37
3.2.3 Link asymmetry on channel 40 and 44 37
3.2.4 Quantile-Quantile plots of the link asymmetry 38
3.2.5 Absolute and relative PDR differences for channel 40 39
3.2.6 Distribution of the node degree on channel 40 39
3.2.7 Link ranges on all channels 41
3.2.8 Scatterplot of the PDR for each link over the distance on channel 40 42
3.2.9 Pseudo-color plot of the PDR for each link over the distance on channel 40 43
3.2.10 Number of links on channel 40 44
3.2.11 Network diameter and average shortest paths on channel 13 45
3.2.12 Fraction of the unidirectional links on channel 40 45
3.2.13 Network Fragility on channel 40 46
3.2.14 Topology of the DES-Testbed on channel 40 47

A.1.1 Absolute and relative PDR differences on channel 44 51
A.1.2 Scatter-plot of the PDR for each link over the distance on channel 44 54
A.1.3 Pseudo-color plot of the PDR for each link over the distance on channel 44 55
A.1.4 Number of links in the testbed for different packet sizes on channel 44 56
A.1.5 Fraction of the unidirectional links on channel 44 56
A.1.6 Network Fragility on channel 44 57

A.2.1 Dependency of ETX on the packet delivery ratios 58
A.2.2 Difference of the ETX value compared to PDR 58
A.3.1 Distribution of the link ranges 59
A.4.1 Node degree distribution 60
A.5.1 Scatter-plot of the PDR for each bidirectional link on channel 13 . . 62
A.5.2 Pseudo-color plot of the PDR for each bidirectional link on channel 13 63
A.5.3 Surface-plot of the PDR for each bidirectional link on channel 13 . 64
A.5.4 Scatter-plot of the PDR for each bidirectional link on channel 40 . . 65
A.5.5 Pseudo-color plot of the PDR for each bidirectional link on channel 13 66
A.5.6 Surface-plot of the PDR for each bidirectional link on channel 13 . 67

B.1.1 Distribution of the packet delivery ratio on channel 1 70
B.1.2 Link asymmetry on channel 1 71
B.1.3 Distribution of the node degree measured on channel 1 72
B.1.4 Scatter plot of the PDR for each link over the distance on channel 1 74
B.1.5 Pseudo-color plot of the PDR for each link over the distance on channel 1 75
B.1.6 Number of links on channel 1 76
B.1.7 Fraction of the unidirectional links on channel 1 76
B.1.8 Network fragility on channel 1 77
B.2.1 Distribution of the packet delivery ratio on channel 7 78
B.2.2 Link asymmetry on channel 7 79
B.2.3 Distribution of the node degree measured on channel 7 80
B.2.4 Scatter plot of the PDR for each link over the distance on channel 7 81
B.2.5 Pseudo-color plot of the PDR for each link over the distance on channel 7 82
B.2.6 Number of links on channel 7 83
B.2.7 Fraction of the unidirectional links on channel 7 83
B.2.8 Network fragility on channel 7 84

List of Tables

2.1.1 Overview of the node deployment in the DES-Testbed 9
2.2.1 Parameters of the experiment 10

3.1.1 Moments of the node degree distributions on channel 13 20
3.1.2 Moments of the link range distributions on channel 13 21
3.2.1 Kolmogorov-Smirnov test of the PDR distributions on channel 40 and 44 34
3.2.2 χ^2 test of the PDR distributions on channel 40 and 44 35
3.2.3 Kolmogorov-Smirnov test of the $\mathsf{PDR}_{\mathsf{Asym}}$ distributions on channel 40 and 44 38
3.2.4 Moments of the node degree distributions on channel 40 40
3.2.5 Moments of the link range distributions on channel 40 40

A.1.1 Moments of the node degree distributions on channel 44 52
A.1.2 Moments of the link range distributions on channel 44 53

Notes about the 2nd Revision

This technical report is an update of the publication *Properties and Topology of the DES-Testbed*, number `TR-B-11-02` that was published in March 2011. Besides the correction of some spelling and grammar mistakes, we added an excerpt of results from channel 1 and 7 in the 2.4 GHz band. The data was measured with the same experiment setup described in Chapter 2. The results are available in Appendix B. Some of the figures that were already included in the first revision have been improved, e.g., pseudo-color plots of histograms show transparent bins when they are empty.

Please use the current revision as reference for your own publications and update your bibliography accordingly.

Abstract

The *Distributed Embedded Systems Testbed* (DES-Testbed) is a hybrid wireless mesh and wireless sensor network that has been deployed at *Freie Universität Berlin* and was successively extended from November 2007 to December 2010. This technical report gives an overview of the current topology and the properties of the IEEE 802.11 wireless mesh network that is part of the DES-Testbed. The information that was gathered from an experimental study shall enable researchers to optimize their experiment scenarios, to support the evaluation of experiments, and to derive improved models of real world deployments. The differences of testbeds compared with simulation models and how to evaluate and filter the raw data are addressed. The focus of our study is an up-to-date description of the testbed state and to highlight particular issues. We show that the node degree, link ranges, and packet delivery ratios are not normal distributed and that simple means are not sufficient to describe the properties of a real world wireless network. Significant differences of the results from three channels are discussed. As last, the technical report shows that the DES-Testbed is an overall well connected network that is suited for studies of wireless mesh network and wireless mobile ad-hoc network problems.

CHAPTER 1

Motivation

1.1 Introduction

Testbeds are a tool of scientific research like analytical models or simulation environments. They enable studies in an environment that exhibits the same properties as a real world deployment in a production setting. In contrast to simulation environments, experiments in testbeds will not generate deterministic results because they are subjected to uncontrollable random processes. The topology and quality of the links will change over time depending on environmental conditions that lead to an attenuation of the signals, e.g., humidity or groups of people that act as a black body [1] and due to sources of interference. The interference comes from external sources, like radios that are not part of the testbed, microwave ovens, or even sulfur lamps [2]. Additional and often more severe interference comes from within the testbed as inter and intra flow interference that is generated by data flows and management packets. Nevertheless, testbeds are especially valuable because of these issues as they can show if there are hidden or unknown problems. While protocols and algorithms can be studied in isolated and fully controllable environments, finally they have to work under totally different conditions. A study that assumes an ideal network will inevitable lead to results, that do not hold in the real world.

Simulations are run with (abstract) models for the radio propagation, mobility, and generated data flows [3]. The radio propagation is often modeled in a fairly simple way where the distance between two stations is the dominating (if not only) factor to determine if a communication is possible, i.e., if a link exists. Examples include the *free-space* or *two-ray ground models*. More complex models like the *shadowing model* try to consider some randomness. The probability to successfully receive a packet is still dependent on the distance, yet the larger the distance, the lower the probability. The general focus of such models is often on free-space propagation where obstacles and multi-path propagation are not considered. In contrast, indoor radio propagation is much more difficult to model. In this scenario, the distance will only be one of many important factors that influence the link quality. Stations are deployed in different rooms and thus each wall will attenuate the signal. The structure of the building with multiple floors, different hall and room sizes, and

the position of the stations[1] relatively to their environment have to be considered. As wireless propagation in indoor environments is complex and particular models are not available or there are no commonly accepted models, testbeds are a viable tool for studies.

Like in all domains of science, the applied tools have to be known and understood. Depending on the focus of research and the subject of the study, a coarse granular understanding can be sufficient. In the research field of computer networks, which includes routing and transport layer issues, a general understanding of the network as a weighted and directed graph is required. Without this particular information, only limited conclusions are possible if deviating results are due to different algorithms and parameters or due to the property of the network. Even worse, errors in the experiment setup or execution can remain undetected. A sound understanding of the testbed is required.

This technical report describes an experimental study that was run in the DES-Testbed [4,5] to determine the topology of the network and the properties of the links on different channels. The primary focus is to specify the network as a graph as it is usually discovered by routing protocols and subsequently evaluated to determine routes from a source to a destination. As the discovery is based on broadcast packets that are flooded over the network, the same setup is used to probe the link qualities. The measured data is evaluated to determine the distribution of the *packet deliver ratio* (PDR), link asymmetry, and node degree. The packet size and frequency are discussed as two parameters that have a severe impact in the results. As the data shows, abstract models do not accurately describe the properties of a real world network. This comes at no surprise as they are in fact models of a complex distributed system. As we show, many phenomenons that are often considered to be uncommon and that are rarely modeled in simulations, e.g., asymmetric or unidirectional links are in fact fairly common in real world networks.

1.2 Structure

The reminder of this paper is structured as follows. Chapter 2 gives a brief overview of the current state of the DES-Testbed and explains the experiment setup and parameters. Subsequently, the measured data is evaluated and discussed in Chapter 3. The chapter is split in two parts, discussing the results from two frequency bands. The paper ends with a summary and conclusion in Chapter 4.

[1] More specifically: The position and orientation of the antennas are relevant.

CHAPTER 2

Experiment Setup

This section starts with a brief overview of the DES-Testbed and subsequently describes the setup of the experiment that is discussed in this paper. The introduction focuses only on the IEEE 802.11 wireless mesh network part of the hybrid testbed and omits the wireless sensor network that is also available.

2.1 DES-Testbed

The DES-Testbed has been steadily extended since the deployment of the first nodes in the end of 2007. Currently 111 mesh routers are deployed over three buildings of the faculty of mathematics and computer science over three floors each. At the time of this writing, 107 mesh routers are available for use in experiments and can be booked using the *Testbed Management System* [6]. 3 further nodes are available for testing and use by the testbed maintainers. 1 node is currently offline because of technical issues. 7 of the 107 nodes are attached to the outside walls of two buildings and significantly improve the connection of all three buildings since their deployment. An overview of the node deployment of the DES-Testbed is shown in Table 2.1.1 and Figure 2.1.2. On average there is a router every 8.00 to 8.25 meter in each building if we simply consider the occupied space and the number of routers. We call this value the *statistical average distance* (SAD). The space is a volume calculated based on the minimum and maximum coordinates of the routers in the corresponding building respectively the whole testbed. Therefore SAD is a metric that assumes a uniform deployment. While the true distribution is not uniform, the calculated density is overall very high. Although there is significant free space between the building, the average distance between the routers in the whole testbed is still below 14 m. We learn from the SAD that the deployment in the three buildings has a common density, i.e., there is a proportional relationship between the number of routers and the size of the building. Of course, when the routers positions are evaluated, the average distance increases as shown in Figure 2.1.1. The *actual average distance* (AAD) is much higher. AAD is calculated based on the coordinates of all N routers in the particular building respectively the whole

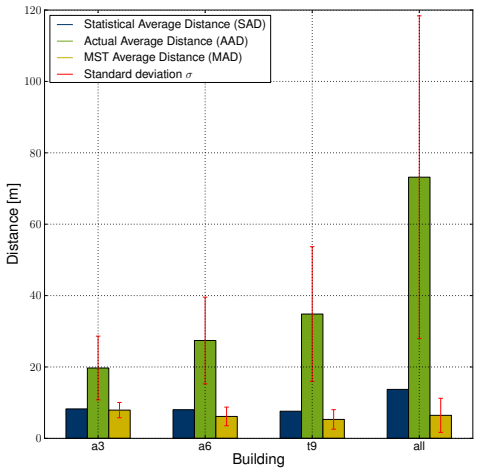

Figure 2.1.1: Distance between the routers

testbed.

$$AAD = \frac{\sum_{i=1}^{N} \sum_{j=1, i \neq j}^{N} d_{i,j}}{N \times (N-1)} \tag{2.1}$$

$d_{i,j}$ is the euclidean distance between the two routers i and j. The difference of the AAD values and SAD highlights the non-uniform deployment. If we create a *minimum spanning tree* (MST) based on the distances of all routers we get another metric for the average distances: *MST average distance* (MAD). MAD is the mean of all edges in the MST graph that are weighted by the distance. Thus if routing would be only based on the MST, the transceivers would only have to cover a distance of less than 10 m. As we will discuss in the following sections, distance is not an optimal measure for routing as there is no clear correlation with the quality of the link; at least in an indoor scenario.

2.1.1 Wireless Interfaces

Each mesh router has three wireless network interface cards that are configured to three orthogonal default channels. The first card is a LogiLink WL0025 IEEE 802.11b/g USB dongle based on the RT2501U architecture with an RT2571W BB/MAC IC and RT2528 RF IC that is configured to channel 13 (2.472 GHz). The second and third card are Atheros-based MiniPCI cards (WLM54SAG) and are configured to channel 40 (5.200 GHz) and channel 44 (5.220 GHz). Channel 11 is the highest one in the 2.4 GHz range that is used in the campus wireless network. It partially overlaps with channel 13. Channel 40 and 44 are not used in the campus network at this time. This configuration was not changed for the experiment.

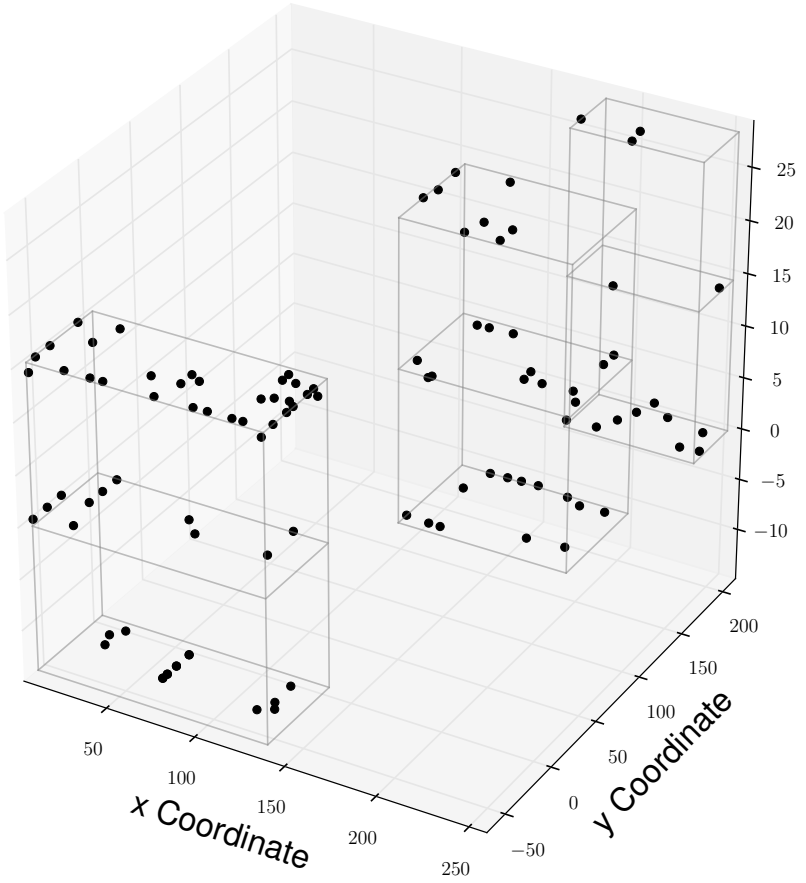

Figure 2.1.2: Position of the nodes in the testbed. Additionally, the contours of the three buildings and the floors are depicted. The vertical position of the nodes are not accurate, to enable a better view of the deployment. Subsequent sections of this report provide figures with accurate z-coordinates.

	Arnimallee 3	Arnimallee 6	Takustraße 9	All
Indoor	14	33	53	100
Outdoor	0	3	4	7
Total	14	36	57	107
Floors	1st, 2nd, 3rd	1st, 2nd, 3rd	basement, 1st, 2nd	

Table 2.1.1: Overview of the node deployment in the DES-Testbed

2.2 Experiment Parameters

The goal of this experiment was to probe the link quality and derive all further information from this data. A common approach to get the link quality, respectively the packet delivery ratio, is to periodically sent broadcast packets from each node. Each node that receives a packet from a neighbor stores this information so that a post-processing of the data is possible. Proactive routing protocols like the *Opti-*

Parameter	Values
Number of Nodes	105
Channels	13, 40, 44
$\text{Packet}_{\text{Size}}$ [Byte]	128, 384, 640, 896, 1152, 1408
$\text{Packet}_{\text{Interval}}$ [sec]	1
Duration per configuration	30 min $\Rightarrow \approx$ 1800 packets

Table 2.2.1: Parameters of the experiment

mized Link State Routing (OLSR) [7] apply exactly the same scheme and base their route selection on the gathered information. Each node has complete knowledge of the network topology and calculates the next best hop for each destination based on a shortest path algorithm. Reactive routing protocols like the *Ad hoc On-Demand Distance Vector* (AODV) routing protocol [8] flood messages over the network that are also forwarded as link layer broadcast. In the case of IEEE 802.11, broadcast frames are sent with a low data rate from the `BSSBasicRateSet` [9] and thus with other modulation schemes than unicast frames.

For the experiment, a modified version of our gossip routing [10,11] daemon based on the *Distributed Embedded Systems Simple and Extensible Routing-Framework for Testbeds* (DES-SERT) [12, 13] was run to generate packets and to log their reception. Hello packets of a particular size were sent every second by each of the 105 mesh routers that participated in the experiment. Each configuration was run for 30 minutes and used one of the network cards configured to one of the three channels. Therefore the experiment took $30 \times 3 \times 6 = 540$ minutes and in total about 10 hours because of the configuration overhead. The duration is a compromise between the accuracy to probe the quality (longer is more accurate) and the fact that the link qualities can change over time due to external interferences. The packet interval could have been further reduced, e.g., to 0.1 s to get an even more extensive data base but $1 - 2$ s is a common interval used by routing protocols for their neighbor discovery and allows accurate conclusions for this application scenario. About 1800 packets were sent for each configuration from each router. As not all nodes started and ceased to send packets at the same time[1], there is a difference of up to 5 packets that are sent per router. The deviating number of packets is considered for the calculation of the PDR metric that is introduced and applied in the following chapters.

[1] The routing daemons are controlled over SSH sessions. Although multiplexing is enabled and the connections remain open, a simultaneous start/stop cannot be ensured.

CHAPTER 3

Evaluation

The evaluation is split in two major parts: results from the 2.4 GHz band in Section 3.1 and the results from the 5 GHz band in Section 3.2. Aside from different results, the first part gives more specific information about the figures and graphs that are included in this technical report and the data they represent. This information is not repeated in the second section and all figure formats and formulas remain the same if not otherwise noted. Instead, the second part additionally compares and discusses the results from both frequency bands.

The following sections will often refer to terms from graph theory, e.g., edges and vertices. A slightly different terminology is usually used in the wireless networking research community. Thus this technical report will often refer, e.g., to edges as links and vertices as nodes or routers. The link metrics that are discussed in the following sections are equivalent to the weights in a weighted graph. The following general notions are used in this chapter:

- The graph G consists of a set of vertices V and a set of edges E: $G = (V, E)$
- An edge $e_{a,b}$ can also be represented as the tuple of nodes that it connects: (a, b)
- Edges are unidirectional if not otherwise noted: $e_{a,b} \in E \not\Rightarrow e_{b,a} \in E$
- A suffix ν like G_ν represents a subgraph that complies to a condition specified by ν
- E_ν are the edges in G_ν
- $||S||$ represents the number of elements in the set S
- N represents the number of nodes/routers in the network, i.e., $N = ||V||$
- $|f|$ is the absolute value of f which can be either a function or a value

In addition, the following symbols are used for statistical values:

To learn about the properties of the DES-Testbed and the network topology, the following metrics will be evaluated:

- Node degree, the number of neighbors of a node

μ	average respectively the mean of a distribution
σ	standard deviation
$\tilde{x}$	median of the sample x
γ	skewness of the distribution
Mode	element that occurs with the highest frequency in the sample

- Link quality measured by the packet delivery ratio
- Link asymmetry, different link qualities in the opposite directions
- Fraction of unidirectional links
- Network diameter
- Average shortest path and average distances
- Link ranges
- Number of links
- Network fragility

These metrics enable to describe the network as a graph and the overall meshness[1]. In most cases a single value of these metrics is not sufficient to fully characterize the testbed. Therefore, the distribution or density functions are presented for the data.

3.1 Results from the 2.4 GHz Band

3.1.1 Packet Delivery Ratio

Figure 3.1.1a shows the *cumulative distribution function* (CDF) of the *packet delivery ratio* (PDR) measured with different packet sizes. The PDR can be calculated for each (directed) link/edge $e_{s,r}$ connecting source s with receiver r by evaluating the number of received packets at node r as a fraction of the number of packets $\|p_s\|$ sent by s.

$$\mathrm{PDR}(e_{s,r}) = \frac{\|e_{s,r}\|}{\|p_s\|} \tag{3.1}$$

$$\mathrm{PDR} \rightarrow [0,1] \tag{3.2}$$

$\|e_{s,r}\|$ represents the absolute number of times a link was detected based on the periodically sent broadcast packets, i.e., the number of received packets during the

[1] The term *meshness* or *degree of meshness* can be found in some graph theory related publications. Unfortunately there is no common definition that is accepted. In our context meshness refers to the overall quality of the network incorporating the node degree, quality of the links, etc.

experiment. If no packets are received there is no edge in the graph.

$$\|e_{s,r}\| = 0 \equiv \mathsf{PDR} = 0.0 \tag{3.3}$$
$$\|e_{s,r}\| = 0 \equiv e_{s,r} \notin \mathsf{E} \tag{3.4}$$
$$\mathsf{PDR} \geq 0.0 \equiv \mathsf{PDR} > 0.0 \tag{3.5}$$

Equation (3.5) applies as there cannot be an edge with $\mathsf{PDR} = 0.0$ by our definition. All CDF plots in this report show the percentiles of the empirical distribution.

Each of the 6 graphs in Figure 3.1.1a represents the empirical distribution of the PDR for each link between two mesh routers, i.e., bidirectional links contribute two data points and unidirectional links only one. In a hypothetical scenario where half of the packets are lost over all links, the graph would show a vertical edge at $\mathsf{PDR} = 0.5$ going from $\mathsf{CDF} = 0.0$ to $\mathsf{CDF} = 1.0$. Thus the more the CDF increases for higher PDR values, the better the overall link quality in the whole testbed.

The packet size of the Hello packets, as introduced in Section 2.2, is the most important parameter in the experiment that shows an effect on the measured data. We observe that the packet delivery ratio distribution from the 128 Bytes scenario deviates from the others. When the packet size is increased to 384 Bytes, the distribution changes but further increments of the packet size show only a limited effect. Surprisingly, the graph for packet size 1408 Bytes does not fully follow this trend: it crosses most of the others at $\mathsf{PDR} \approx 0.5$. This phenomenon can also be observed in several of the following figures and is easily explained: the number of links is not constant. When the packet size moves beyond a specific threshold, several (low quality) links vanish and thus a larger fraction of higher quality links remains[2].

For comparison, Figure 3.1.1b shows a histogram of the PDR with 40 bins of equal size for $[0, 1]$, i.e., one bin has a size of 0.025. The ordinate does not show the complete $[0, 1]$ interval, to make the fraction[3] of the empirical distribution in the bin better visible[4]. As in the CDF plot, we observe that the PDR of the links is not normal distributed but that there is a high frequency of low quality links as well as high quality links: a bounded bimodal distribution or two truncated normal distributions with peaks near $\mathsf{PDR} = 0.0$ and $\mathsf{PDR} = 1.0$. In the mid-range the distribution more or less resembles a uniform distribution which is caused by the overlap of the two normal distributions.

Interestingly, there is a spike in the histogram for packet size 128 Bytes at $\mathsf{PDR} = 0.75$ that seems to move to the left side towards a lower PDR when the packet size is increased. This can be an effect of the binning and we have to consider that the spikes also do not have to represent the same set of nodes. The phenomenon can be seen as a diagonal in Figure 3.1.1c that shows the histograms as pseudo-color plot. We can observe, that the PDR distribution is affected by the packet size. Surprisingly, the frequency of the links in the left most bin ($\mathsf{PDR} < 0.025$) does not

[2]Please note that only a larger fraction remains and not an absolute number! This fact has also to be considered for the metrics in several of the following sections.

[3]All histograms in this technical report show fractions respectively the relative frequency of the data.

[4]The same applies for all other histograms in this technical report. To compare the frequencies in two different histograms, the scales of the ordinate axes have to be considered as they can differ.

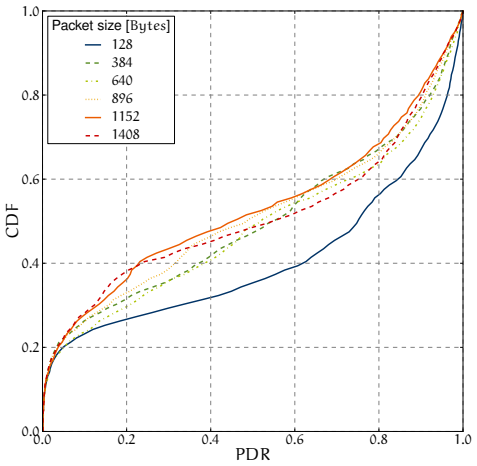

(a) Cumulative distribution function

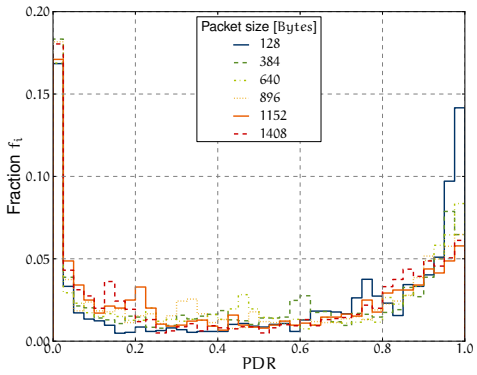

(b) Histogram with 40 bins of equal size

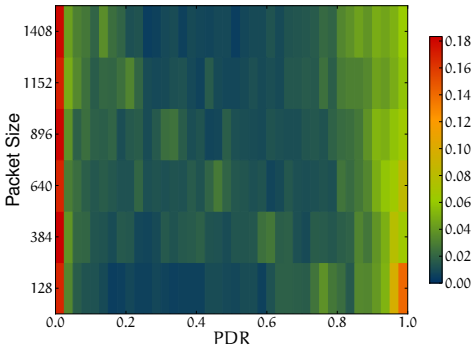

(c) Pseudo-color plot with 40 bins of equal size. The color represents the fraction of links in the bin with a particular PDR.

Figure 3.1.1: Distribution of the packet delivery ratio on channel 13

significantly change. We conclude from the data that although the packet size has an overall negative effect on the link PDR, there is always a constant fraction of very low quality links. Routing protocols will have to consider this fact and select newly discovered neighbors only as next hops toward a destination when the link quality has been determined accurately.

The PDR probability density function could also be described as a bathtub curve [14]. This shape is often found in reliability theory to model or depict the probability for devices to fail: high initial failure rate (production defects), high failure rate after extended time (end of life time), and low failure rate in between. It is often modeled, respectively the data fitted, by *Beta* or *Weibull* distributions. For example, the PDR distribution is similar to the Beta distribution with parameters $0 < \alpha, \beta < 1$, location $p = 0$, shape $q = 1$. While the shape is similar to the empirical bimodal distribution, it cannot represent the third peak discussed in the previous paragraph. A detailed evaluation of the data is required before a fitting statistical distribution can be provided.

3.1.2 Link Asymmetry

Figure 3.1.2 gives an insight into the link asymmetry. A link e is asymmetric[5] if the following condition applies:

$$\mathsf{PDR}(e_{s,r}) \neq \mathsf{PDR}(e_{r,s}) \tag{3.6}$$

As this is a fairly strict constraint we relax it to:

$$|\mathsf{PDR}(e_{s,r}) - \mathsf{PDR}(e_{r,s})| > \epsilon \tag{3.7}$$

Each graph shows the cumulative distribution function of the PDR difference in both directions, called $\mathsf{PDR}_{\mathrm{Asym}}$, for each (bidirectional) link e.

$$\mathsf{PDR}_{\mathrm{Asym}}(a,b) = |\mathsf{PDR}(e_{a,b}) - \mathsf{PDR}(e_{b,a})| \tag{3.8}$$

$$\mathsf{PDR}_{\mathrm{Asym}} \rightarrow [0,1] \tag{3.9}$$

For example, if $\mathsf{PDR}(e_{a,b}) = 0.6$ and $\mathsf{PDR}(e_{b,a}) = 0.8$, then $\mathsf{PDR}_{\mathrm{Asym}} = 0.2$. Lower values are thus better and unidirectional links are by definition not considered in this metric. The more the distribution function increases for higher $\mathsf{PDR}_{\mathrm{Asym}}$ values, the more links exhibit strong asymmetry.

When the packet size is 128 Bytes, about 80% of the links satisfy $\mathsf{PDR}_{\mathrm{Asym}} \leq 0.2$, i.e., they show a low asymmetry. We can also derive from the figure, that there are very few links that can be considered symmetric, depending on the definition of this property. Even when we attribute $\mathsf{PDR}_{\mathrm{Asym}} \leq 0.05$ (corresponding to $\epsilon > 0.05$ in Equation (3.6)) to measurement errors and external sources of errors, only 20% of the links are symmetric. We also learn from the distribution functions, that an increase of the packet size effects a higher asymmetry. Yet again, there is a significant difference when the packet size goes from 128 to 384 Bytes and very limited difference between the larger values. The histogram as shown in Figure 3.1.2b lets us assume that the $\mathsf{PDR}_{\mathrm{Asym}}$ distribution is normal but truncated on the left side of the peak or that the data follows a power low distribution. For all packet sizes different kurtoses are visible but no clear trend.

As Figure A.5.1 in the appendix shows, most of the asymmetric links have either in one direction a high PDR and the other is slightly better or both have often an already low PDR. The points in the scatter plot accumulate in the lower left and upper right corner. We observe again, that there are few symmetric links, that lie on the diagonal. The increasing packet size leads to a shift of the points towards the upper left and lower right corners.

Link asymmetry leads to an inaccurate view of the network when symmetric metrics like *Expected Transmission Count* (ETX) [15] are applied[6]: Some links are overestimated in one direction and underestimated in the other. Figure A.2.2 in the appendix shows the difference between the PDR and ETX values, where:

$$\mathsf{ETX}(s,r) = \frac{1}{\mathsf{PDR}(e_{s,r}) \times \mathsf{PDR}(e_{r,s})} \tag{3.10}$$

$$\mathsf{ETX} \rightarrow [1,\infty] \tag{3.11}$$

[5] Do not confuse this definition of asymmetry with the one that is used to describe routes. Asymmetric routes between a source and destination do not consist of the same set of nodes.

[6] This has also an effect on metrics that are based on ETX, e.g., ETT and transitively WCETT.

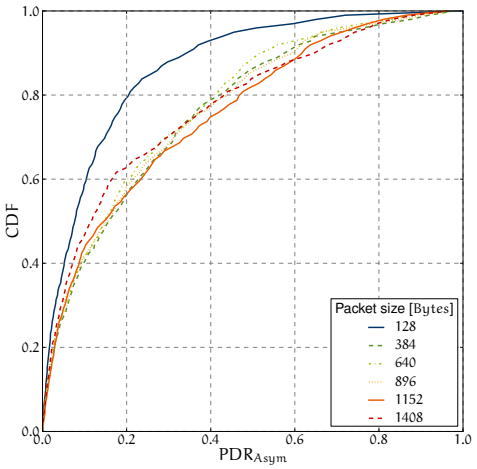

(a) Cumulative distribution

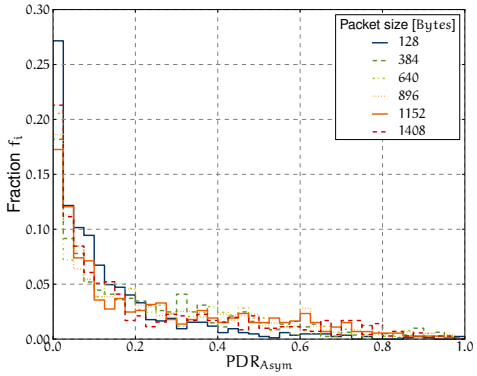

(b) Histogram with 40 bins

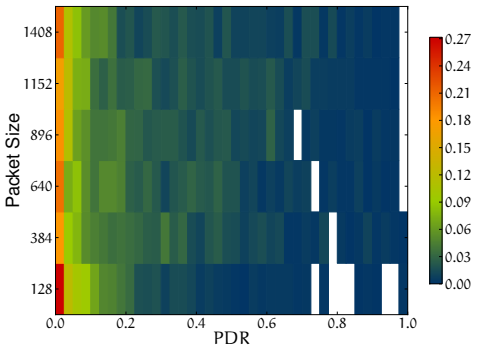

(c) Pseudo-color plot with 40 bins

Figure 3.1.2: Link asymmetry on channel 13. The PDR difference of each bidirectional link (PDR_{Asym}) is depicted as measure of the link asymmetry.

$$ETX_{Diff}(s,r) = \sqrt{1/ETX(s,r)} - PDR(e_{s,r}) \quad (3.12)$$

$$= \sqrt{PDR(e_{s,r}) \times PDR(e_{r,s})} - PDR(e_{s,r}) \quad (3.13)$$

$$ETX_{Diff} \rightarrow [-1,0] \quad (3.14)$$

As shown in Figure A.2.2a, the ETX value often deviates from the PDR value. Of course the ETX metric has a different meaning and intention compared to PDR yet the problem remains that a routing protocol might under- or overestimate the quality of a link because of the averaging. As last, we can derive from the data that the distribution of the difference between ETX and the PDR is dependent on the packet size: the larger the packets, the more the ETX_{Diff} distribution is skewed to the left towards -1. Again, the data measured with the largest packet size deviates from this trend which we attribute to the lower number of links that are available in this scenario.

We can conclude that ETX, at least for some links, inaccurately describes the quality due to distinct asymmetry and that link asymmetry is a common and not a rare case. Regardless of the packet size, there are always asymmetries.

3.1.3 Impact of the Packet Size

Figure 3.1.3 shows the degree of PDR changes when the packet size increased. The absolute (Figure 3.1.3a) and relative (Figure 3.1.3b) difference of the PDR is plotted based on the results that where achieved when the packet size was 128 Bytes; the minimum size used in the experiments. Links can only contribute to the result when they existed for packet size $\alpha = 128$ Bytes and the other size β_i ($\alpha < \beta_i$). That means, at least one packet was received over the (directed) link for packet size α and for β. If communication was not possible anymore over a particular link for β_i then it is ignored for the α, β_i data set and in the corresponding CDF[7].

$$\mathrm{Abs}(\mathrm{PDR}_{\mathrm{Diff}}(a, b, \alpha, \beta)) = \mathrm{PDR}(e_{a,b}, \beta) - \mathrm{PDR}(e_{a,b}, \alpha) \quad (3.15)$$

$$\mathrm{Abs}(\mathrm{PDR}_{\mathrm{Diff}}) \rightarrow [-1, 1] \quad (3.16)$$

$\mathrm{PDR}(e_{a,b}, \beta)$ is the packet delivery ratio for the link from node a to node b that was measured with packet size β. The relative PDR difference is calculated in the same manner:

$$\mathrm{Rel}(\mathrm{PDR}_{\mathrm{Diff}}(a, b, \alpha, \beta)) = \frac{\mathrm{Abs}(\mathrm{PDR}_{\mathrm{Diff}}(a, b, \alpha, \beta))}{\mathrm{PDR}(e_{a,b}, \alpha)} \quad (3.17)$$

$$\mathrm{Rel}(\mathrm{PDR}_{\mathrm{Diff}}) \rightarrow [-1, \infty] \quad (3.18)$$

These two metrics allow a comparison of what would happen when routes are discovered with small sized packets and then data packets of larger size are transmitted. Further on, there are routing protocols like the *Dynamic Source Routing* (DSR) protocol [16], where the route discovery packets increase in size when they travel from the source node towards a destination and thus may be lost due to the dependency of the link quality on the packet size[8]. The colored dashed horizontal lines in both figures show where the graphs cross the vertical line at 0.0. Therefore the left region represents the fraction of links that decreased in PDR and the right region the fraction of links that improved when the packet size increased from α to β. Independent of the packet size, more than 80% of the links experienced a (expected) PDR decrease. Some links improved their PDR (significantly) which happens especially for low quality links and this can be considered "noise" in the data. For example, 1 packet (out of about 1800) was received over a link when the packet size was $\alpha = 128$ Bytes and 2 packets are received for a particular larger packet size β, resulting in a relative improvement of 2.0. The graphs in Figure 3.1.3b are cut off at $\mathrm{Rel}(\mathrm{PDR}_{\mathrm{Diff}}) = 1.0$ as some links improved by several hundred percents because of this phenomenon.

We can deduce from the results that 10%–20% of the links show $\mathrm{Abs}(\mathrm{PDR}_{\mathrm{Diff}}) \geq 0.5$. This is quite high, especially considering that the PDR is in the interval $[0.0, 1.0]$. About 60% of the links decreased in quality by $\mathrm{Abs}(\mathrm{PDR}_{\mathrm{Diff}}) \geq 0.1$. When we assume that $-0.1 \leq \mathrm{Abs}(\mathrm{PDR}_{\mathrm{Diff}}) \leq 0.1$ is within normal bounds[9] due to

[7] If the link is available for $\beta_j > \beta_i$ than it will contribute to the particular data set α, β_j. This can happen in some rare cases.

[8] The size in route discovery packets can be increased due to the accumulation of the addresses of the traversed node in the header and additionally because of piggybacked data, e.g., link metrics.

[9] Marked by the additional dotted vertical lines in Figure 3.1.3a.

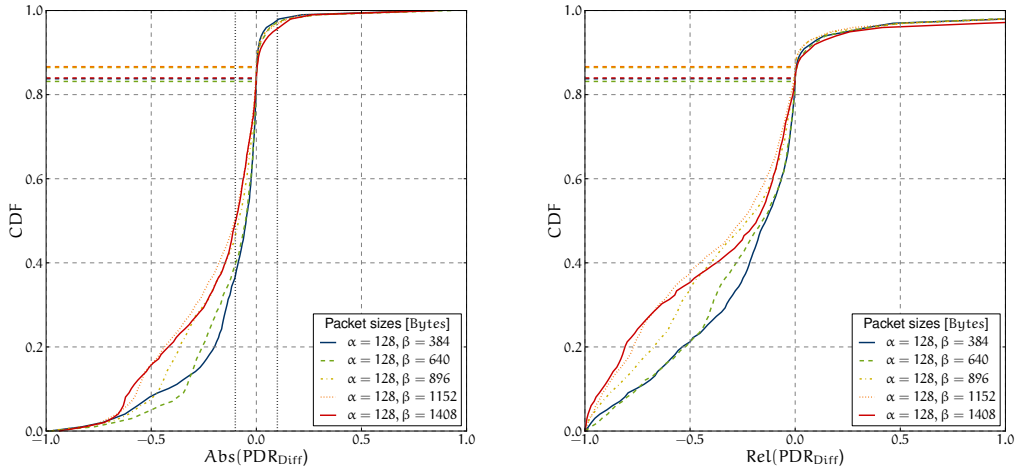

(a) Absolute PDR difference (b) Relative PDR difference

Figure 3.1.3: Absolute and relative difference in PDR for different packet sizes on channel 13

measurement errors, external sources of interference, etc, then around 50% of the links kept their PDR. Of course, with a stricter condition, a lower fraction of links has to be considered as unaffected.

We conclude that a high fraction of the links is affected by the packet size. In addition, it should always be considered that several links vanished for larger packet sizes which is not represented in the graphs. The number of links is discussed in Section 3.1.6. Nevertheless, the results show the dynamics of the PDR that has to be expected in real world scenarios.

3.1.4 Node Degree

The distribution of the node degree is depicted in Figure 3.1.4a for each packet size. The vertical colored dashed lines represent the average node degree in the particular scenario. For each node r the degree d_G is calculated as follows based on its neighborhood N_G set:

$$N_G(r) = \{s \mid s \in V \wedge e_{s,r} \in E\} \tag{3.19}$$

$$d_G(r) = \|N_G(r)\| \tag{3.20}$$

$$d_G(r) \rightarrow [0, N-1] \tag{3.21}$$

s is a node from which r received a packet over link $e_{s,r}$. Thus the node degree is equivalent to the number of incoming edges of the vertex in graph G.

We observe that when the packet size increases, the maximum and average node degree decrease. The maximum node degree moves from 43 to 32 and the average node degree decreases from 17.92 to 15.40. It is important to understand the impact of the approach how the node degree has been determined to assess the data. The naive procedure as described above is fairly simple: If a mesh router received a packet from a previously unknown neighbor, the node degree is incremented. Thus, even a single packet received in the 30 min duration has an effect. Neighborhood discovery

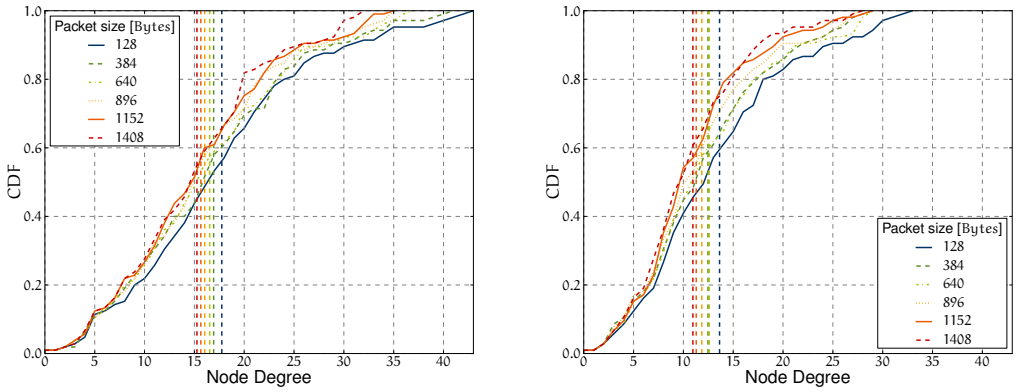

(a) Graph $G_{PDR>0.0}$ (b) Subgraph $G_{PDR\geq 0.10}$

Figure 3.1.4: Distribution of the node degree measured on channel 13

protocols, e.g., NHDP [17] or the ones included in routing protocols deal with low quality links in several ways. Some protocols do not accept nodes as neighbors before a particular number of packets has been received (in a specific timespan) while others remove nodes from their neighbor set if no subsequent packets are received for a specific time. Hybrid approaches are also possible. If we apply the first approach and remove all edges from the graph with $PDR < t$ (subgraph $G_{PDR\geq t}$), the maximum and average node degrees change as shown in Figure 3.1.4b. For the subgraph the node degree is calculated as follows:

$$G_{PDR\geq t} \subseteq G \tag{3.22}$$

$$d_{G_{PDR\geq t}}(r) = \left|\left|N_{G_{PDR\geq t}}(r)\right|\right| \tag{3.23}$$

This raises the question which threshold should be used. Some filtering has to be applied to cleanup the data but it has to be guaranteed that we do not remove edges from the graph that are required for the connectivity of the graph when we try to determine a more accurate average node degree. One node is isolated in $G_{PDR\geq 0.10}$ but is was already isolated in G[10]. The filtering of low quality links is further discussed in the next sections. Table 3.1.1 summarizes the maximum and average node degrees measured for each (sub-)graph and packet size. An additional graphical representation of the node degree distribution is also available in Section A.4.

3.1.5 Distance

Figure 3.1.6 shows the PDR for each link over the Euclidean distance (also called link range) between the two mesh routers based on the information that has been manually determined and stored in the central testbed database[11]. Each symbol represents one (unidirectional) link. In some cases, bidirectional links that are repre-

[10] The node is connected by an unidirectional link with the others and could not receive packets from any other node. Its packets were nevertheless received by other nodes.

[11] The position of the mesh routers has an absolute error of $\approx$ 1 m due to the measurement approach and the fact that routers can be slightly repositioned.

Packet Size [Bytes]	Subgraph	Max	Mode	μ	σ	$\tilde{d}_G$	γ
128	$G_{PDR>0}$	43	5	17.75	9.40	17.0	0.61
	$G_{PDR\geq 0.10}$	33	9	13.63	7.54	13.0	0.71
384	$G_{PDR>0}$	41	16	16.93	8.98	16.0	0.53
	$G_{PDR\geq 0.10}$	29	8	12.47	6.66	12.0	0.56
640	$G_{PDR>0}$	37	16	16.53	8.58	16.0	0.44
	$G_{PDR\geq 0.10}$	29	9	12.59	6.84	11.0	0.71
896	$G_{PDR>0}$	35	15	16.04	8.12	15.0	0.45
	$G_{PDR\geq 0.10}$	28	10	11.85	6.37	11.0	0.73
1152	$G_{PDR>0}$	35	16	15.65	7.98	15.0	0.43
	$G_{PDR\geq 0.10}$	29	8	11.29	5.82	10.0	0.86
1408	$G_{PDR>0}$	32	20	15.26	7.51	15.0	0.33
	$G_{PDR\geq 0.10}$	28	9	10.95	5.61	10.0	0.81

Table 3.1.1: Moments of the node degree distributions on channel 13

sented by two symbols above of each other are recognizable. Three kinds of symbols and colors are used to represent different type of links:

- Links between mesh routers that are attached to the outside walls of the buildings (▼ Outdoor Link)
- Links between mesh routers that are deployed inside the buildings (● Indoor Link)
- Links between mesh routers where one node is deployed outside and the other inside (× Indoor/Outdoor Link)

In addition, the median $\tilde{x}$ and mean μ of the PDR and Euclidean distance are represented by dashed and dotted lines on each axis. Figure 3.1.5 shows the distribution as pseudo-color plots as the scatter plots hide the number of data points that fall on the same position.

We observe that the increasing packet size shows only a negligible effect on the median and mean of the Euclidean distance. This is an indicator that long distance links experience the same effects as short distance links: The PDR decreases but the links are still existent or, alternatively, that short and long distance links vanish at the same rate. In contrast, the median and mean of the PDR decrease with larger packet sizes but going from packet size 1152 Bytes to 1408 Bytes they actually improve again. This is most probably an effect of different number of links that was already discussed in Section 3.1.1. Most importantly, no clear linear, logarithmic, or

Packet size [Bytes]	Mode [m]	μ [m]	σ [m]	$\tilde{x}$ [m]	γ
128	2.57	25.92	18.03	23.19	1.17
384	2.57	25.38	17.84	22.42	1.20
640	2.57	25.21	17.83	22.23	1.20
896	2.57	24.77	17.63	21.67	1.23
1152	2.57	24.37	17.26	21.40	1.24
1408	2.57	24.37	17.47	20.86	1.20

Table 3.1.2: Moments of the link range distributions on channel 13

otherwise anti-proportional relationship between the PDR and Euclidean distance can be derived from the figures. The outdoor links on their own show some kind of linear relationship but the sample size with about 22 links is too low for an accurate conclusion. Outdoor mesh routers do not necessarily have better quality links than the other routers as the radio propagation does not happen in free-space and experiences attenuation, shadowing, scattering, and multi-path effects. Indoor/Outdoor links can be available over equal distances with the same or even a higher PDR. As last, we observe that most indoor links are below 50 m and that there are two larger clouds of symbols in the top left and bottom part of the plots representing high quality and very low quality links. The average and median distances of the links are limitedly affected by the packet size but the variance is too high for more accurate conclusions. Table 3.1.2 summarizes the most important information about the link ranges.

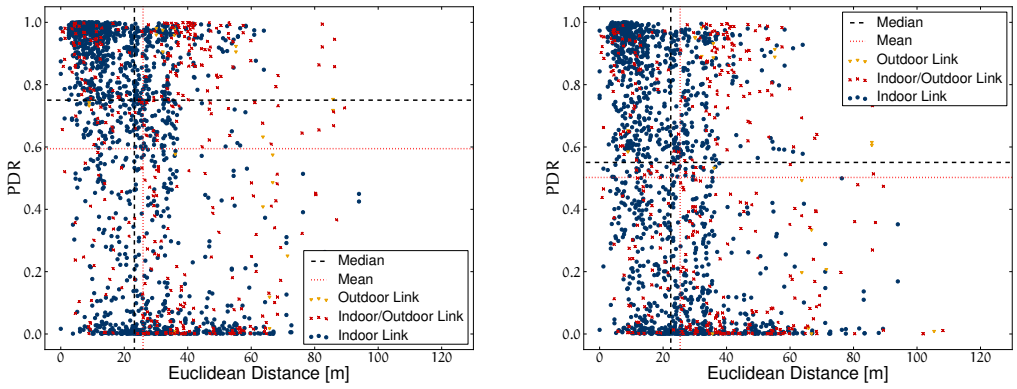

(a) Packet size 128 Bytes

(b) Packet size 384 Bytes

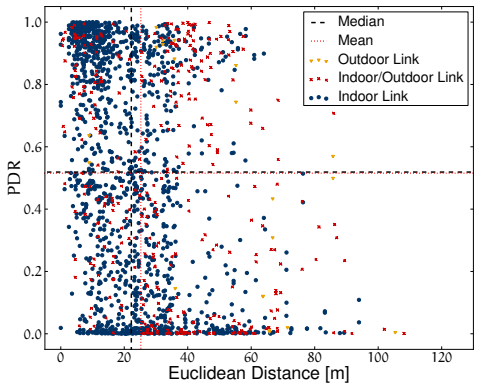

(c) Packet size 640 Bytes

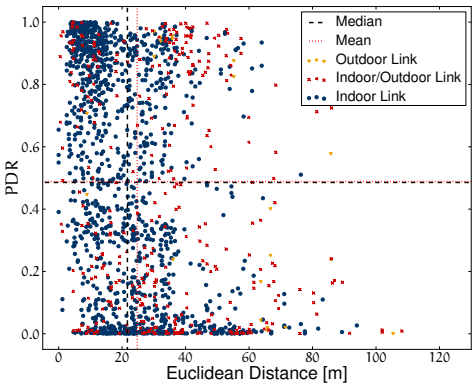

(d) Packet size 896 Bytes

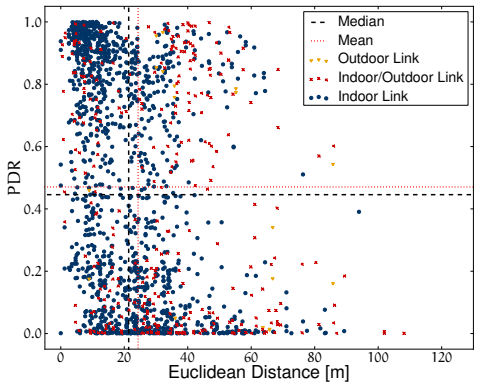

(e) Packet size 1152 Bytes

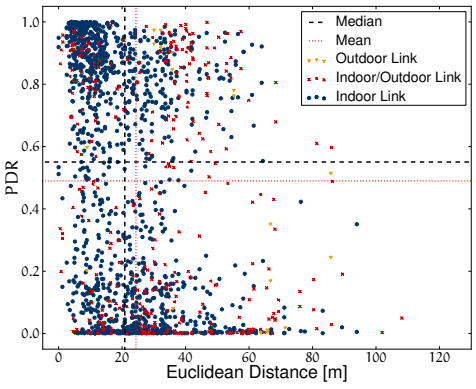

(f) Packet size 1408 Bytes

Figure 3.1.5: Scatter plot of the PDR for each link over the distance of the two corresponding mesh routers on channel 13

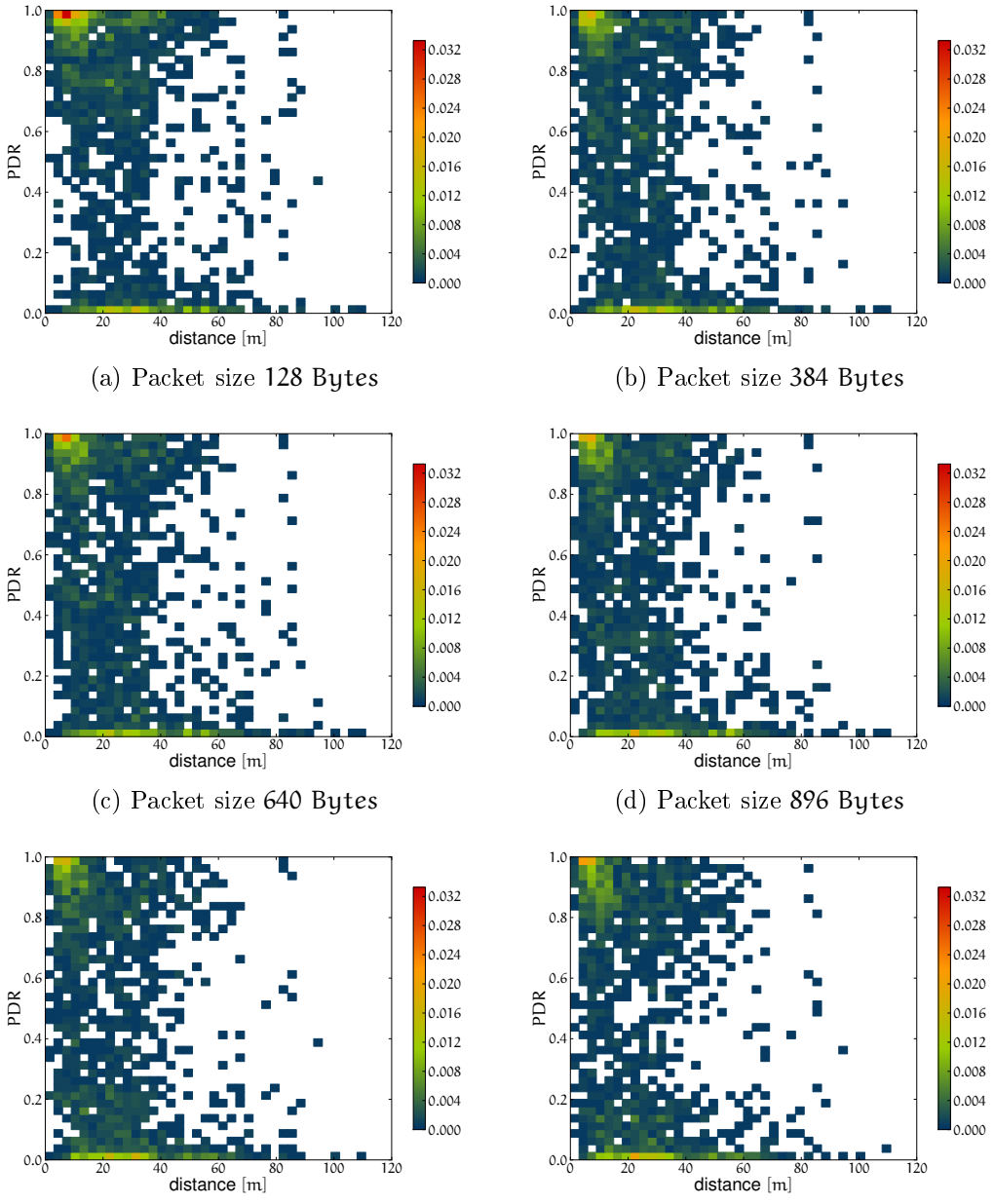

(a) Packet size 128 Bytes

(b) Packet size 384 Bytes

(c) Packet size 640 Bytes

(d) Packet size 896 Bytes

(e) Packet size 1152 Bytes

(f) Packet size 1408 Bytes

Figure 3.1.6: Pseudo-color plot of the PDR for each link over the distance of the two corresponding mesh routers on channel 13. The color represents the fraction of the data points that are in the particular bin.

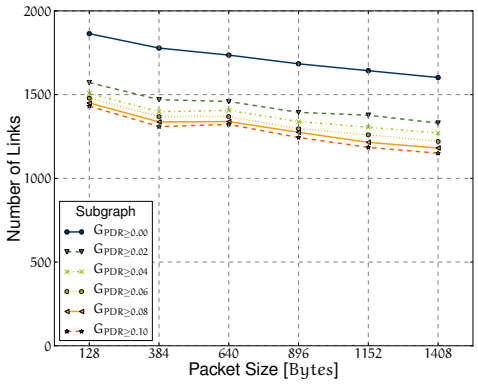

Figure 3.1.7: Number of links in the network for different packet sizes on channel 13. The number of links is determined in the denoted subgraphs.

3.1.6 Number of Links

The number of links $||E||$ can easily be determined by counting the distinct sources s of packets that each mesh router r received. A received packet represents an edge e in the network graph from node s and node r. When the node degree is already available, the number of links can be calculated based on the neighborhood information.

$$E = \{e_{s,r} \mid s, r \in V \wedge \|e_{s,r}\| > 0\} \tag{3.24}$$

$$\|E\| = \sum_{i=1}^{N} d_G(r_i) \tag{3.25}$$

$$\|E\| \in \left[0, (N-1)^2\right] \tag{3.26}$$

As represented in the formulas, $||E||$ contains bidirectional links twice: once for each direction.

Figure 3.1.7 shows the total number of links for each packet size. An increased packet size leads to an overall decrease in the number of links. As the graph also contains many low quality links, the total number of links is determined in several subgraphs $G_{PDR \geq t}$. All edges in the subgraph comply to the following condition:

$$E_{PDR \geq t} = \{e \mid PDR(e) \geq t, e \in E\} \tag{3.27}$$

Of course, the higher the threshold t, the less edges are left in the subgraph. Surprisingly in $G_{PDR \geq 0.10}$ and for packet size 640 Bytes, the total number increases compared to the previous value of packet size 384 Bytes. We consider this as an effect of measurement errors caused by changing environmental conditions. Overall, more than 200 links (between 14.0% and 19.6% depending on the particular value t) vanish when the packet size increases up to the highest value.

We can conclude, that the DES-Testbed topology is certainly not a fully meshed graph. The upper limit is given by $||E_{max}|| = N \times (N-1) = 10.920$ links. Thus the degree of meshness if expressed by $\frac{||E||}{||E_{max}||}$ is between 16.5% and 11%.

3.1.7 Diameter and Average Shortest Path

Figure 3.1.8a shows the diameter of the network, i.e., the maximum shortest path (in hops) for all nodes in the network. All nodes can reach each other over at most diameter many hops. Additionally, the average shortest path length is depicted. Both values are calculated as follows:

$$W(u_0, u_k): \quad u_0 \to u_1 \to \ldots \to u_k \tag{3.28}$$

$$\text{distance}(u, v) = \min\{k \mid u \xrightarrow{k} v\} \tag{3.29}$$

$$\varepsilon(u) = \max\{\forall v \in V, \mathit{distance}(u, v)\} \tag{3.30}$$

$$\text{diameter} = \max\{\forall u \in V, \varepsilon(u)\} \tag{3.31}$$

$$\text{avr(shortest path)} = \sum_{u,v \in V} \frac{\mathit{distance}(u, v)}{N(N-1)} \tag{3.32}$$

Where W is a walk from node u_0 to node u_k with length k, the distance between two nodes u and v is the minimal length (shortest path) for a walk, the eccentricity ε of a node is its maximum distance, and the diameter is the maximum eccentricity of all nodes. The average shortest path is the average of all distances of all node pairs.

Like in the previous sections, we calculate these values after low quality links have been removed from the graph, i.e., the subgraph $G_{PDR \geq t}$ is used. If the graph is not strongly connected (see Section 3.1.9), then the largest component is used for evaluation. The shortest paths and diameter are determined on a directed graph. Due to the discrete domain of the diameter metric, the particular graphs overlap in the figure.

Overall, the diameter increases from 6 to 8 hops when the packet size is increased but the data do not show a monotone correlation. The diameter actually falls back to 7 hops for some of the results measured with packet size 1408 Bytes. This can be a measurement effect respectively a consequence of the experiment execution: the topology was probed with each packet size one after another and not at the same time. As shown in Figure 3.1.1a, the distribution of the PDR for the largest packet size deviated from the others. Nevertheless, for packet size 1408 Bytes and $t \geq 0.06$ the diameter is also at 8 hops. The average shortest path, as shown by the dashed lines in the same figure, increases slightly with increased packet size and the lower number of links shows some effect but the average shortest path does not increase beyond 3. While our results show a low average shortest path metric, the this does not imply that the route is actually usable for data transfer in common application scenarios. For example, the PDR over a three hop path in $G_{PDR \geq 0.1}$ can be as low as 0.1^3.

A different approach has been applied to create Figure 3.1.8b to visualize the hop distance of the routers. The average distance[12] (ordinate) is shown for each of the nodes that are lined up on the abscissa. The nodes/distances are ordered by their average distance and thus a particular node does not necessarily have the same position on the abscissa for the different packet sizes that represent the different graphs. In contrast to the previous approach where all links of less than a particular PDR where ignored when applying the algorithm, the average distances are calculated on

[12] Average distance of a particular node to all other nodes.

a graph where the edges are weighted by the ETX metric [15] (see Equation (3.10)). As the ETX metric implicitly describes the PDR of bidirectional links, the graphs contain no unidirectional links. Additionally, all links with $\mathsf{ETX} > 2.0$ are removed, i.e., there are only edges left in the graph where (statistically) a packet has to be transmitted at most twice over each particular link to be successfully received and acknowledged[13].

$$G_{ETX \leq t} \subseteq G \tag{3.33}$$

$$E_{G_{ETX \leq t}} = \{e_{s,r} \mid ETX(e_{s,r}) \leq t, \forall e \in E\} \tag{3.34}$$

As shown in Figure A.2.1, in the worst case $\mathsf{ETX} = 2.0$ describes a link that is perfect in one direction ($\mathsf{PDR} = 1.0$) and looses half of the packets in the other ($\mathsf{PDR} = 0.5$). If the ETX value is increased further, an even more distinct link asymmetry is possible. Thus we deem $\mathsf{ETX} = 2.0$ as an acceptable choice to determine the shortest paths, especially as ETX is used as an additive path metric and thus the latent error increases.

We learn from Figure 3.1.8b that the number of nodes in the largest connected component shrinks when the packet size is increased. Further on, there is a proportional relationship between the packet size and the average distances for packet sizes 128 to 640 Bytes that is lost as soon as the graph becomes to sparse at packet size 896 Bytes. Surprisingly, all average distances of the nodes are above the average shortest path for all links that are depicted in Figure 3.1.8a. This means that a significant number of paths that were determined with the first approach contain links that are either unidirectional or have a higher ETX value and would not be used by routing protocols applying the ETX metric with our parametrization.

We do not give a definite answer how a simple metric like the average shortest path respectively the distance should be calculated in a wireless multi-hop network but as shown in this section, the results can significantly deviate. In contrast, in simulations where, depending on the radio model, communication is often possible in a perfect way up to a specific distance, the average shortest path can be intuitively calculated. Unfortunately, this simple approach is not applicable in the real world.

3.1.8 Unidirectional Links

Figure 3.1.9a shows the fraction of the unidirectional links E_{uni} determined for each packet size. The set of unidirectional links can be determined indirectly by the number of bidirectional links E_{bi}.

$$E_{bi} = \{e_{u,v} \mid e_{u,v} \in E \wedge e_{v,u} \in E\} \tag{3.35}$$

$$E_{uni} = E \setminus E_{bi} \tag{3.36}$$

The lowest graph in Figure 3.1.9a represents the evaluation of the raw data (the complete graph G) where a link is considered bidirectional when at least one packet was received by node r from node s and vice versa. We observe that about $10-12\%$

[13] The ETX link metric is defined for the network layer and calculated based on network layer information. The data link layer can nevertheless provide an arbitrary number of retransmissions that are transparent for the upper layers.

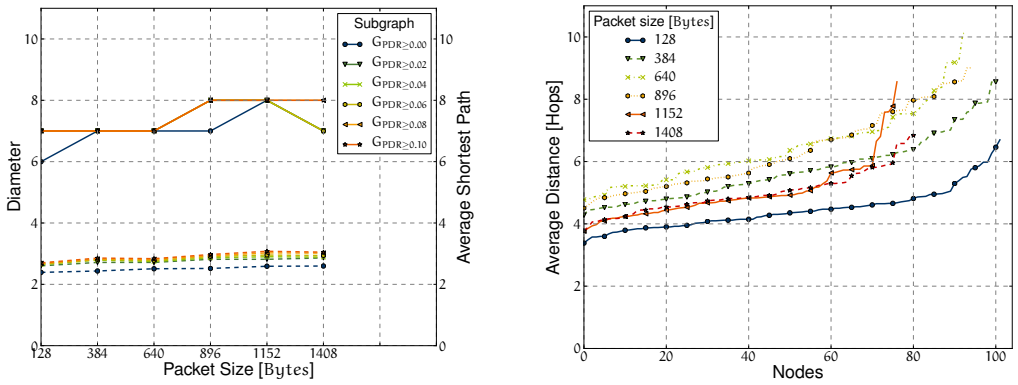

(a) Network diameter (solid lines) and average shortest path (dashed lines) for each packet size in the subgraph $G_{PDR\geq t}$.

(b) Average distance for each packet and for each node in $G_{ETX\leq2.0}$

Figure 3.1.8: Network diameter and shortest paths on channel 13

of the links are unidirectional in this scenario. As links with low PDR in one direction are borderline bidirectional, we apply a PDR threshold t that has to be met in both directions before the link is counted towards the bidirectional fraction.

$$E_{bi,PDR\geq t} = \{e_{u,v} \mid PDR(e_{u,v}) \geq t \wedge PDR(e_{v,u}) \geq t\} \quad (3.37)$$

$$G_{bi,PDR\geq t} = (V, E_{bi,PDR\geq t}) \quad (3.38)$$

The fraction of unidirectional links increases above 20% in $G_{bi,PDR\geq0.02}$ and in $G_{bi,PDR\geq0.1}$ nearly 40% of the links are unidirectional. Unidirectional links, especially of this magnitude, are rarely modeled in simulations but have high significance for the study and performance evaluation of routing protocols. E_{uni} as defined in Equation (3.35) includes also links that have a low PDR (below t) in both directions. If we compensate the values for these low quality links, the fraction of unidirectional links decreases again as shown in Figure 3.1.9b.

$$E_{PDR<t} = \{e_{u,v} \mid PDR(e_{u,v}) < t \wedge PDR(e_{v,u}) < t\} \quad (3.39)$$

$$E_{uni,PDR\geq t} = E \setminus (E_{bi,PDR\geq t} \cup E_{PDR<t}) \quad (3.40)$$

Nevertheless, the fraction stays above 20% for all but the smallest packet size and $t > 0$. If the links in $E_{PDR<t}$ should be considered as asymmetric is up for discussion.

We conclude from the large gap between the graphs for $G_{bi,PDR\geq0.00}$ and $G_{bi,PDR\geq0.02}$ that several nodes received few packets only due to rare events and environmental conditions: $PDR < 0.02$ means less than 36 of 1800 packets were received. These links can also be seen near the left and bottom edges in Figure A.5.1.

3.1.9 Network Fragility

Figure 3.1.10a shows the number of strongly connected components in the network. A strongly connected component is a subgraph in which each node can be reached from the others (and vice versa).

$$G_{strong} \subseteq G \quad (3.41)$$

$$V_{strong} = \{v \mid distance(v,u) \neq \infty \wedge distance(u,v) \neq \infty, \forall u,v \in V_{strong}\} \quad (3.42)$$

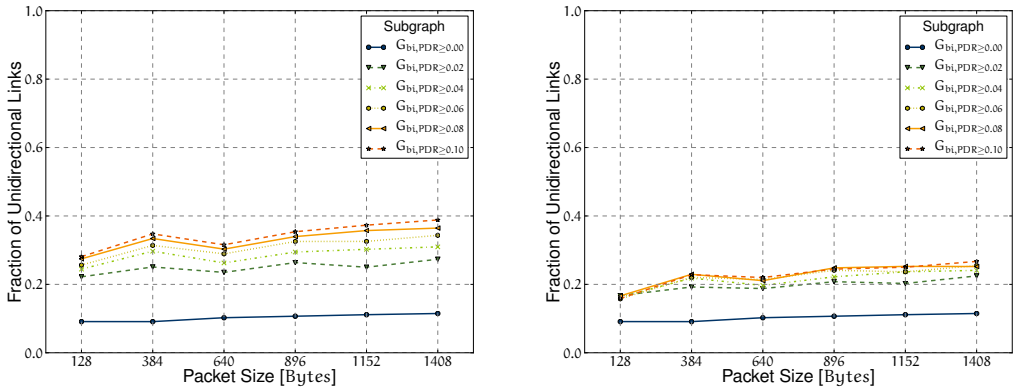

(a) Fraction of unidirectional links including $E_{PDR<t}$

(b) Fraction of unidirectional links excluding $E_{PDR<t}$

Figure 3.1.9: Fraction of the unidirectional links in particular subgraphs on channel 13.

As shown in the left hand side of Figure 3.1.10a, the network is not strongly connected as there are two components. One mesh router is only connected by a unidirectional link with the main component. As discussed in the other sections, low quality links should be ignored by routing protocols. So what happens, when edges are successively removed from the graph that have a PDR below a particular threshold? We define the (spanning) subgraph $G_{PDR\geq t}$ as follows:

$$G_{PDR\geq t} \subseteq G \tag{3.43}$$

$$E_{G_{PDR\geq t}} = \{e \mid PDR(e) \geq t, e \in E\} \tag{3.44}$$

The abscissa shows the subgraph $G_{PDR\geq t}$, i.e., it specifies the minimum PDR of links that are in the graph. We observe that with higher values, the graph partitions in more and more strongly connected components but that the graph $G_{PDR\geq 0.25}$ still has relatively few components: nodes break only off the "main component".

Figure 3.1.10b shows the number of mesh routers in the largest strongly connected component. This gives a better insight and more fine granular view. Often times when planning experiments, it is not important how many components a graph consists of but what the largest number of nodes is that can reach each other. For example, when a study requires that all links should have $PDR \geq t$ than this metric allows to derive how many mesh routers are available at most for the experiment. The dotted graphs (belonging to the ordinate on the right hand side) show the fraction of links in $G_{PDR\geq t}$ removed from G.

The packet size has an effect on the number of components and the number of mesh routers in the largest component: the larger the packet size, the more components and the less routers in the largest component. Yet again, we can observe that the graph for packet size 1408 Bytes does not follow this trend. Starting at $PDR \geq 0.45$, the number of mesh routers is larger than what was measured with packet size 1152 Bytes. Firstly, this can be attributed to the fact that a lower fraction of edges was removed from the graph (as shown with the dotted graphs). Secondly, Figure 3.1.1a and Figure 3.1.2 showed a better distribution of the PDR and

PDR_{Asym} metrics. Therefore it is plausible that the graph for packet size 1408 Bytes shows a lower fragility and breaks later when more and more edges are removed.

As last, Figure 3.1.10c shows the number of strongly connected components plotted over the number of nodes in the largest strongly connected component. Each point in the graphs corresponds to a particular $G_{PDR \geq t}$ value on the abscissae of the previous two figures: the number of strongly connected components and nodes in the largest connected component form a tuple for a particular t of $G_{PDR \geq t}$. We observe that there is no linear relationship between the two metrics[14]. There are long vertical and horizontal slopes and only some points are on the diagonal. The vertical slopes represent a change in the number of strongly connected components while the number of nodes in the largest strongly connected component stays constant, i.e., nodes do not "break" from this largest component but smaller ones. The horizontal slopes represent a (nearly) constant number of strongly connected components while groups of nodes break from the largest component.

We conclude from the results that while the network topology can be improved, routing protocols can ignore at least the worst links ($PDR < 0.2$) when calculating shortest paths in the DES-Testbed.

3.1.10 Topology

As there are over 1100 links in the testbed, the topology is difficult to represent in a clear way. Nevertheless to give a rough overview, Figure 3.1.11 shows the network as it was probed with the packet sizes 128 and 1408 Bytes. The PDR of the links is represented by colors (see the scale on the color-bar) and additionally by size: the higher the PDR, the thicker the edge in the graph. Thick yellow edges represent high quality links and thin red edges are links with low PDR.

The decrease in PDR when the packet size increased is clearly visible but especially distinct for the building in the front left. Fortunately, none of the buildings or floors gets isolated.

[14] The dashed diagonal line is plotted for comparison.

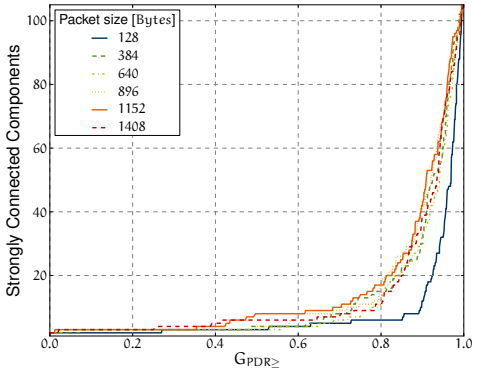

(a) Number of strongly connected components

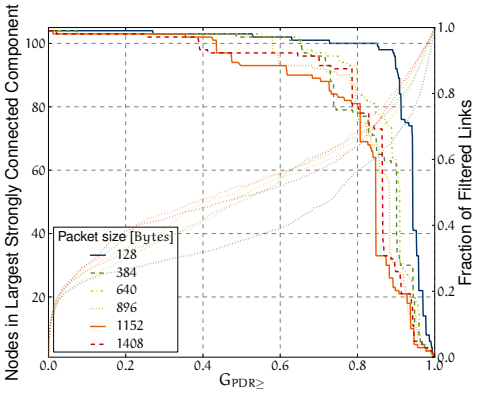

(b) Number of nodes in the largest strongly connected component

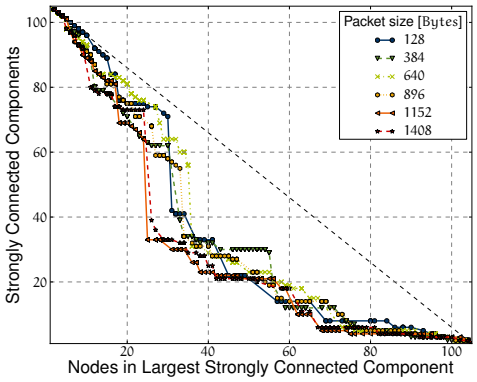

(c) Number of strongly connected components plotted over the number of nodes in the largest strongly connected component

Figure 3.1.10: Network fragility on channel 13

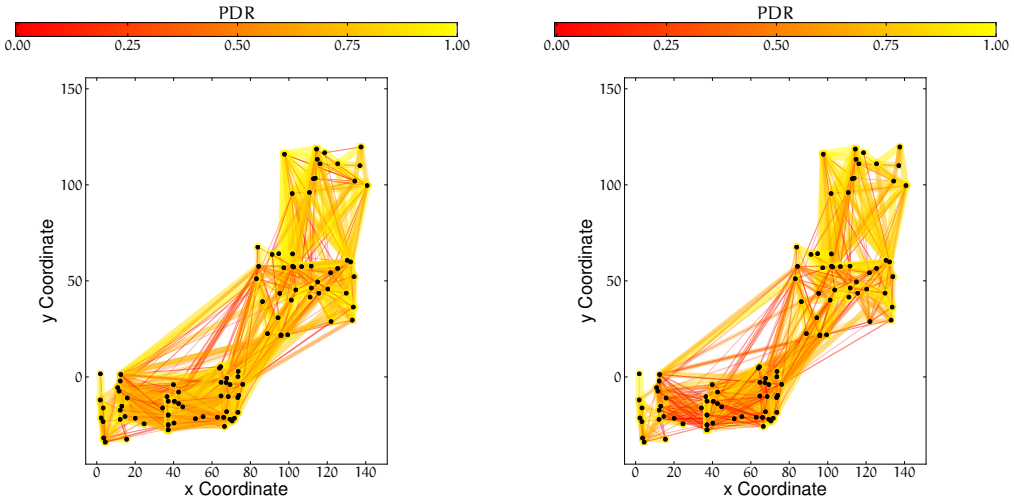

(a) Packet size 128 Bytes

(b) Packet size 1408 Bytes

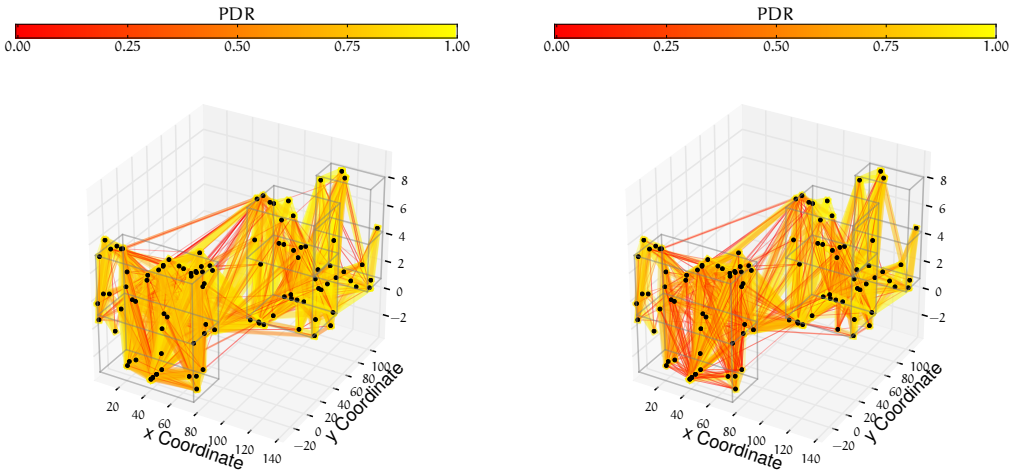

(c) Packet size 128 Bytes

(d) Packet size 1408 Bytes

Figure 3.1.11: Topology of the DES-Testbed on channel 13 for two selected packet sizes. The two-dimensional representations shows the floors slightly skewed against each other to minimize the visual overlap of nodes.

3.2 Results from the 5 GHz Band

This section presents the results from channel 40 and 44. As the data is very similar in most cases, not all figures are included in this section for channel 44. They are available in the appendix for comparison.

3.2.1 Packet Delivery Ratio

Figure 3.2.1 shows the cumulative distribution function of the packet delivery ratio measured with different packet sizes as well as the relative frequency of the PDR as pseudo-color plots[15]. Compared with the results from the 2.4 GHz band, we observe a much higher quality of the links. Whereas on channel 13 only 30% to 45% of the links had $PDR \geq 0.8$, nearly 80% are now above this level. Further on, the distributions of the PDR shows less influence from the packet sizes. This is especially true for the lower quality links. Links that fall in the bin $0.8 \leq PDR \leq 0.95$ show some effect and the best links ($PDR > 0.975$), that actually encompass a fraction of more than 0.5, are unaffected.

The differences of the results from the two frequency bands are clearly visible. An in-detail discussion of the specific reasons for that phenomenon are not in the focus of this technical report but as we will see in the following, the total number of links might be one important factor. The distribution of the PDR nevertheless seems bimodal as there is still a peak for the lowest bin but that has only a quarter of the height compared to the data from channel 13.

The results from channel 40 and 44 can be considered similar. The quantile-quantile plot of the percentiles in Figure 3.2.2a shows that both distributions of the PDR are linearly related but not equal. Channel 40 has slightly better links but the difference is relatively small. Nevertheless, a *Kolmogorov-Smirnov* (K-S) test of the two samples rejected that the samples come from the same distribution (null hypothesis H_0) in most cases. The K-S test considers the maximum distance between the CDF curves of both empirical distributions: $D = \max|F_{s_1}(x) - F_{s_2}(x)|$. Where F_{s_i} is the empirical distribution function of the samples s_i at x and D is the K-S statistic. The K-S test is a two-sided test for H_0 that two independent samples are from the same (continuous) distribution. The critical value D_{crit} [18] is approximated as follows:

$$D_{crit} = c(\alpha)\sqrt{\frac{||S_1|| + ||S_2||}{||S_1|| \times ||S_2||}} \tag{3.45}$$

$$c(0.05) = 1.36 \tag{3.46}$$

$$c(0.10) = 1.22 \tag{3.47}$$

α is the confidence level and $||S_i||$ is the size of sample S_i. In this case, S_i is a list of PDR values. The results of the test are summarized in Table 3.2.1. The distributions are only similar but they are not equal. In contrast, the quantile-quantile plot of the PDR from channel 40 and channel 13 in Figure 3.2.2b highlights the difference

[15] Please note that the scales for both plots and the plot in the previous section are different.

between the two frequency bands. The links on channel 13 are without a doubt much worse, independent of the packet size.

Besides the K-S test, a χ^2 two sample test[16] was applied to compare the empirical distributions. The results are summarized in Table 3.2.2. The χ^2 test compares the frequency of the data based on a histogram.

$$\chi^2 = \sum_{i=1}^{k} \frac{(K_1 \times \text{freq}(S_{40}, i) - K_2 \times \text{freq}(S_{44}, i))^2}{\text{freq}(S_{40}, i) + \text{freq}(S_{44}, i)} \tag{3.48}$$

$$K_1 = \sqrt{\frac{\sum_{i=1}^{k} \text{freq}(S_{40}, i)}{\sum_{i=1}^{k} \text{freq}(S_{44}, i)}} \tag{3.49}$$

$$K_2 = \sqrt{\frac{\sum_{i=1}^{k} \text{freq}(S_{44}, i)}{\sum_{i=1}^{k} \text{freq}(S_{40}, i)}} \tag{3.50}$$

$$\tag{3.51}$$

Where χ^2 is the test statistic, S_{40} and S_{44} are the samples, freq is a function returning the observed frequency in the i-th bin, and K_1 and K_2 are scaling constants[17]. For the test, the number of bins is dynamically adjusted for both samples so that at least five observations are in each bin. Thus there are no empty bins and the degrees of freedom df is given by the number of bins minus one. The χ^2 accepts the null-hypothesis more often than the K-S test but for the specified confidence levels we cannot assume that the distributions of the PDR are from the same population.

3.2.2 Link Asymmetry

The link asymmetry is less distinct on channel 40 compared to the previous results. As shown in Figure 3.2.3, up to 90% of the links have $PDR_{Asym} \leq 0.2$ and 50% have $PDR_{Asym} \leq 0.05$. The packet size shows only an effect for links with low asymmetry ($PDR_{Asym} \leq 0.2$), while links with higher asymmetries are unaffected. As for channel 13, the distributions for both data sets seem like truncated normal distributions with peaks near $PDR_{Asym} = 0$ but with different kurtoses: the peaks have more than twice the height compared with channel 13.

The results from channel 40 and 44 can be considered similar but not equal as shown in the quantile-quantile plot in Figure 3.2.3a. A K-S test rejected the null-hypothesis that the samples come from the same distribution for different confidence levels. The results of the test are summarized in Table 3.2.3. The higher asymmetry on channel 13 is clearly visible in Figure 3.2.3. The distributions for packet size 128 Bytes are the ones that are the most similar yet for larger packet sizes there is a significant difference.

The low link asymmetry on channel 40 has also an influence on the ETX_{Diff} values. As shown in Figure A.2.2b, ETX accurately describes the quality for nearly 75% of the links. This fact is especially surprising as the reciprocal ETX value will always be smaller than the two PDR values used for the computation. The improved

[16] This special type of χ^2 test is also called identity χ^2 test.

[17] Required because the data sets differ in size.

Packet size	$\|S_{40}\|$	$\|S_{44}\|$	D	D_{crit}	p-value	α	H_0
128	1064	1028	0.122	0.071	0.000	0.01	rejected
128	1064	1028	0.122	0.059	0.000	0.05	rejected
128	1064	1028	0.122	0.053	0.000	0.10	rejected
384	1040	996	0.155	0.072	0.000	0.01	rejected
384	1040	996	0.155	0.060	0.000	0.05	rejected
384	1040	996	0.155	0.054	0.000	0.10	rejected
640	1052	982	0.044	0.072	0.275	0.01	accepted
640	1052	982	0.044	0.060	0.275	0.05	accepted
640	1052	982	0.044	0.054	0.275	0.10	accepted
896	1026	971	0.086	0.073	0.001	0.01	rejected
896	1026	971	0.086	0.061	0.001	0.05	rejected
896	1026	971	0.086	0.055	0.001	0.10	rejected
1152	1024	949	0.061	0.073	0.050	0.01	accepted
1152	1024	949	0.061	0.061	0.050	0.05	accepted
1152	1024	949	0.061	0.055	0.050	0.10	rejected
1408	1034	947	0.122	0.073	0.000	0.01	rejected
1408	1034	947	0.122	0.061	0.000	0.05	rejected
1408	1034	947	0.122	0.055	0.000	0.10	rejected

Table 3.2.1: Kolmogorov-Smirnov test of the PDR distributions on channel 40 and 44

link asymmetry results in a much more accurate view of the network topology when ETX is used as routing metric. The packet size shows only a minor effect on the ETX_{Diff} distribution.

3.2.3 Impact of the Packet Size

Figure 3.2.5 shows how the PDR of each link changed when the packet size was increased as cumulative distribution function. As discussed in the previous two sections, the links were mostly unaffected by increased packet sizes. Whereas on channel 13 about 85% of the links decreased in quality, on channel 40 only around 70% show a decrease. The important difference is in the magnitude of the decreased PDR. If we apply the same limit[18] as in Section 3.1.3, then between 75% and 85% of the links kept their PDR when the packet size was increased. Even for links that decrease in quality, the difference is not as high as on channel 13: less than 5% of the links decrease by $Abs(PDR_{Diff}) \geq 0.5$. We observe from Figure 3.2.5b that less than 10% of the links experienced a halving of their PDR.

[18] $Abs(PDR_{Diff}) \in [-0.1, 0.1]$ is considered to be within normal bounds, i.e., the link was unaffected.

Packet size	$\|S_{40}\|$	$\|S_{44}\|$	χ^2	χ^2_{crit}	df	p-value	α	H_0
128	1064	1028	17.219	29.141	14	0.052	0.01	accepted
128	1064	1028	17.219	23.685	14	0.052	0.05	accepted
128	1064	1028	17.219	21.064	14	0.052	0.10	rejected
384	1040	996	16.871	27.688	13	0.047	0.01	accepted
384	1040	996	16.871	22.362	13	0.047	0.05	rejected
384	1040	996	16.871	19.812	13	0.047	0.10	rejected
640	1052	982	22.766	32.000	16	0.028	0.01	accepted
640	1052	982	22.766	26.296	16	0.028	0.05	rejected
640	1052	982	22.766	23.542	16	0.028	0.10	rejected
896	1026	971	15.660	27.688	13	0.057	0.01	accepted
896	1026	971	15.660	22.362	13	0.057	0.05	accepted
896	1026	971	15.660	19.812	13	0.057	0.10	rejected
1152	1024	949	35.594	34.805	18	0.002	0.01	rejected
1152	1024	949	35.594	28.869	18	0.002	0.05	rejected
1152	1024	949	35.594	25.989	18	0.002	0.10	rejected
1408	1034	947	17.592	27.688	13	0.041	0.01	accepted
1408	1034	947	17.592	22.362	13	0.041	0.05	rejected
1408	1034	947	17.592	19.812	13	0.041	0.10	rejected

Table 3.2.2: χ^2 test of the PDR distributions on channel 40 and 44

3.2.4 Node Degree

The node degree distribution is depicted in Figure 3.2.6a measured for all scenarios[19]. The packet size shows little effect on the distribution of the node degree: maximum and average are only affected to a very limited degree. Both values are actually much lower than on channel 13 for G and $G_{PDR \geq 0.10}$ (see Table 3.2.4). The difference between the average node degrees in G and $G_{PDR \geq 0.10}$ is also much lower as fewer links have $PDR < 0.1$.

At this point we come to the conclusion that the overall higher PDR and lower asymmetry on 5 GHz can be attributed to the fact that the nodes have less neighbors and when a link exists, it often has a high PDR. Maybe less long range links with a low quality exist in the topology? This hypothesis will be discussed in the next section.

3.2.5 Distance

Figure 3.2.8 shows the PDR for each link over the Euclidean distance between the two corresponding mesh routers. The scatter plots look noticeably different from

[19] The number of links is also available in Table 3.2.1.

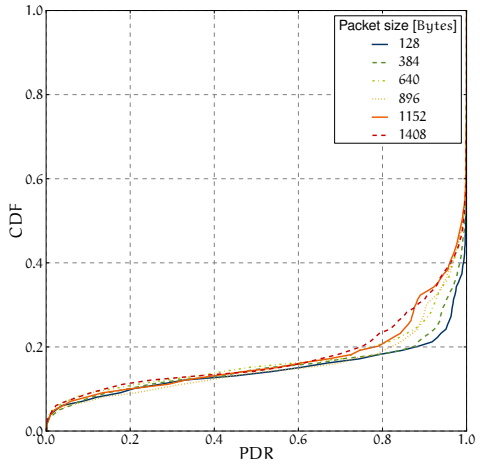

(a) CDF of the PDR on channel 40

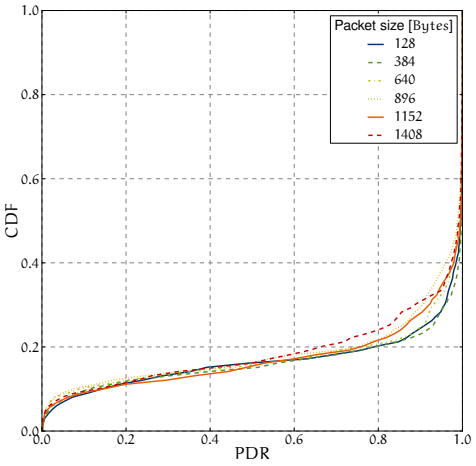

(b) CDF of the PDR on channel 44

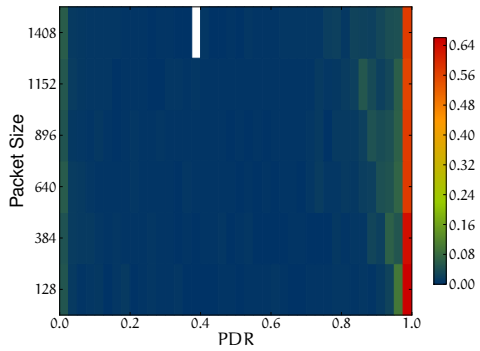

(c) Pseudo-color plot of the PDR distribution on channel 40

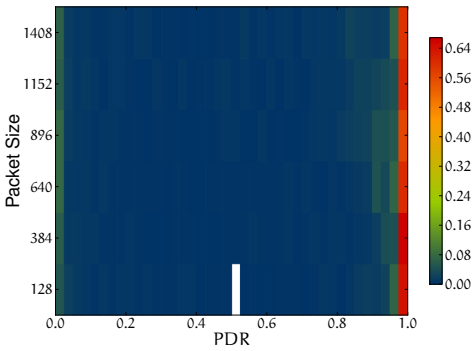

(d) Pseudo-color plot of the PDR distribution on channel 44

Figure 3.2.1: Distribution of the packet delivery ratio on channel 40 and 44

what was depicted in Section 3.1.5. The accumulation of data points in the top-left and bottom region is much more developed. Fewer data points are in between these clusters: the links are either very good or very bad. Like for channel 13, there is no clearly visible relationship between the distance and the PDR. Only for the links between outdoor nodes, a linear relationship is indicated. Figure 3.2.9 shows the distribution as pseudo-color plots.

The data partially confirms the assumption that links on the 5 GHz band exhibit higher attenuation effects and thus have a lower maximum range. The median and average distances are overall lower compared to the 2.4 GHz data (compare Table 3.2.5). Figure 3.2.7 depicts the median and average distances that where measured for the particular packet sizes. As the standard deviation is very high, it is not shown in the figure, as well as confidence intervals. Due to its high value, that is calculated assuming a normal distribution of the data[20], only limited conclusions are possible concerning the channel-maximum-distance relationship. The mean and median distances on channel 13 decrease monotonously when the packet size is increased but this effect is not present on the other two channels where they stay

[20]The appendix contains some additional information about the distribution in Section A.3.

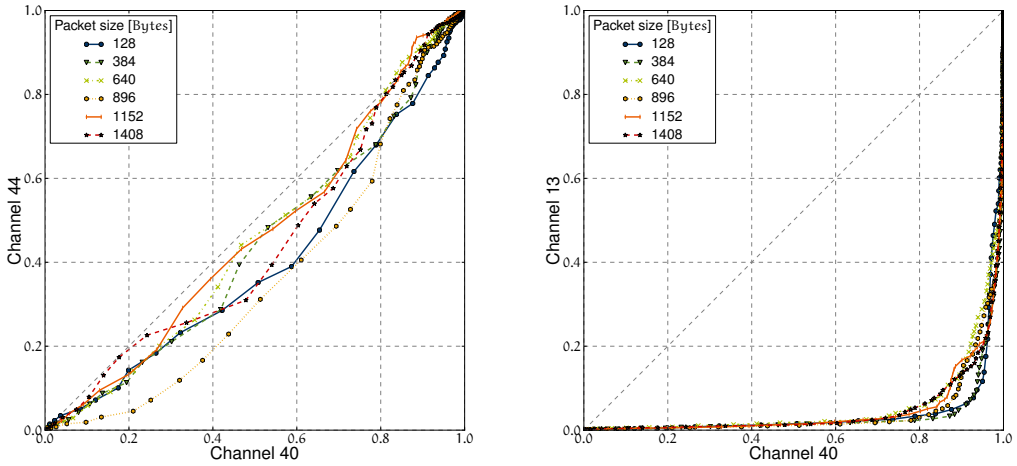

(a) Channel 40 versus channel 44 (b) Channel 40 versus channel 13

Figure 3.2.2: Quantile-Quantile plots of the PDR. The figures show the percentiles for each pair of empirical distributions.

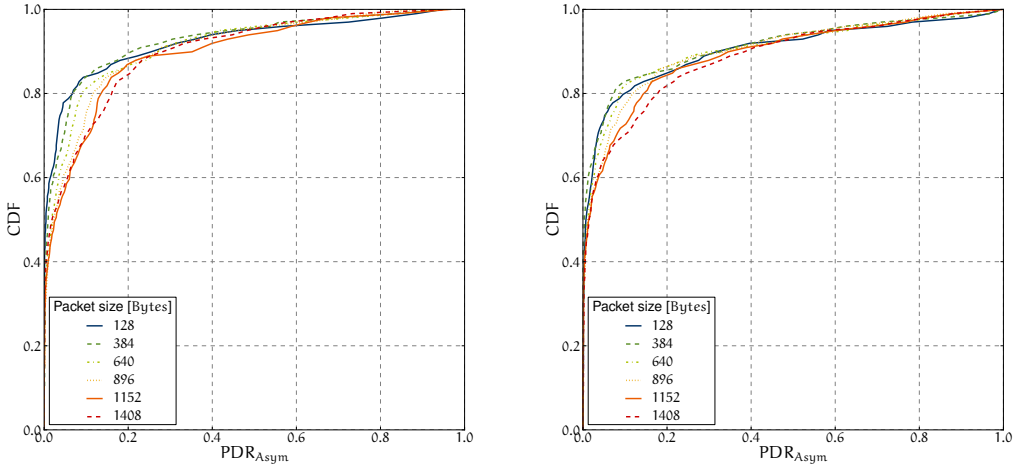

(a) Channel 40 (b) Channel 44

Figure 3.2.3: Link asymmetry on channel 40 and 44. The cumulative distribution of the PDR_{Asym} is depicted as measure of the link asymmetry.

constant.

We conclude from the results, that approaches that are commonly applied to describe the distances/ranges of links make little sense for a real world deployment. It is not sufficient to provide only the average and standard deviation as the assumption that the data is normal distributed does not hold. Figure A.3.1 shows the frequency of the link ranges as a histogram. The data resembles a χ distribution with more than one degree of freedom ($k \geq 1$) but a full statistical comparison is yet required for accurate conclusions.

Packet size	$\|S_{40}\|$	$\|S_{44}\|$	D	D_{crit}	p-value	α	H_0
128	986	920	0.130	0.075	0.000	0.01	rejected
128	986	920	0.130	0.062	0.000	0.05	rejected
128	986	920	0.130	0.056	0.000	0.10	rejected
384	958	886	0.239	0.076	0.000	0.01	rejected
384	958	886	0.239	0.063	0.000	0.05	rejected
384	958	886	0.239	0.057	0.000	0.10	rejected
640	982	870	0.073	0.076	0.014	0.01	accepted
640	982	870	0.073	0.063	0.014	0.05	rejected
640	982	870	0.073	0.057	0.014	0.10	rejected
896	960	856	0.091	0.077	0.001	0.01	rejected
896	960	856	0.091	0.064	0.001	0.05	rejected
896	960	856	0.091	0.057	0.001	0.10	rejected
1152	958	840	0.078	0.077	0.008	0.01	rejected
1152	958	840	0.078	0.064	0.008	0.05	rejected
1152	958	840	0.078	0.058	0.008	0.10	rejected
1408	972	838	0.138	0.077	0.000	0.01	rejected
1408	972	838	0.138	0.064	0.000	0.05	rejected
1408	972	838	0.138	0.058	0.000	0.10	rejected

Table 3.2.3: Kolmogorov-Smirnov test of the PDR_{Asym} distributions on channel 40 and 44

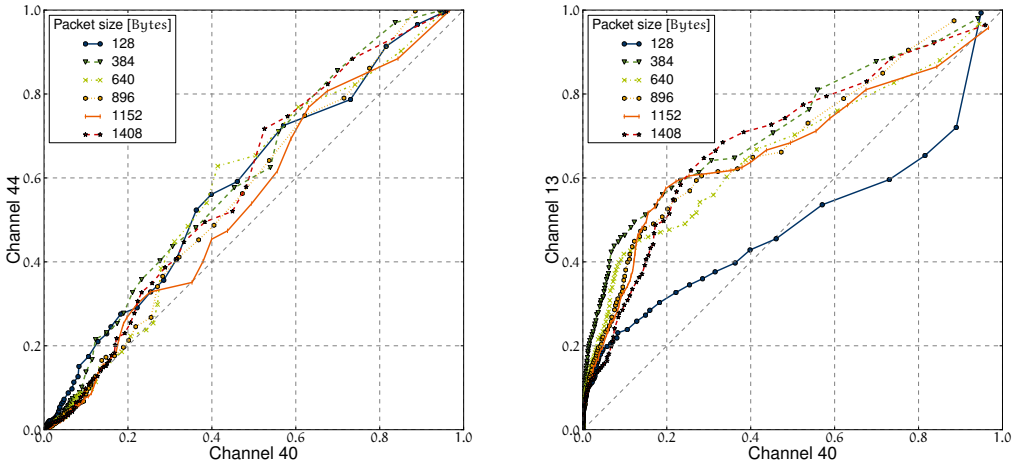

(a) Channel 40 versus channel 44 (b) Channel 40 versus channel 13

Figure 3.2.4: Quantile-Quantile plots of the link asymmetry. The figures show the percentiles for each pair of empirical distributions.

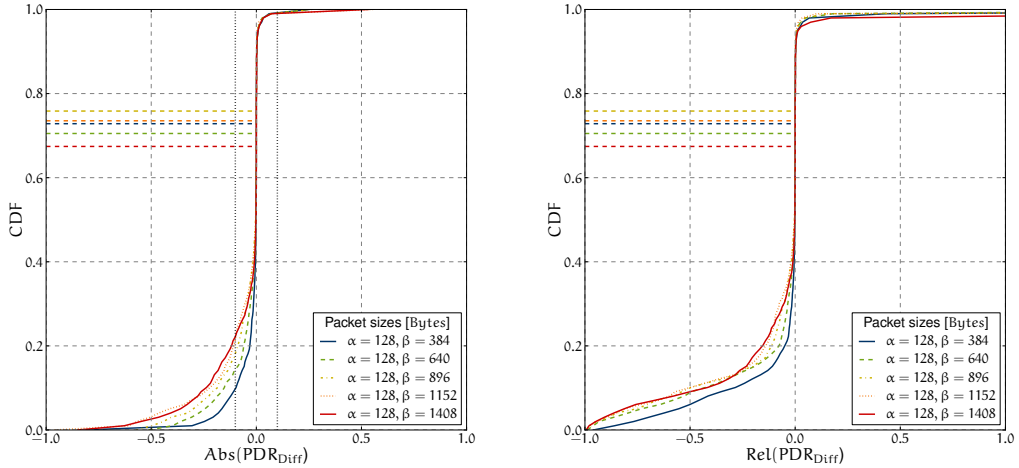

(a) Absolute PDR difference (b) Relative PDR difference

Figure 3.2.5: Absolute and relative difference in PDR for different packet sizes and channel 40

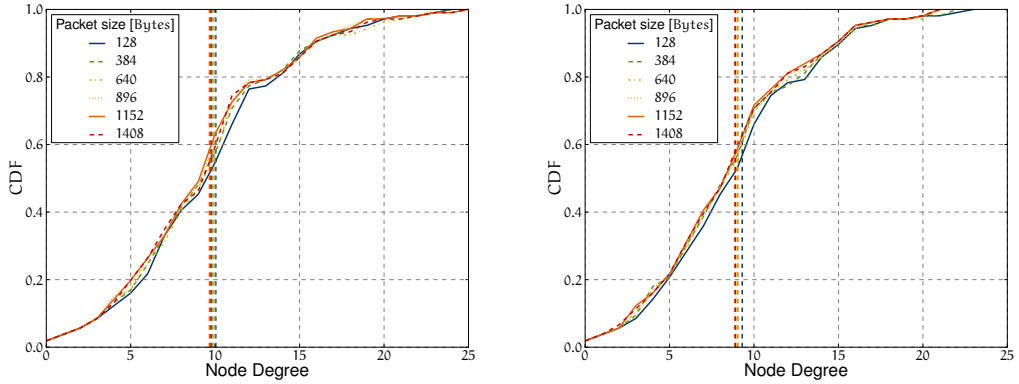

(a) Graph $G_{PDR>0.0}$ (b) Subgraph $G_{PDR\geq 0.10}$

Figure 3.2.6: Distribution of the node degree on channel 40 measured for different packet sizes

Packet Size [Bytes]	G	Max	Mode	μ	σ	$\tilde{d}_G$	γ
128	$G_{PDR>0}$	24	7	10.04	4.89	10.0	0.38
	$G_{PDR\geq 0.10}$	23	10	9.30	4.60	9.0	0.45
384	$G_{PDR>0}$	24	11	9.81	4.84	10.0	0.45
	$G_{PDR\geq 0.10}$	22	10	9.04	4.57	9.0	0.49
640	$G_{PDR>0}$	25	11	9.92	5.02	10.0	0.55
	$G_{PDR\geq 0.10}$	21	10	9.04	4.54	9.0	0.43
896	$G_{PDR>0}$	23	10	9.68	4.80	10.0	0.44
	$G_{PDR\geq 0.10}$	21	10	9.00	4.50	9.0	0.44
1152	$G_{PDR>0}$	25	10	9.66	4.89	10.0	0.54
	$G_{PDR\geq 0.10}$	21	10	8.87	4.47	9.0	0.45
1408	$G_{PDR>0}$	25	11	9.75	4.99	10.0	0.56
	$G_{PDR\geq 0.10}$	21	9	8.90	4.48	9.0	0.44

Table 3.2.4: Moments of the node degree distributions on channel 40

Packet size [Bytes]	Mode [m]	μ [m]	σ [m]	$\tilde{x}$ [m]	γ
128	2.57	21.23	15.68	16.04	1.16
384	2.57	21.10	15.72	15.82	1.17
640	2.57	21.23	15.79	16.03	1.20
896	2.57	20.86	15.35	15.82	1.16
1152	2.57	20.95	15.46	15.83	1.16
1408	2.57	21.29	15.84	16.03	1.16

Table 3.2.5: Moments of the link range distributions on channel 40

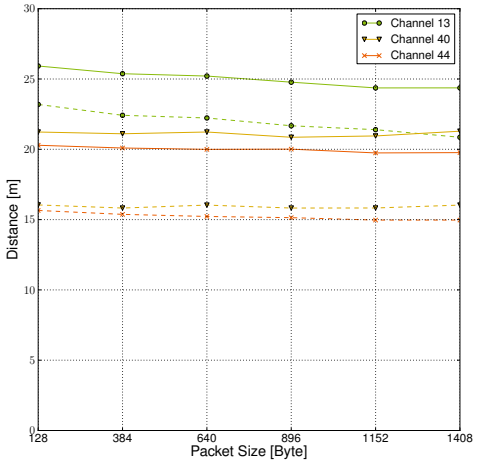

Figure 3.2.7: Link ranges for particular packet sizes on different channels. The solid lines represent the average and the dashed lines the median.

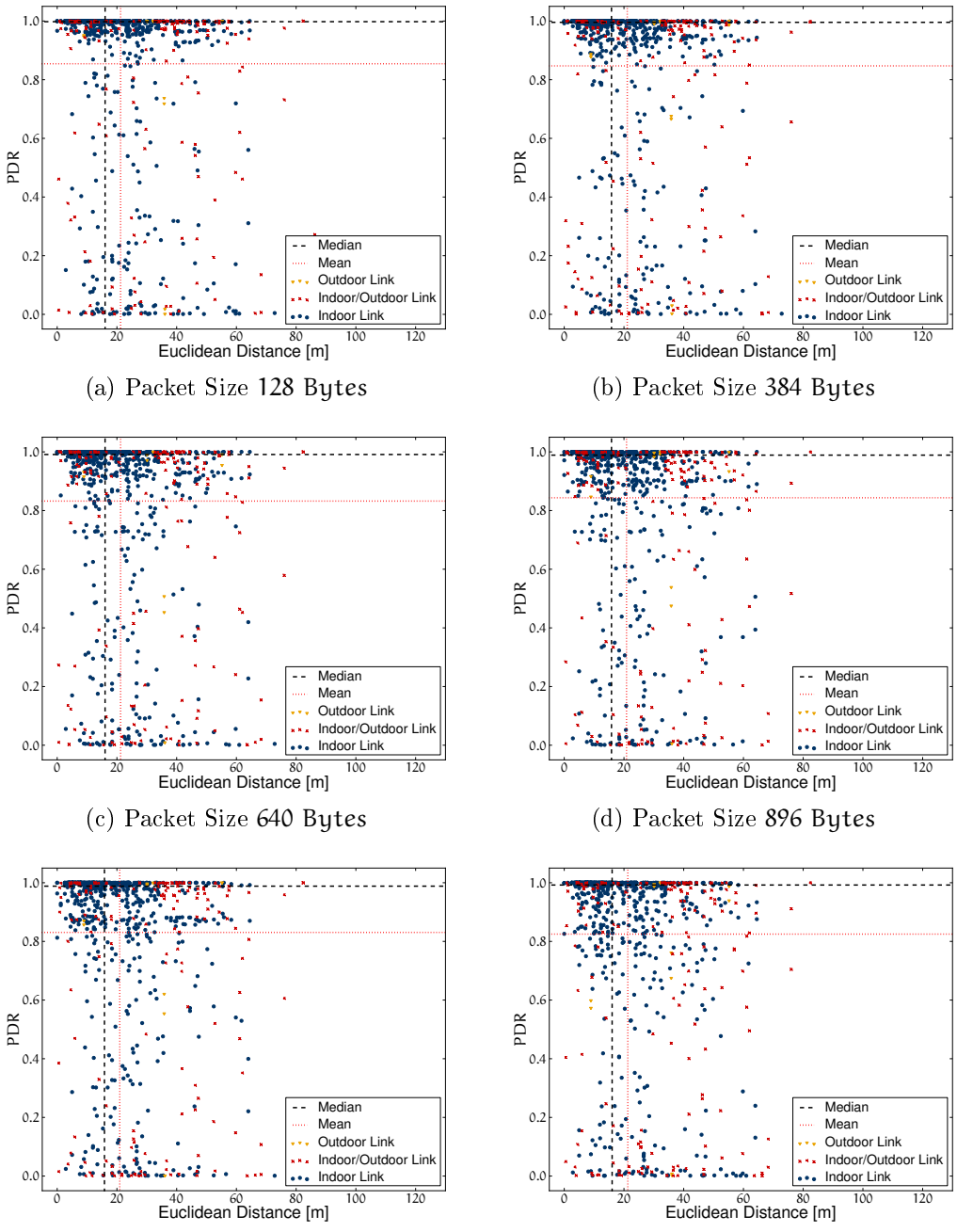

(a) Packet Size 128 Bytes

(b) Packet Size 384 Bytes

(c) Packet Size 640 Bytes

(d) Packet Size 896 Bytes

(e) Packet Size 1152 Bytes

(f) Packet Size 1408 Bytes

Figure 3.2.8: Scatterplot of the PDR for each link over the distance of the two corresponding mesh routers on channel 40

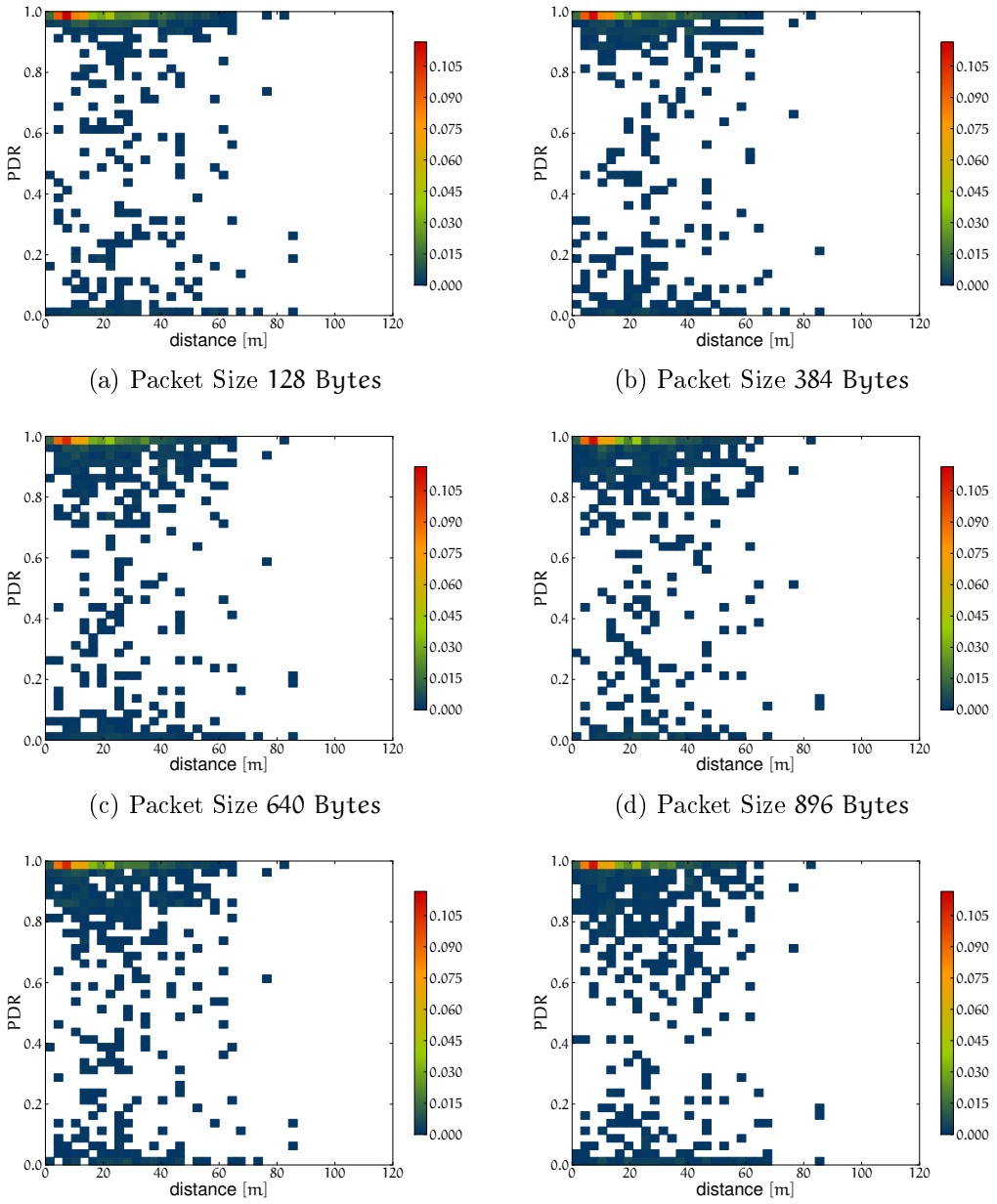

(a) Packet Size 128 Bytes

(b) Packet Size 384 Bytes

(c) Packet Size 640 Bytes

(d) Packet Size 896 Bytes

(e) Packet Size 1152 Bytes

(f) Packet Size 1408 Bytes

Figure 3.2.9: Pseudo-color plot of the PDR for each link over the distance of the two corresponding mesh routers on channel 40. The color represents the fraction.

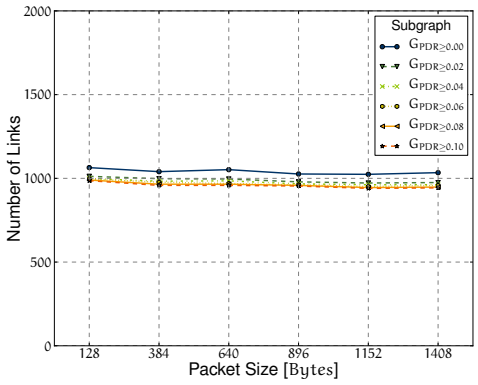

Figure 3.2.10: Number of links in the network for different packet sizes on channel 40. The number of links is determined in the denoted subgraphs.

3.2.6 Number of Links

Figure 3.2.10 shows the total number of links measured for each packet size. Like for the data gathered from channel 13, we consider the subgraph $G_{PDR\geq t}$. In contrast to Figure 3.1.7 we do not observe the same effect of the packet size on the number of links that stays more or less constant. Around 1000 links exist in each of the graphs which is lower than the 1600-1150 links on channel 13. We assume that the overall deviating results from the two frequency bands are caused by the different number of links: there are less links on 5 GHz but they have high(-er) PDR.

3.2.7 Diameter and Average Shortest Path

Figure 3.2.11a shows the diameter of the network and the average shortest path for all packet sizes in different subgraphs $G_{PDR\geq t}$. The diameter is higher than for channel 13: 6-8 versus 7-11 hops. The average shortest path for all nodes is increased by about 1 hop.

Figure 3.2.11b also shows a deviating result. It depicts the average distance for each node based on the ETX graph as introduced in Section 3.1.7. We observe that the largest strongly connected component of the graph has always the same number of nodes. Further on, larger packet sizes do not increase the average distance of each node which is represented by the overlapping graphs. Like for channel 13, the average distance for each node in the ETX graph is higher than what is determined on the graph with unidirectional links, that includes links with $ETX > 2.0$. Surprisingly, for larger packet sizes, the maximum average distance on channel 40 is below the maximum average distance on channel 13.

3.2.8 Unidirectional Links

Figure 3.2.12 shows the fraction of the unidirectional links determined for each packet size for the two sets as introduced in Section 3.1.8. Channel 40 has more bidirectional links. We observe that less than 8% of the links are unidirectional even when the links in $E_{PDR<t}$ are included in E_{uni}. In the subgraph $G_{bi,PDR\geq0.10}$ there are still $< 15\%$ unidirectional links. Further on, the packet size has no effect on the

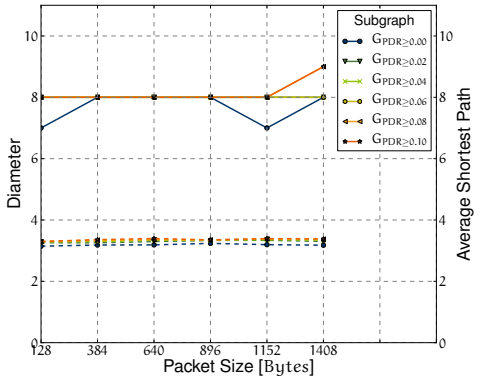

(a) Network diameter (solid lines) and average shortest path (dashed lines) for each packet size after filtering links below the denoted PDR.

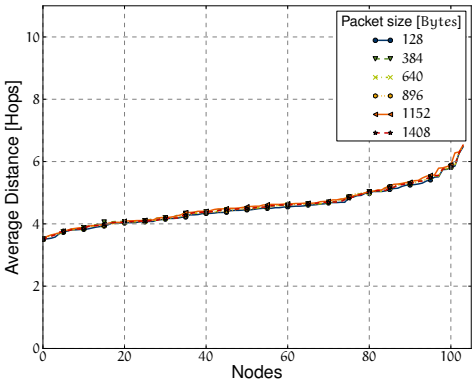

(b) Average distance for each packet and for each node in the network graph where all links have ETX $\leq$ 2.0.

Figure 3.2.11: Network diameter and shortest paths on channel 13

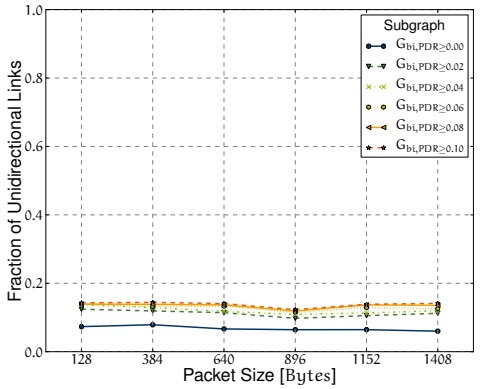

(a) Fraction of unidirectional link including $E_{PDR<t}$

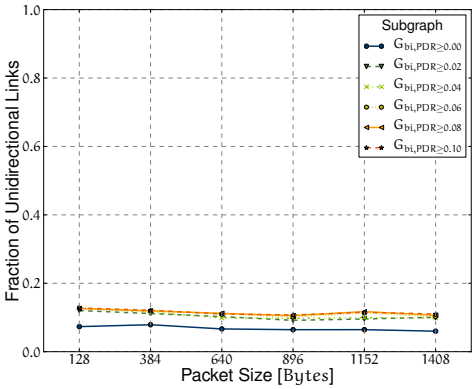

(b) Fraction of unidirectional links excluding $E_{PDR<t}$

Figure 3.2.12: Fraction of the unidirectional links in particular subgraphs on channel 40.

fraction as it was the case in the 2.4 GHz data. Channel 44 shows a larger fraction of unidirectional links compared to channel 40 as shown in Figure A.1.5 but it still stays below the 20% mark. When the links in $E_{PDR<t}$ are not counted towards the unidirection fractions as depicted in Figure 3.2.12b, nearly 90% of the links are not unidirectional.

3.2.9 Network Fragility

Figure 3.2.13a shows the number of strongly connected components in the network and highlights the overall higher PDR on channel 40. Even the graph $G_{PDR\geq0.8}$ is still strongly connected. As soon as it starts to partition, single nodes get isolated which is represented by the number of nodes in the largest strongly connected component in Figure 3.2.13c. At the first sight, Figure 3.2.13c shows as stronger linear relation

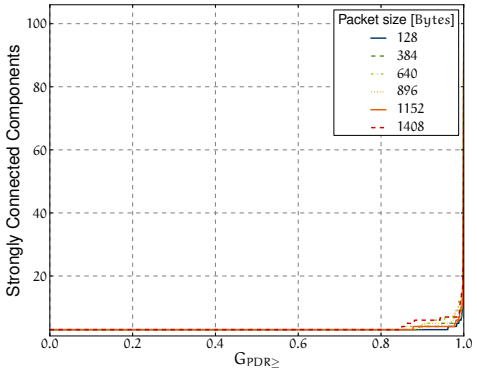

(a) Number of strongly connected components

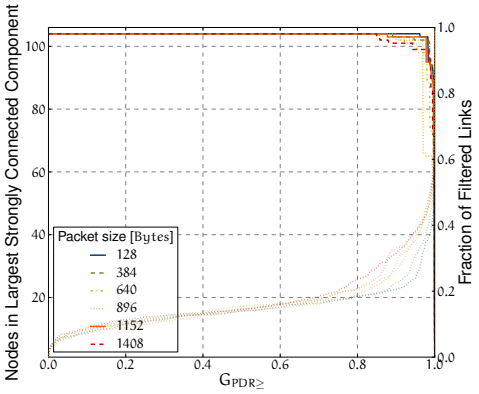

(b) Number of nodes in the largest strongly connected component

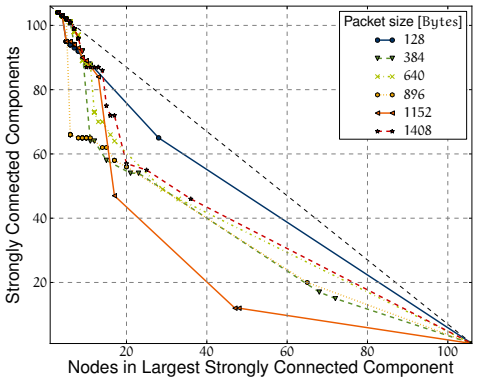

(c) Number of strongly connected components plotted over the number of nodes in the largest strongly connected component

Figure 3.2.13: Network Fragility on channel 40

of the number of strongly connected components and number of nodes in the largest strongly connected component which is a misinterpretation. The shape of the graphs depicted in the figure is determined by the available data points (see the markers). As the metrics do not change in value for most $G_{PDR\geq t}$, nearly all points are found in the lower-right of the figure: the graph is one large strongly connected component. Most other data points are in the top-left corner when the graph is nearly fully partitioned. As the transition is rather abrupt, there are few data points in between that lead to the linear looking shape.

We conclude that the network is less fragile on channel 40 than on channel 13. The packet size has no strong effect on this metric as the network starts to "break" at $PDR \geq 0.85$ for each but the smallest size. Therefore, the 5 GHz band should be used for experiments where the network is assumed to be a strongly connected graph with high quality links independent of the packet size.

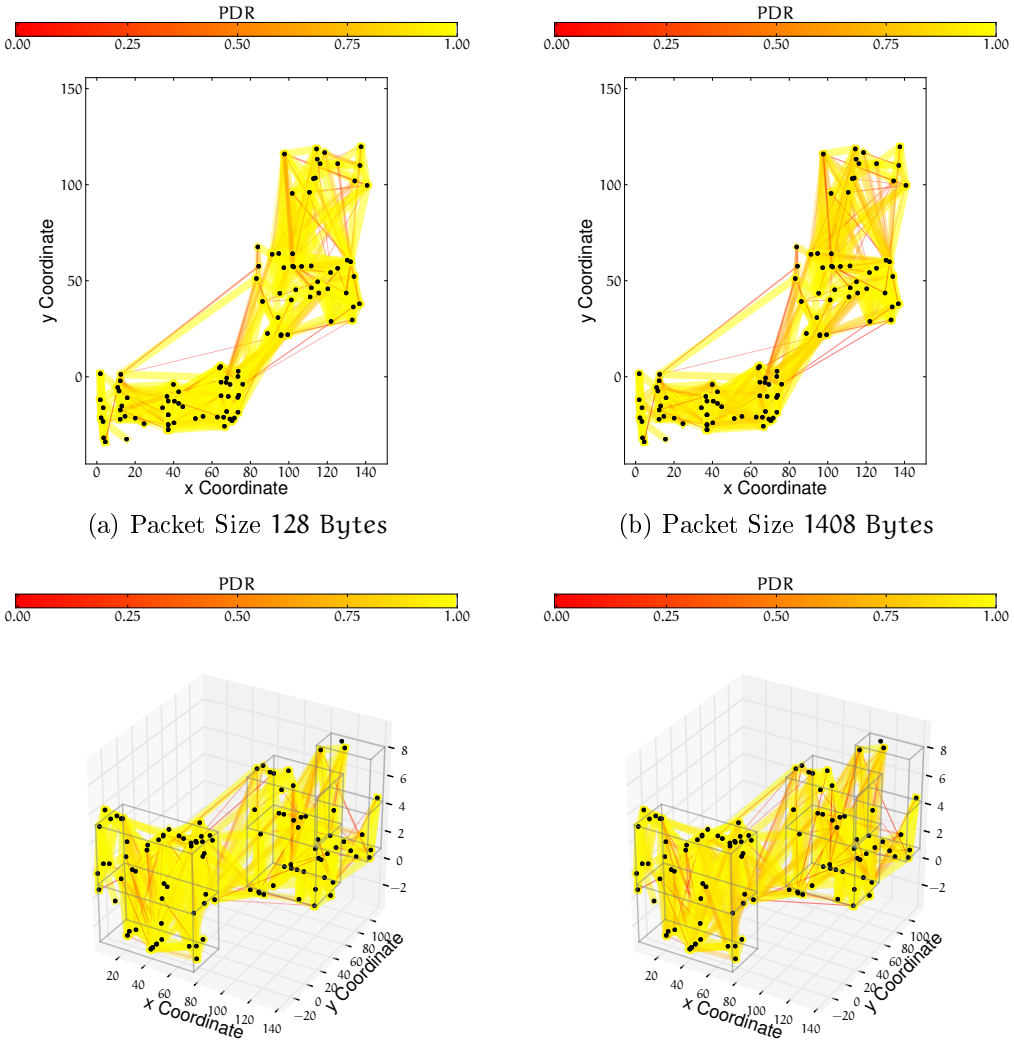

(a) Packet Size 128 Bytes

(b) Packet Size 1408 Bytes

(c) Packet Size 128 Bytes

(d) Packet Size 1408 Bytes

Figure 3.2.14: Topology of the DES-Testbed on channel 40 for two selected packet sizes. The two-dimensional representation shows the floors slightly skewed to each other to minimize the overlap of nodes.

3.2.10 Topology

Figure 3.2.14 shows the topology of the network. Compared to the figures representing channel 13, the higher PDR is clearly visible. The increased packet size (from 128 to 1408 Bytes) decreases the PDR for links that are uniformly distributed over the testbed. No regions can be visually determined that are significantly stronger (or less) affected.

CHAPTER 4

Conclusion

In this technical report we discussed the results of an experiment to probe the topology of the DES-Testbed to learn critical information about the network which shall help to improve subsequent studies. There are several statements that can be made based on the evaluation of the measured data. The DES-Testbed has significantly different link qualities on the 2.4 and 5 GHz band. Where there are many links with low or average PDR on channel 13, the links on channel 40 and 44 are in general better. We learned from the data that the PDR shows a bimodal distribution and there is a particular fraction of very low PDR links independent of the channel.

The network shows a higher node degree on channel 13 but this does not lead to a higher meshness, i.e., a well connected and stable network. When links are successively removed from the graph ordered from the lowest to the highest PDR (creating the subgraph $G_{PDR \geq t}$), the graph partitions much earlier. The packet size has also a significant effect on the link quality, quantity, and symmetry which was not observed on the higher frequency band. Nevertheless, link asymmetry and unidirectionality are common and not rare occurrences like it is often assumed. Even on channel 40 and 44, 90% of the links differ by up to 0.2 in the PDR in both directions and around 10% of the links are unidirectional.

Although very simple metrics that are commonly used in publications were applied to document the DES-Testbed's topology, several questions remain. Depending on the applied neighborhood discovery approach respectively a particular protocol, the (average) number of neighbors can be in a large interval. It is up for discussion, if a node is a neighbor when 1 packet is successfully received, when 10% of the packets are received, or do we even require $PDR \geq 0.5$ to consider the node as a neighbor? Further on, the size of the packets that were used to probe the network should be considered. Network protocols that rely on this information to enable, e.g., routing, probabilistic flooding, or reliable broadcast will get an incomplete or even false view of the network as a graph. It makes little sense to discover a route from a source to a destination with small size (broadcast) discovery packets, when the route is eventually not capable to transfer larger unicast data packets[1]. This highlights how important a complete understanding of the network topology actu-

[1] The same problem also arises for multicast over IEEE 802.11.

ally is. We additionally discussed the property of the average shortest path and the average distance of the nodes. Depending on the graph used for the calculations, several different values can be the result.

We learned from the experiment that, as expected, there is no relationship between the link ranges and the PDR: proximity does not ensure a high quality link. Indoor radio propagation is complex and will probably never show such relationship, but our results also show that such an assumption does not even hold for the outdoor links. Free-space communication cannot be assumed and most transmissions will experience reflection, refraction, multi-path propagation and further effects. While we can already state that (simple) simulation models do not accurately represent the DES-Testbed, we will study the relationship of the RSSI, PDR, and distance in the next experiments.

As last, we showed that the ETX metric will over- or underestimate the quality of several links. This is especially true for channel 13 with its more distinct link asymmetry. Whether this fact is significant for routing protocols has yet to be evaluated.

The measured data of this study will be used for graph based simulation starting with focus on flooding, gossip routing, and route discovery issues. This will enable a comparison of experiments that were already run in the testbed. Subsequently, we will try to provide a complete statistical model for our testbed to create random graphs that exhibit the same properties as the DES-Testbed.

APPENDIX A

Additional Figures and Discussion

This section provides the remaining figures and tables depicting the results from channel 44 that were omitted from the previous sections as the results are similar to that of channel 40. In addition, figures are included that show the differences of the ETX and PDR metrics, histograms of the link range distributions, and several figures showing the frequency of asymmetric links in the testbed.

A.1 Additional Figures for Channel 44

A.1.1 Impact of the Packet Size

An increased packet size has the same effect on the PDR on channel 44 as on channel 40 as shown in Figure A.1.1: the larger the packets, the more the links decrease in quality. The decrease ($\mathsf{Abs}(\mathsf{PDR}_{\mathsf{Diff}})$) is noticeable but not as severe as on channel 13. If there is a decrease, it is rarely higher than 0.5.

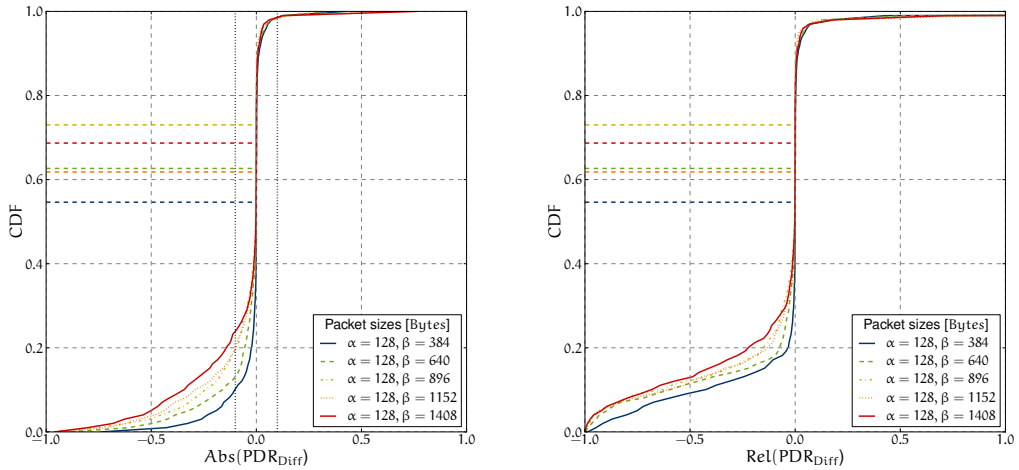

(a) Absolute PDR difference

(b) Relative PDR difference

Figure A.1.1: Absolute and relative differences of the links for different packet sizes on channel 44.

A.1.2 Node Degree

The node degree distribution as shown in Table A.1.1 is very similar to channel 40. The average is slightly lower but this applies also to the standard deviation.

Packet Size [Bytes]	G	Max	Mode	μ	σ	$\tilde{d}_G$	γ
128	$G_{PDR>0}$	24	10	9.70	4.76	10.0	0.37
	$G_{PDR\geq0.10}$	23	5	8.83	4.44	9.0	0.47
384	$G_{PDR>0}$	23	10	9.40	4.59	9.5	0.37
	$G_{PDR\geq0.10}$	23	10	8.50	4.32	8.0	0.54
640	$G_{PDR>0}$	23	10	9.26	4.59	9.0	0.45
	$G_{PDR\geq0.10}$	23	10	8.31	4.27	8.0	0.57
896	$G_{PDR>0}$	23	10	9.16	4.52	9.0	0.47
	$G_{PDR\geq0.10}$	22	8	8.18	4.19	8.0	0.52
1152	$G_{PDR>0}$	23	10	8.95	4.41	9.0	0.54
	$G_{PDR\geq0.10}$	21	8	8.11	4.14	8.0	0.48
1408	$G_{PDR>0}$	23	10	8.93	4.47	9.0	0.54
	$G_{PDR\geq0.10}$	20	10	8.08	4.12	8.0	0.45

Table A.1.1: Moments of the node degree distributions on channel 44

A.1.3 Distance

The lower node degree as shown in the previous section can be explained by the lower link ranges on channel 44. Table A.1.2 shows that while the mode is equal, the average, median, and standard deviation are lower. γ is higher which means that the distribution is more skewed. Section A.3 shows the corresponding density as histograms.

Packet size [Bytes]	Mode [m]	μ [m]	σ [m]	$\tilde{x}$ [m]	γ
128	2.57	20.29	14.59	15.65	1.21
384	2.57	20.09	14.55	15.37	1.23
640	2.57	20.00	14.35	15.22	1.18
896	2.57	20.01	14.43	15.14	1.19
1152	2.57	19.74	14.28	14.97	1.20
1408	2.57	19.76	14.32	14.97	1.20

Table A.1.2: Moments of the link range distributions on channel 44

The link ranges are depicted in Figure A.1.2 for each packet size. As on channel 40, we observe two accumulations in the scatter plots. One is in the top left area that represents high PDR links over short distances while the other is in the lower left region representing very low quality links. Like on the other two channels, we notice no clear relationship between the PDR and distance. The increased packet size affects only some of the links. They move out of the top left cloud towards the bottom in the figures but this effect is less distinct than on channel 13.

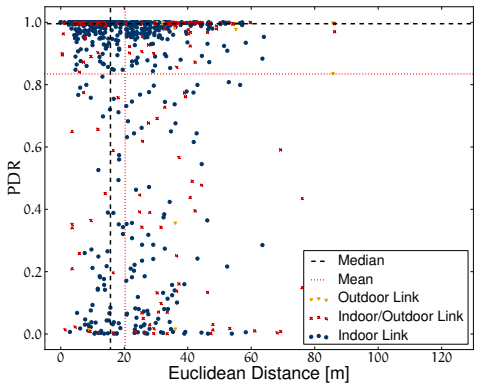

(a) Packet size 128 Bytes

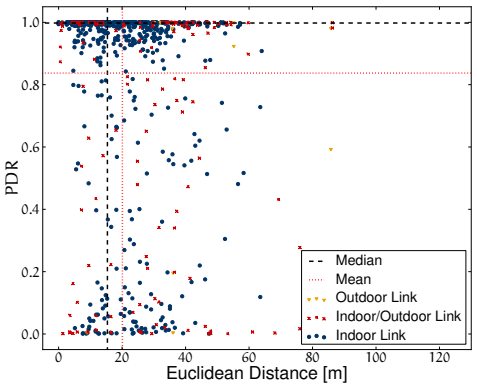

(b) Packet size 384 Bytes

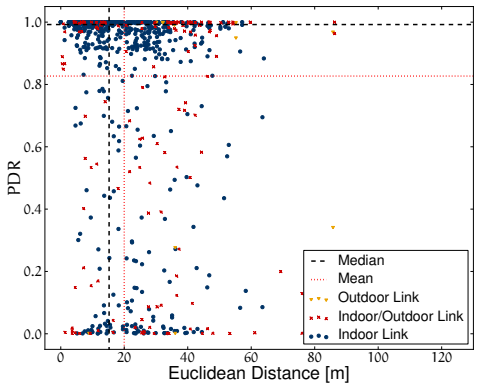

(c) Packet size 640 Bytes

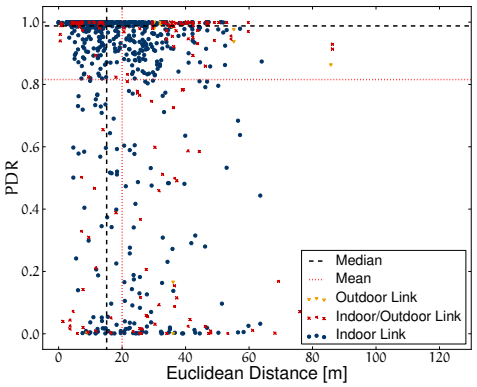

(d) Packet size 896 Bytes

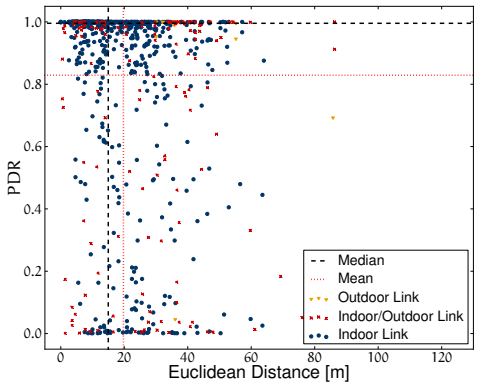

(e) Packet size 1152 Bytes

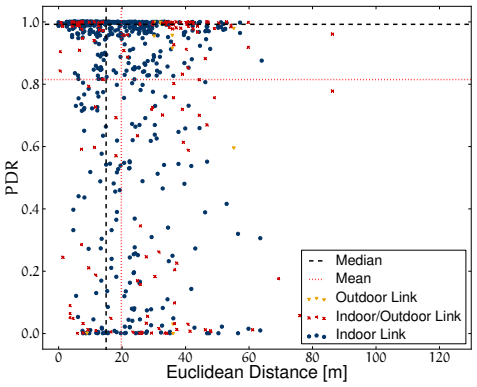

(f) Packet size 1408 Bytes

Figure A.1.2: Scatter-plot of the PDR for each link over the distance of the two corresponding mesh routers

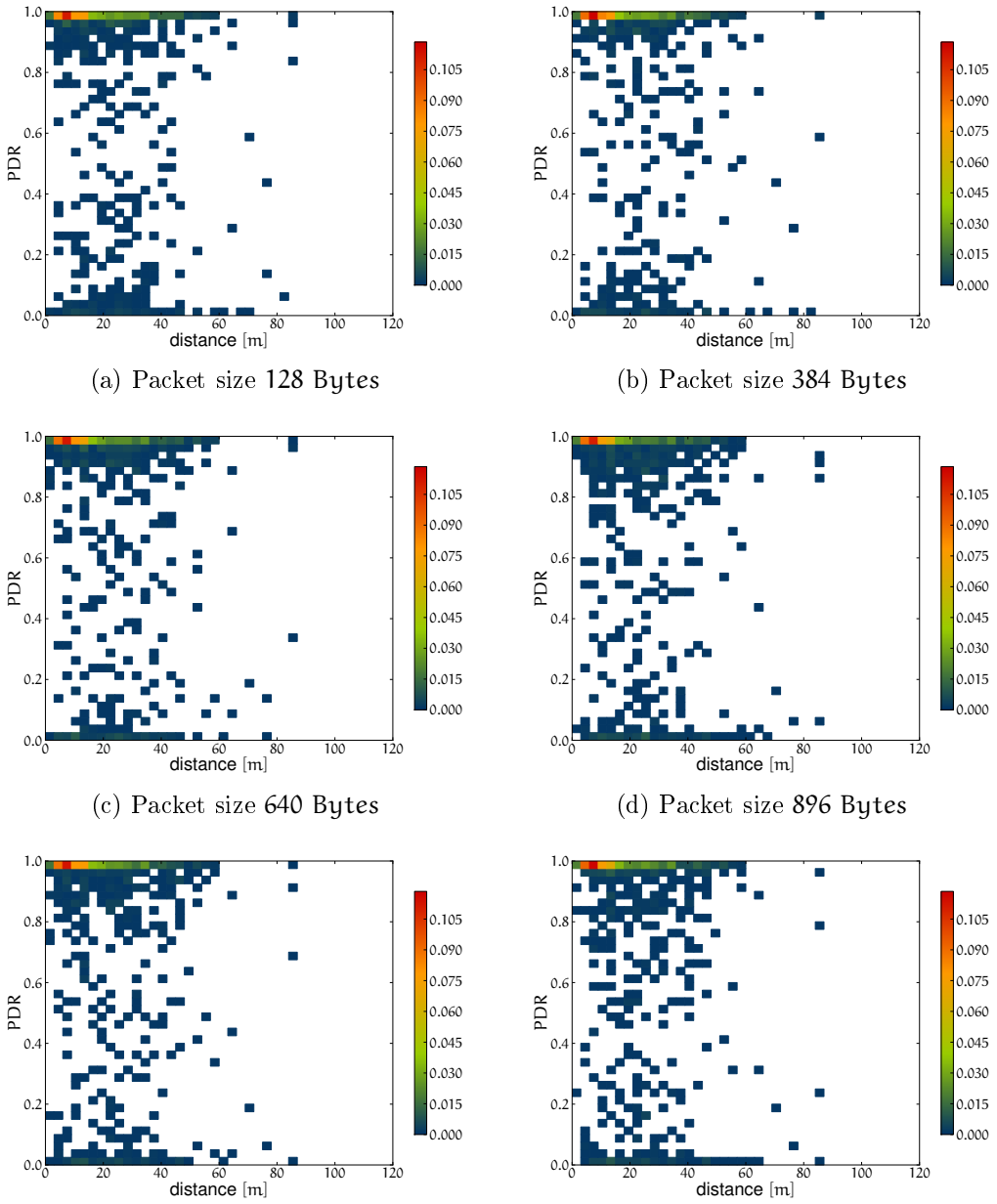

(a) Packet size 128 Bytes

(b) Packet size 384 Bytes

(c) Packet size 640 Bytes

(d) Packet size 896 Bytes

(e) Packet size 1152 Bytes

(f) Packet size 1408 Bytes

Figure A.1.3: Pseudo-color plot of the PDR for each link over the distance of the two corresponding mesh routers on channel 44. The color represents the fraction.

A.1.4 Number of Links

The number of links as shown in Figure A.1.4 is mostly unaffected be the increased packet size but there is a monotone decrease. Compared to the other two channels, channel 44 has the lowest number of links.

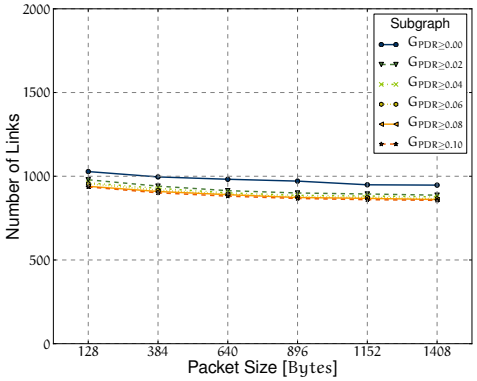

Figure A.1.4: Number of links in the testbed for different packet sizes on channel 44. The number of links is determined in the denoted subgraphs.

A.1.5 Unidirectional Links

A fraction of less than 20% of the links is unidirectional which is higher than on channel 40 but overall lower than on channel 13. The packet size has no clear effect on the fraction.

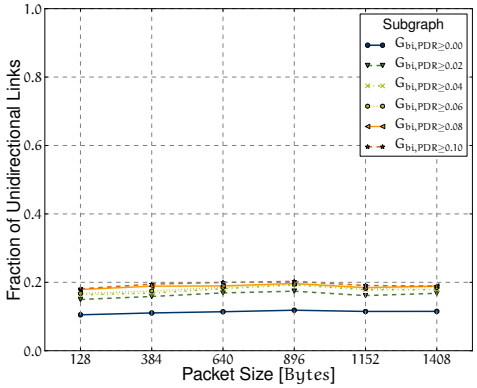

(a) Fraction of unidirectional link including $E_{PDR<t}$

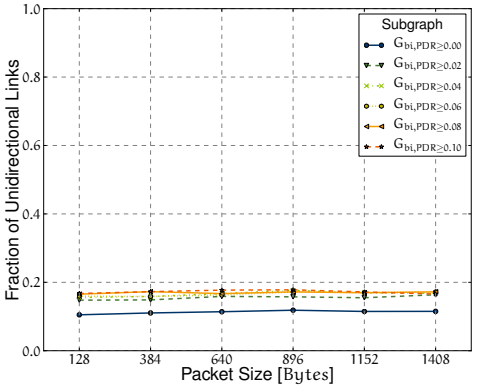

(b) Fraction of unidirectional links excluding $E_{PDR<t}$

Figure A.1.5: Fraction of the unidirectional links in particular subgraphs on channel 44.

A.1.6 Network Fragility

The network shows the same fragility as on channel 40. Only graphs for PDR $\geq$ 0.9 are partitioned, with packet size 1408 Bytes as an exception. When the graph "breaks", only single nodes get isolated before each node is a single strongly connected component.

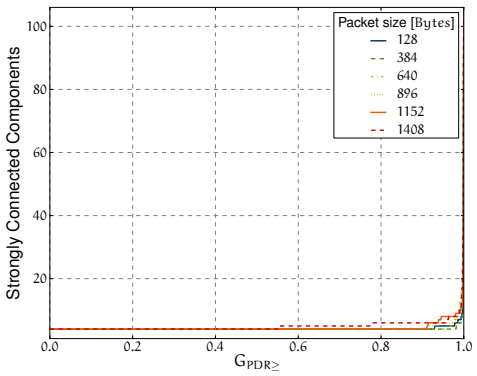

(a) Number of strongly connected components

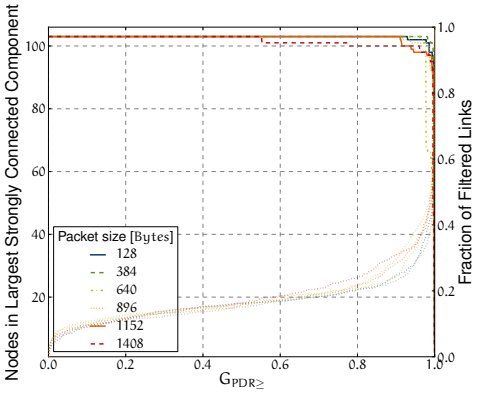

(b) Number of nodes in the largest strongly connected component

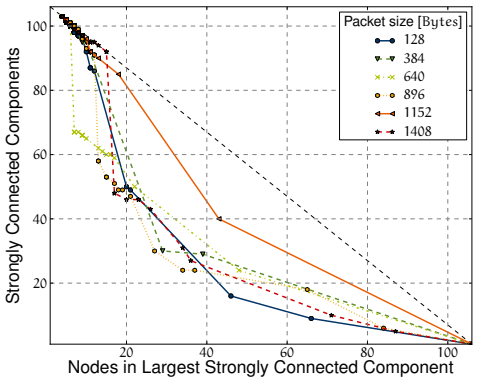

(c) Number of strongly connected components plotted over the number of nodes in the largest strongly connected component

Figure A.1.6: Network Fragility on channel 44

A.2 ETX Metric and PDR Comparison

As discussed in Section 3.1.2, ETX is a symmetric metric that evaluates the so-called forward and backward PDR and assigns each link a value that represents the number of transmissions for a packet that is necessary until it is successfully received and acknowledged. Figure A.2.1 depicts how much the ETX can hide the "true quality" and asymmetry of a link. We observe that an ETX can represent many different links with different qualities. The higher the ETX value, the more the graphs move together. Figure A.2.2 shows the frequency of the ETX-PDR misjudgment as pseudo-color plot (see Section 3.1.2 for the definition). Surprisingly, the misjudgment is only minor for most of the links yet it can be high for some few ones. This effect is much more distinct on channel 13 than on channel 40. In both scenarios, the increasing packet size leads to a higher fraction of misjudged links.

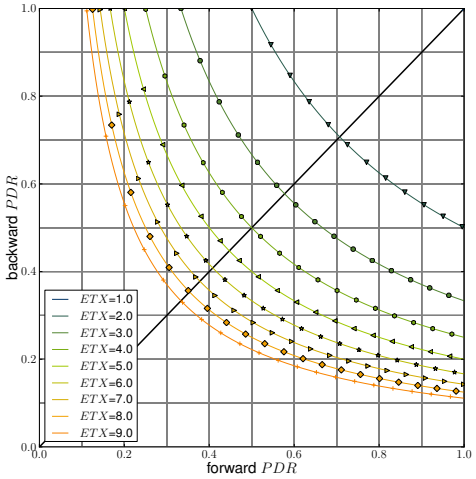

Figure A.2.1: Dependency of ETX on the packet delivery ratios. Each curve represents a particular ETX value of a link. As all points on a curve have the same ETX value, strong asymmetry can remain hidden. The only exception is ETX = 1.0 where the link is perfect in both directions (barely visible in the top right corner).

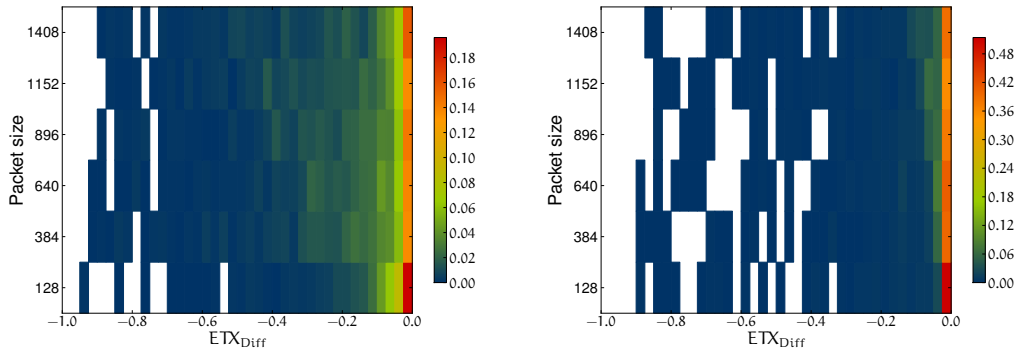

(a) Difference of the ETX value compared to PDR for the links on channel 13

(b) Difference of the ETX value compared to PDR for the links on channel 40

Figure A.2.2: Difference of the ETX value compared to PDR as pseudo-color plot depicting the frequency

A.3 Distribution of the Link Ranges

As shown in Figure A.3.1, the distribution of the link ranges is not Gaussian. The peal of the bell curve is shifted to the left where it is cut off as the distance is always a positive value. Thus there is a short left tail and a long right tail. For channel 13 the distributions seems bimodal as there is a second peak that is partially also in the channel 40 data. Overall, the density of the distribution seem to be χ distributed with $k > 1$ degrees of freedom, but a more detailed statistical analysis is required.

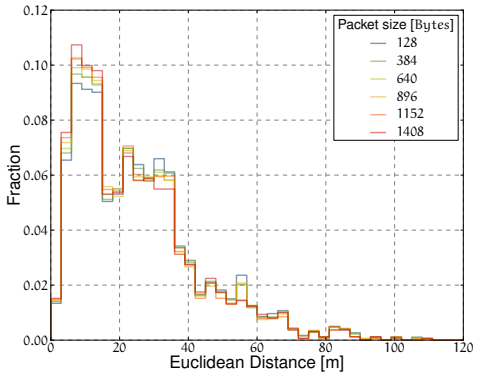

(a) Distribution on channel 13

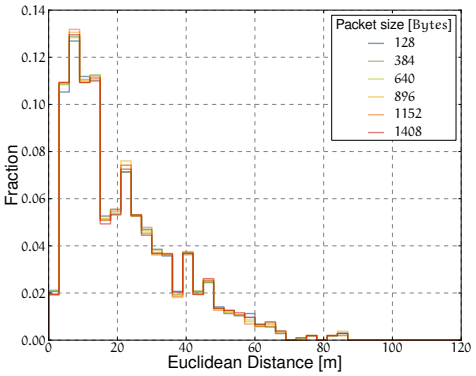

(b) Distribution on channel 40

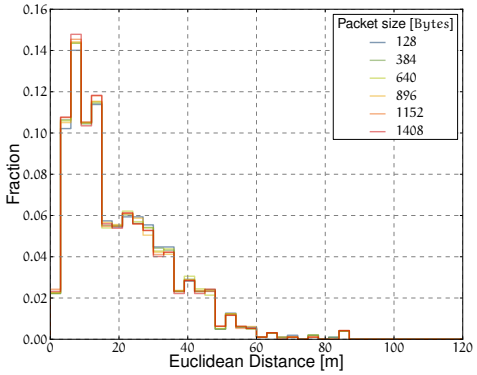

(c) Distribution on channel 44

Figure A.3.1: Distribution of the link ranges represented by histograms with 40 equal-sized bins for the interval $[0, 120]$ m

A.4 Node Degree Distribution

Figure A.4.1 shows the distribution of the node degree for each packet size and the two subgraphs defined in Section 3.1.4 as pseudo-color plot. We observe in Figure A.4.1a that the mode is different for each packet size and shows no clear relationship with the packet size. The mode seems to stabilize in the subgraph $G_{PDR \geq 0.10}$ shown in Figure A.4.1b. The distribution on channel 40 (Figure A.4.1c and Figure A.4.1d) has a more distinct peak. In all cases, the distribution of the node degree is not normal but has a significant skew that results in a longer (and lower) right tail.

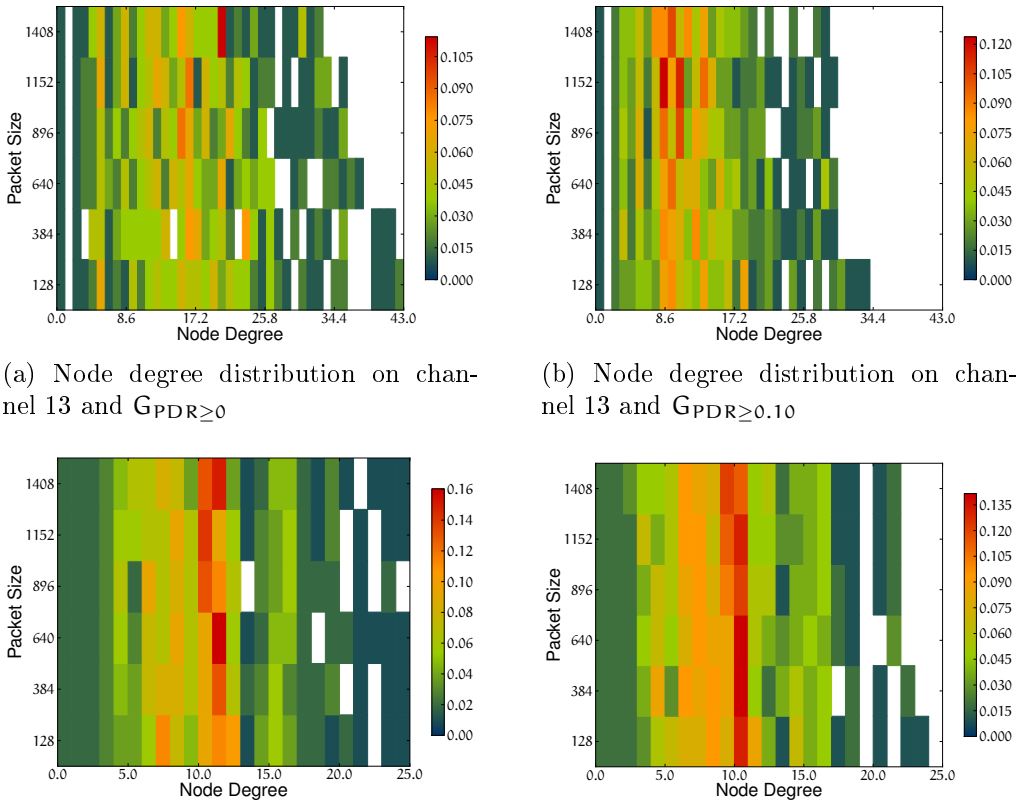

(a) Node degree distribution on channel 13 and $G_{PDR \geq 0}$

(b) Node degree distribution on channel 13 and $G_{PDR \geq 0.10}$

(c) Node degree distribution on channel 40 and $G_{PDR \geq 0}$

(d) Node degree distribution on channel 40 and $G_{PDR \geq 0.10}$

Figure A.4.1: Node degree distribution as pseudo-color plots. Each plot represent a histogram showing the relative frequency of the degrees in the interval $[0, \max(d_G)]$.

A.5 Asymmetry

The following figures depict the frequency of the asymmetric and symmetric links. In all figures the $\mathsf{PDR}(e_{a,b})$ is plotted over $\mathsf{PDR}(e_{b,a})$. As all links are evaluated as two data points, the figures are symmetric. Symmetric links are on a diagonal from $(0,0)$ to $(1,1)$ whereas strong asymmetric links are found near the corners at $(0,1)$ and $(1,0)$. Unidirectional links are not included in the data sets. The total number of links for each packet size is different (Section 3.1.6 and Section 3.2.6).

The data is shown as scatter plots, pseudo-color plots, and surface plots. Each type has particular advantages. Where the scatter plots immediately makes structures/accumulations visible, the others give a better view of the distribution.

As the figures show, there is a significant difference between channel 13 and channel 40[1]. There are many asymmetric links on 2.4 GHz and the frequency of symmetric, high PDR links decreases when the packet size increases. We observe that the affected links do not decrease in PDR equally in both directions as starting with packet size 896 Bytes there are less and less peaks in the center area and a general shift towards the corners. The links on 5 GHz show little influence from the increasing packet size. The asymmetry does not significantly increase.

[1]Figures for channel 44 are not included here but the data is similar to channel 40.

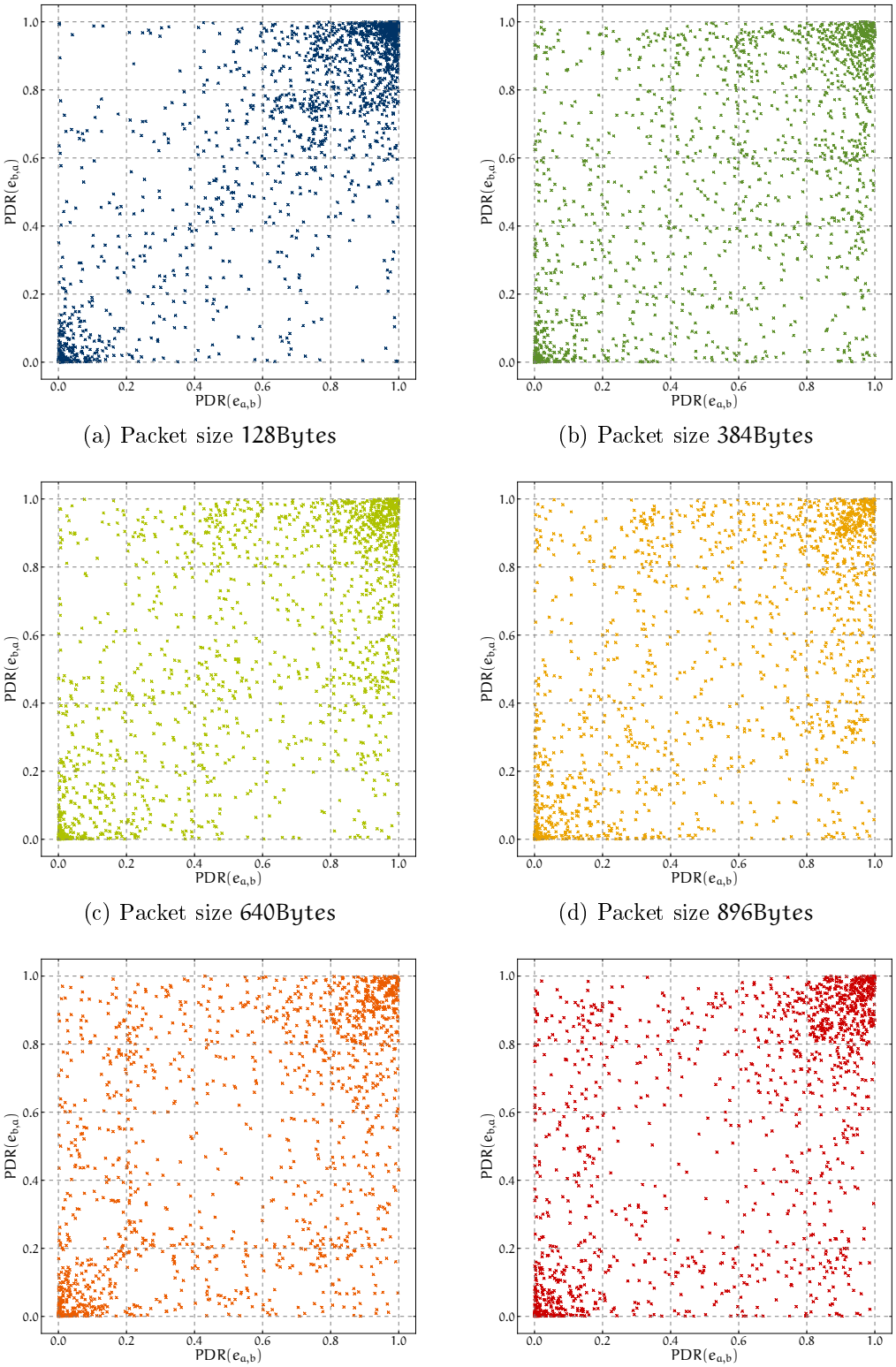

(a) Packet size 128Bytes

(b) Packet size 384Bytes

(c) Packet size 640Bytes

(d) Packet size 896Bytes

(e) Packet size 1152Bytes

(f) Packet size 1408Bytes

Figure A.5.1: Scatter-plot of the PDR for each bidirectional link on channel 13. Each link is plotted twice and thus the figures are symmetric.

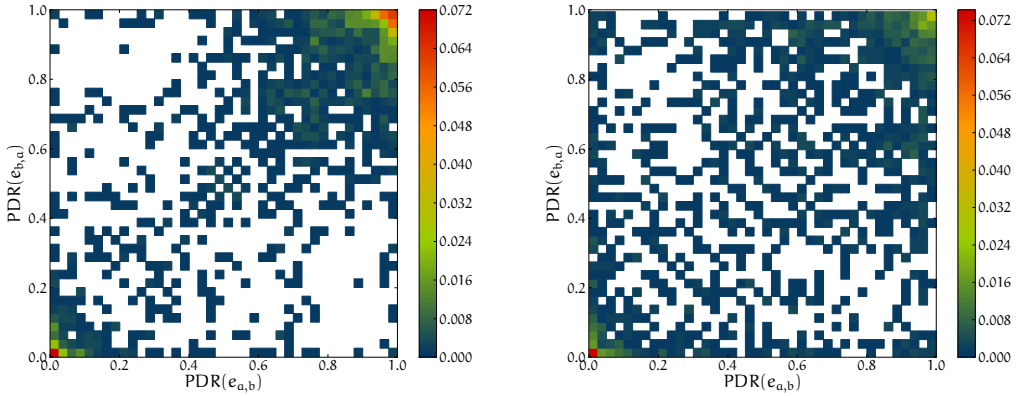

(a) Packet size 128Bytes

(b) Packet size 384Bytes

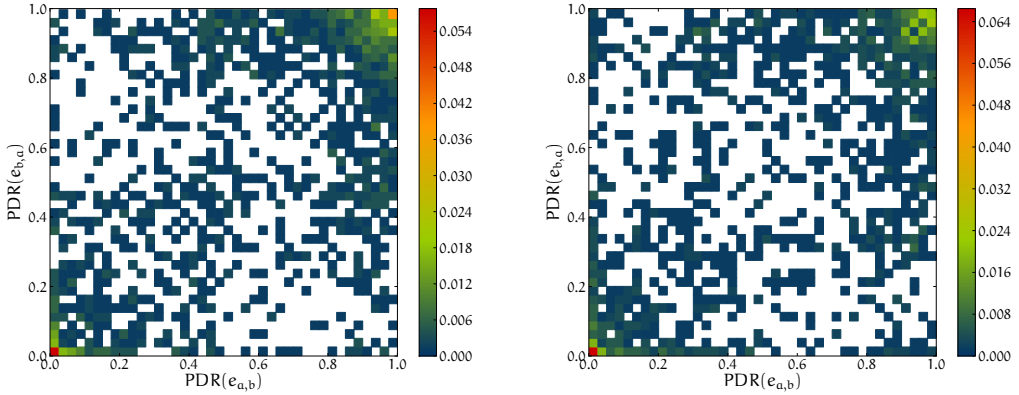

(c) Packet size 640Bytes

(d) Packet size 896Bytes

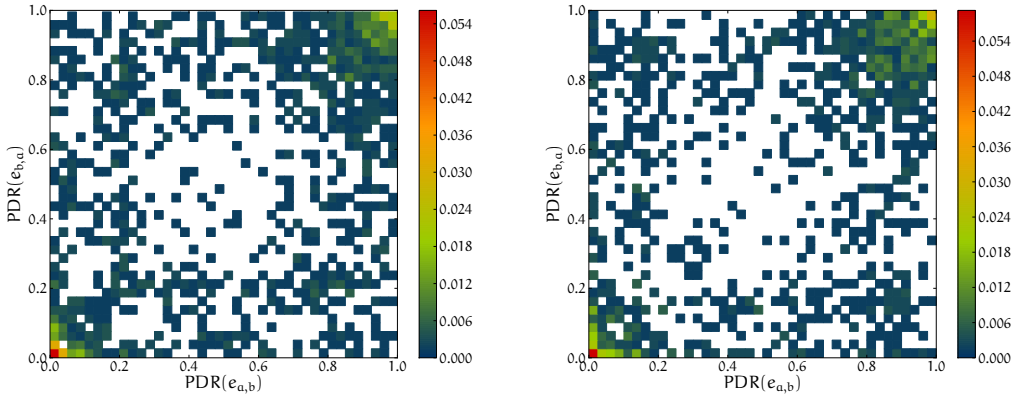

(e) Packet size 1152Bytes

(f) Packet size 1408Bytes

Figure A.5.2: Pseudo-color plot of the PDR for each bidirectional link on channel 13. The frequency is depicted.

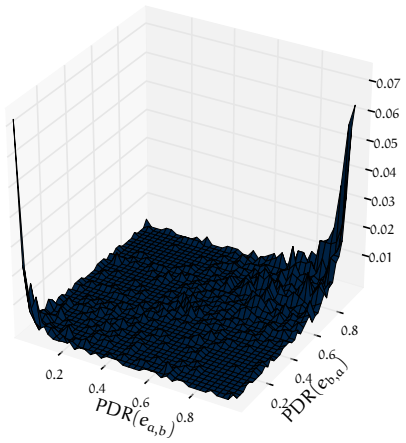

(a) Packet size 128Bytes

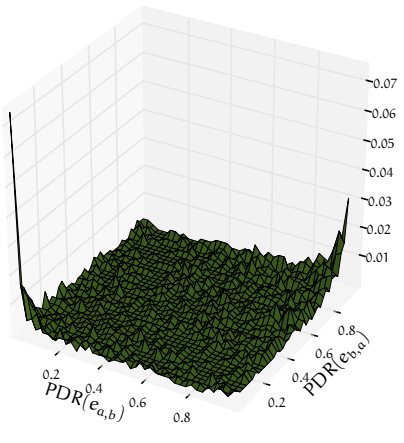

(b) Packet size 384Bytes

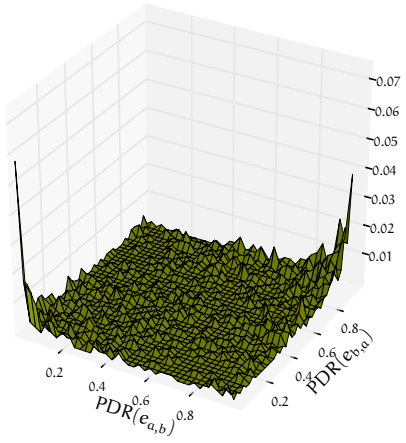

(c) Packet size 640Bytes

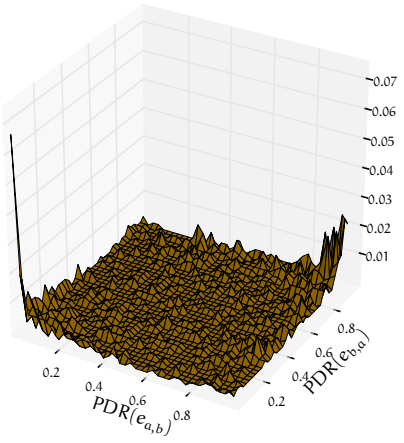

(d) Packet size 896Bytes

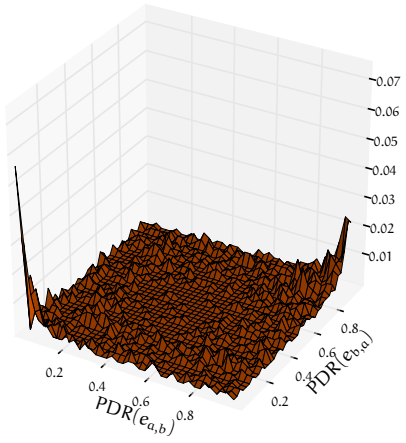

(e) Packet size 1152Bytes

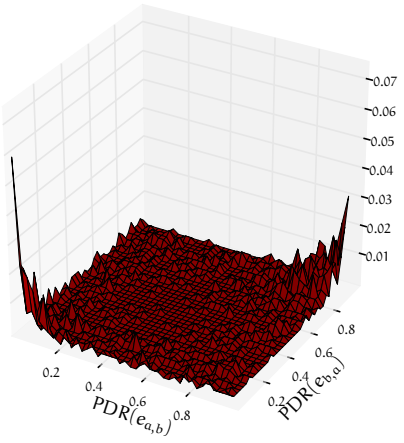

(f) Packet size 1408Bytes

Figure A.5.3: Surface-plot of the PDR for each bidirectional link on channel 13. The frequency is depicted on the vertical axis.

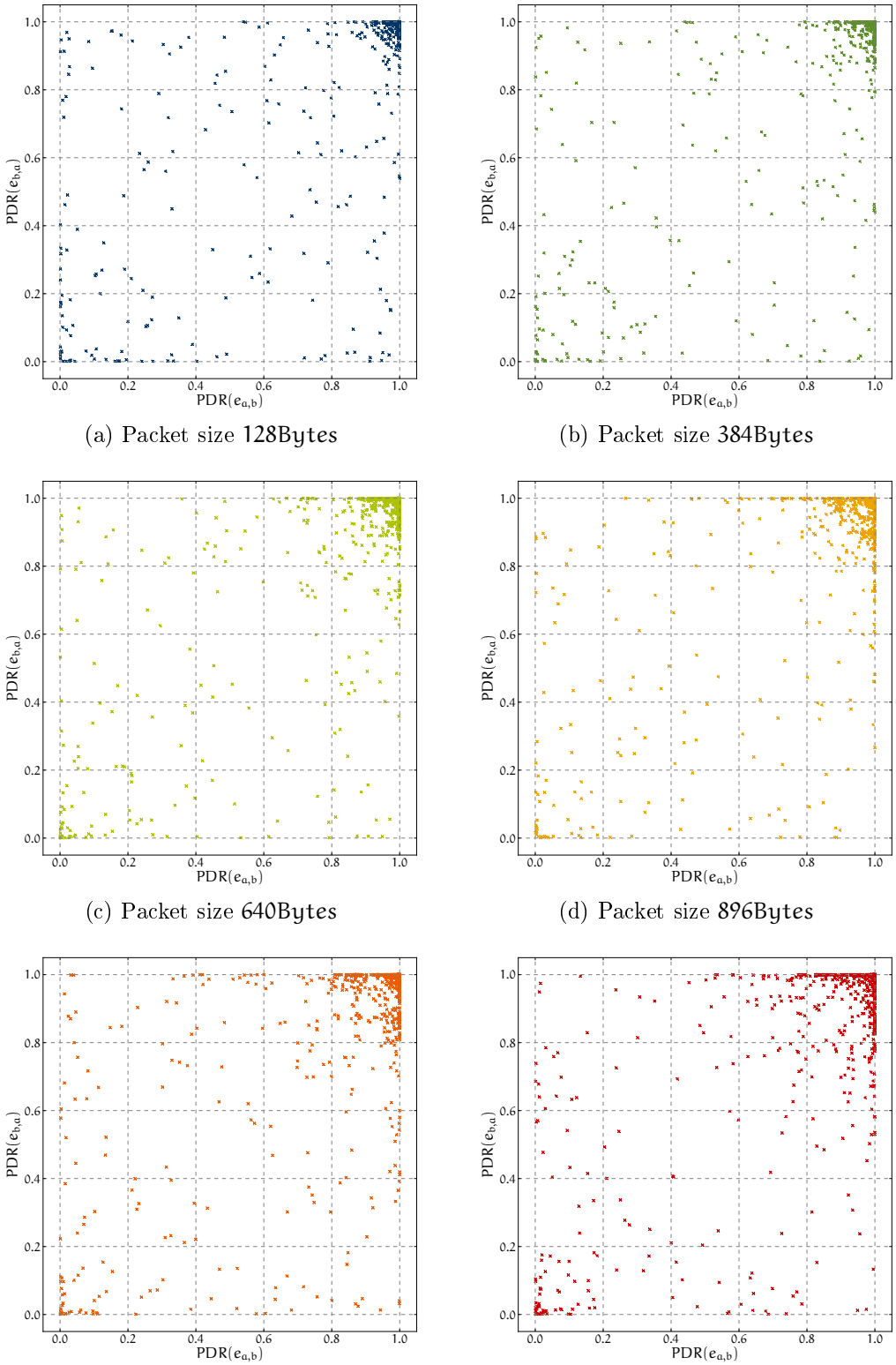

(a) Packet size 128Bytes

(b) Packet size 384Bytes

(c) Packet size 640Bytes

(d) Packet size 896Bytes

(e) Packet size 1152Bytes

(f) Packet size 1408Bytes

Figure A.5.4: Scatter-plot of the PDR for each bidirectional link on channel 40. Each link is plotted twice and thus the figures are symmetric.

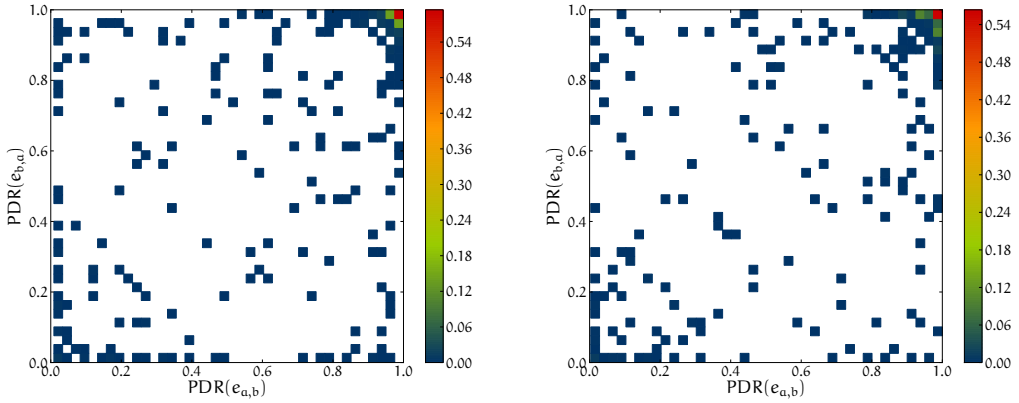

(a) Packet size 128Bytes

(b) Packet size 384Bytes

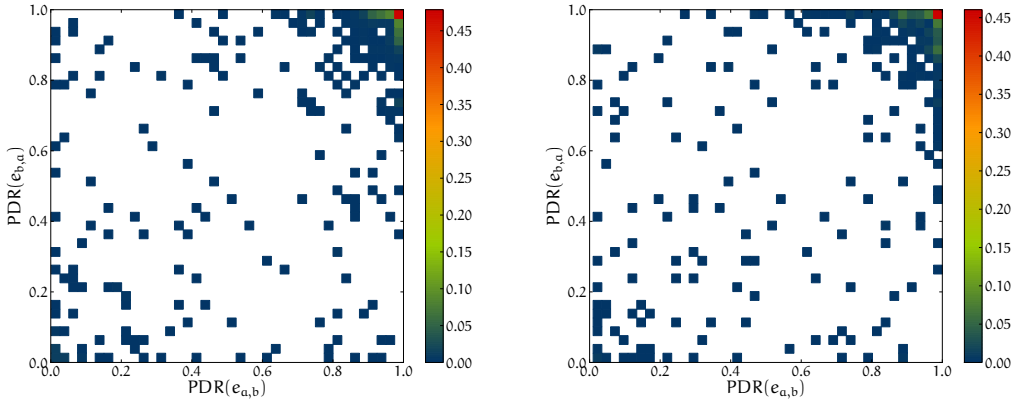

(c) Packet size 640Bytes

(d) Packet size 896Bytes

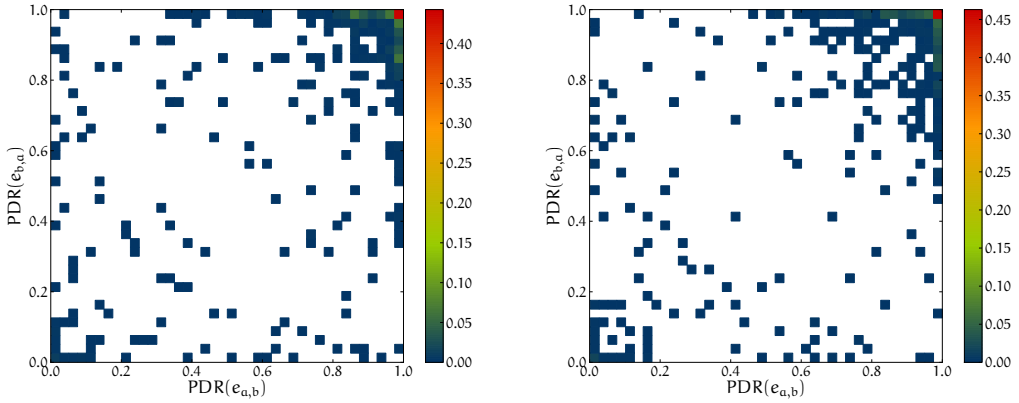

(e) Packet size 1152Bytes

(f) Packet size 1408Bytes

Figure A.5.5: Pseudo-color plot of the PDR for each bidirectional link on channel 13. The frequency is depicted.

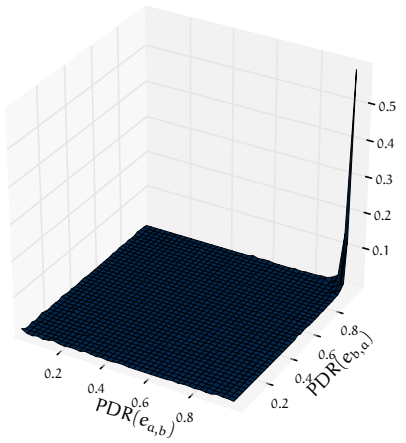

(a) Packet size 128Bytes

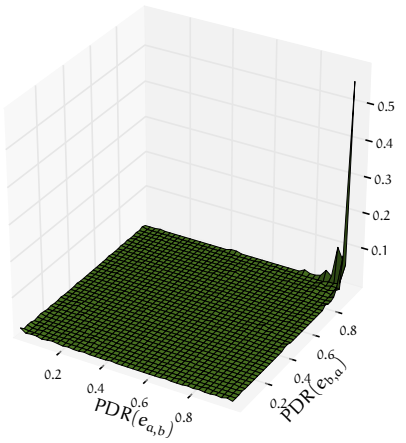

(b) Packet size 384Bytes

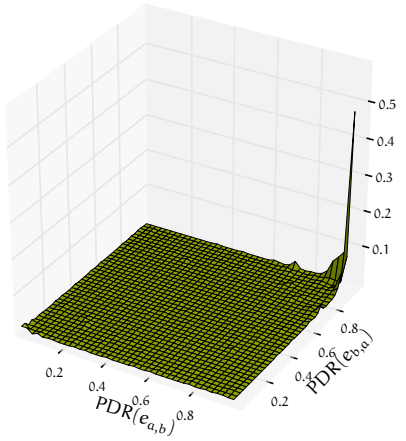

(c) Packet size 640Bytes

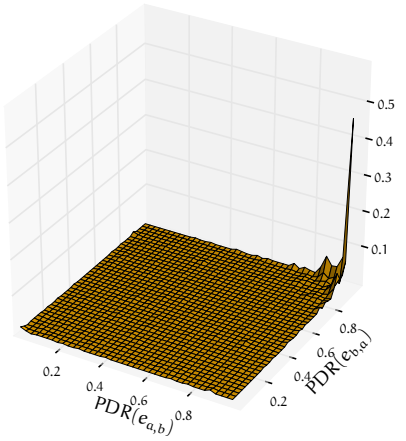

(d) Packet size 896Bytes

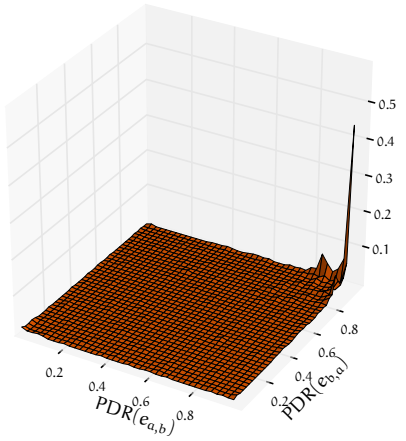

(e) Packet size 1152Bytes

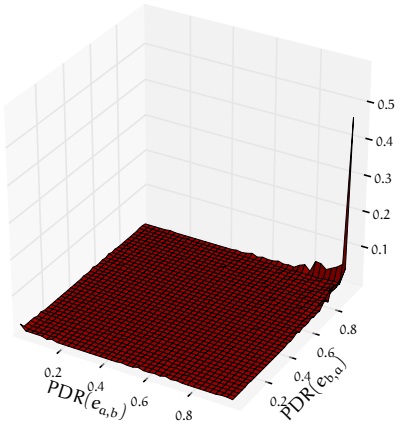

(f) Packet size 1408Bytes

Figure A.5.6: Surface-plot of the PDR for each bidirectional link on channel 13. The frequency is depicted on the vertical axis.

APPENDIX B

Additional Results from the 2.4 GHz Band

The following figures have been added to the 2nd version of this technical report. We run the same experiment again on two additional channels in the 2.4 GHz band: channel 1 and channel 7.

B.1 Channel 1

Channel 1 is used by the campus wireless network and thus there is significantly more interference from the access points. 2.412 GHz is the lowest frequency for IEEE 802.11 devices and thus we should expect the highest number of links as the attenuation by obstacles like walls or floors is lower. The main focus of this section is on a comparison of the data from channel 1 with the data from channel 13 as they are at the opposite ends of the 2.4 GHz band.

B.1.1 Packet Delivery Ratio

The packet delivery ratio on channel 1, as depicted in Figure B.1.1, shows a high number of low quality links. The bimodal distribution like on channel 13 (compare Figure 3.1.1) is less exposed as the right mode is much lower and the distribution's kurtosis is lower. Like for all other channels, we observe that a particular fraction of the links decreases in PDR when the packet size is increased. This can be seen as diagonal pattern in Figure B.1.1c.

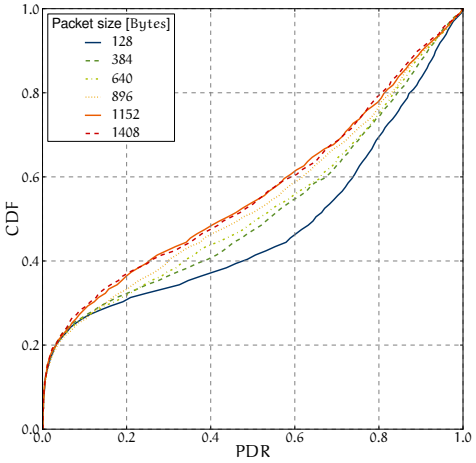

(a) Cumulative distribution function

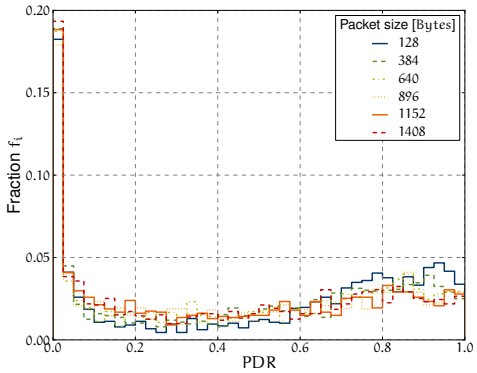

(b) Histogram with 40 bins of equal size

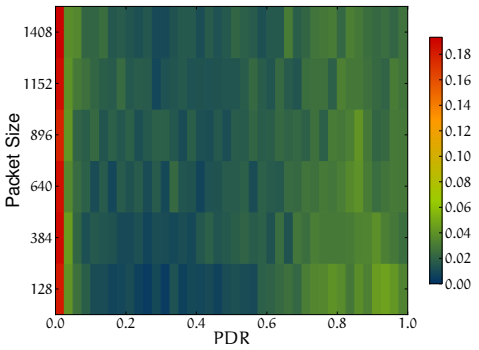

(c) Pseudo-color plot with 40 bins of equal size. The color represents the fraction of links in the bin with a particular PDR.

Figure B.1.1: Distribution of the packet delivery ratio on channel 1

B.1.2 Link Asymmetry

The links show a similar asymmetry distribution as on channel 13 (compare Figure B.1.2 and Figure 3.1.2). In contrast, the increase of the packet size from 128 Bytes to 384 Bytes has a less drastic effect. A high fraction of the links on channel 13 increased their asymmetry which is absent here.

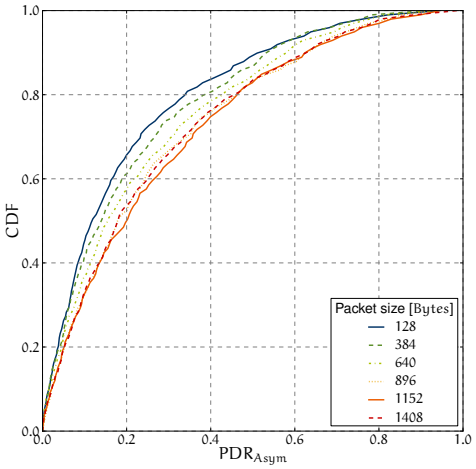

(a) Cumulative distribution

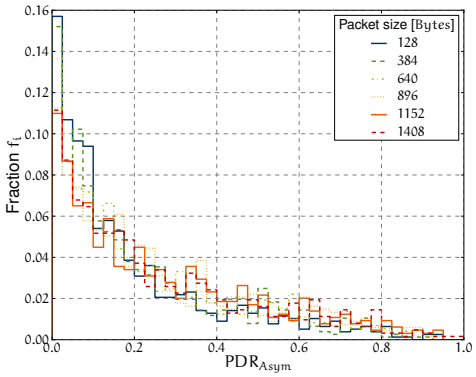

(b) Histogram with 40 bins

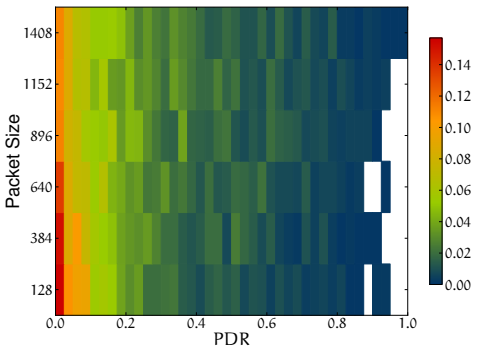

(c) Pseudo-color plot with 40 bins

Figure B.1.2: Link asymmetry on channel 1. The PDR difference of each bidirectional link (PDR_{Asym}) is depicted as measure of the link asymmetry.

B.1.3 Node Degree

The node degree is also very similar to channel 13 and the average is only about one degree lower for all packet sizes (compare Figure B.1.3 and Figure 3.1.4). In contrast, the highest node degree that was measured in the network is lower: about five neighbors less.

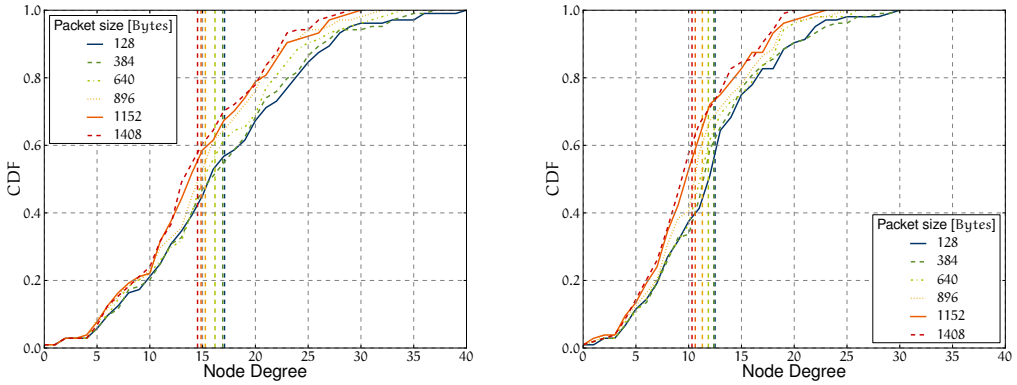

(a) Graph $G_{PDR>0.0}$ (b) Subgraph $G_{PDR\geq 0.10}$

Figure B.1.3: Distribution of the node degree measured on channel 1

B.1.4 Distance

The median and mean distances match the data from channel 13 (compare Figure B.1.4 and Figure 3.1.5). This is no surprise as the nodes are stationary and as soon as a single packet arrives this event adds a data point to the distance sample. If there is a difference in the number of links, it does not show up here. Figure B.1.5 shows the distribution as pseudo-color plots. In contrast to what is seen in Figure 3.1.6, a lower fraction of high quality links over $20 - 60$ m remains when the packet size increases.

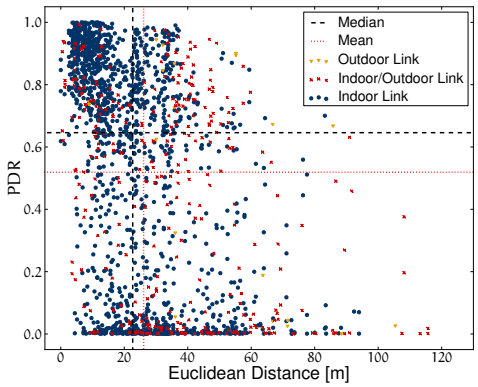

(a) Packet size 128 Bytes

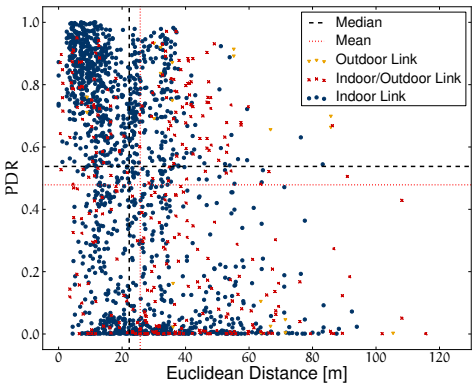

(b) Packet size 384 Bytes

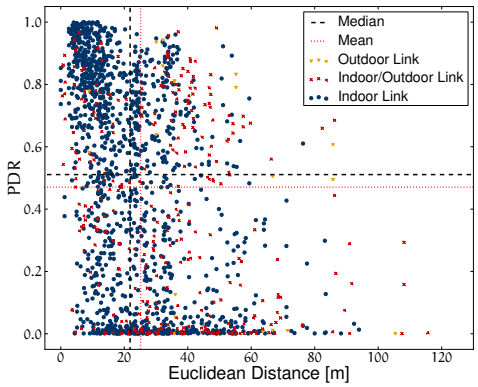

(c) Packet size 640 Bytes

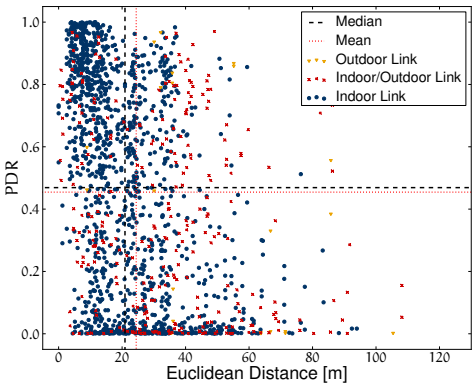

(d) Packet size 896 Bytes

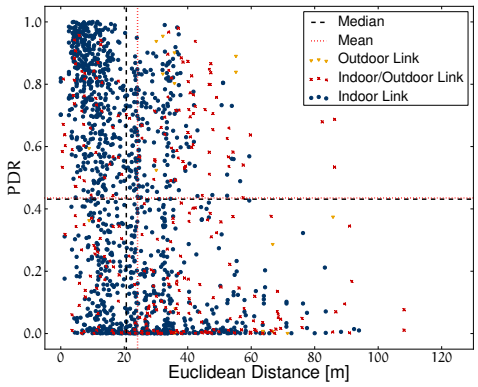

(e) Packet size 1152 Bytes

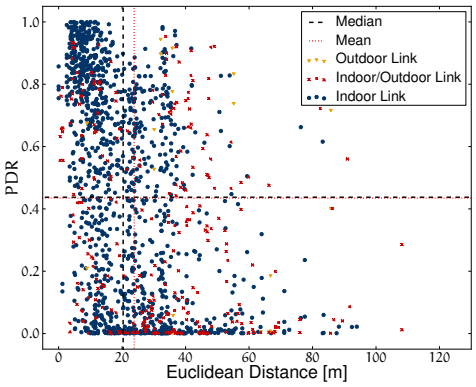

(f) Packet size 1408 Bytes

Figure B.1.4: Scatter plot of the PDR for each link over the distance of the two corresponding mesh routers on channel 1

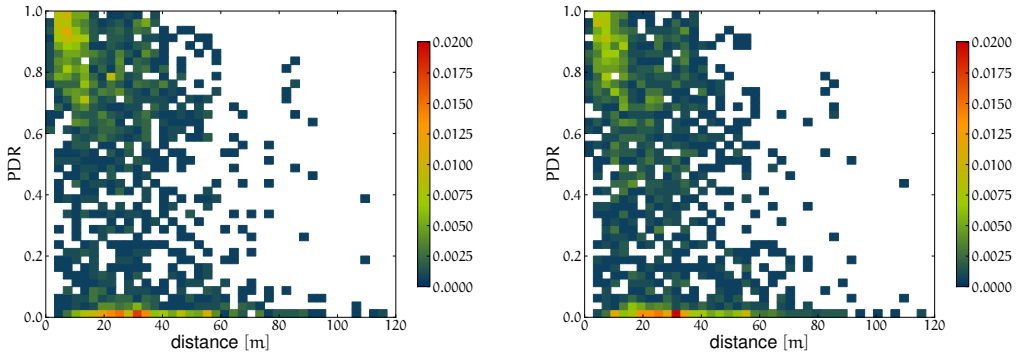

(a) Packet size 128 Bytes

(b) Packet size 384 Bytes

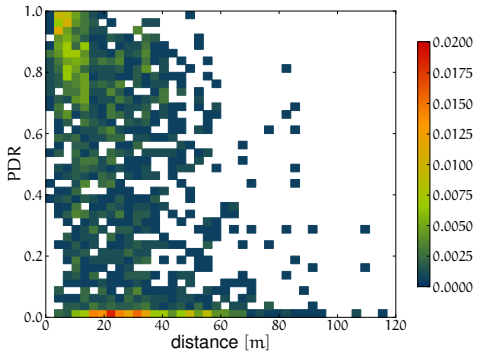

(c) Packet size 640 Bytes

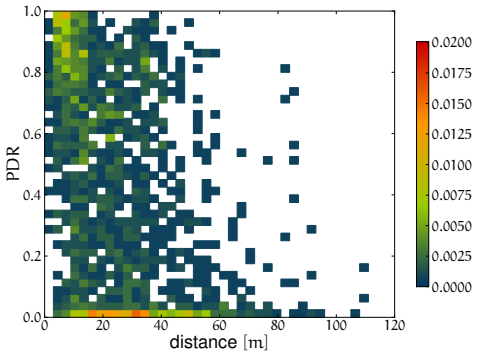

(d) Packet size 896 Bytes

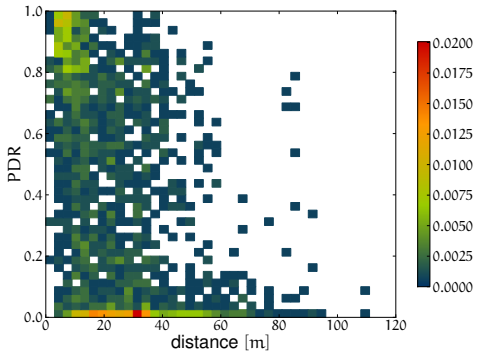

(e) Packet size 1152 Bytes

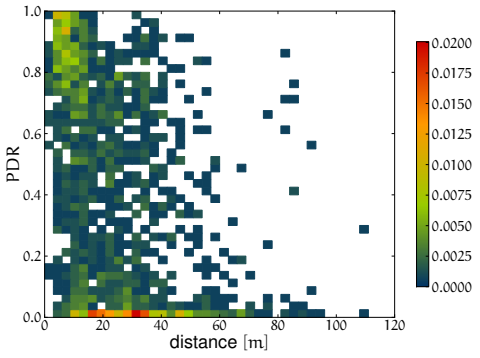

(f) Packet size 1408 Bytes

Figure B.1.5: Pseudo-color plot of the PDR for each link over the distance of the two corresponding mesh routers on channel 1. The color represents the fraction.

B.1.5 Number of Links

The network shows less links on channel 1 than on channel 13 (compare Figure B.1.6 and Figure 3.1.7. This holds for any measured packet packet size and we thus have to assume that the lower number results from the increased interference.

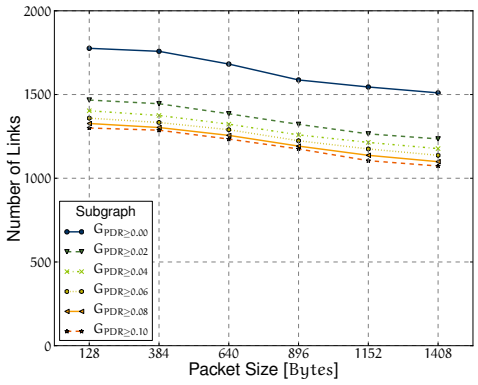

Figure B.1.6: Number of links in the network for different packet sizes on channel 1. The number of links is determined for the denoted subgraphs.

B.1.6 Unidirectional Links

The fraction of unidirectional links is significantly higher than on channel 13 (compare Figure B.1.7 and Figure 3.1.9). For some packet sizes the difference can be about 10%. Interestingly, for packet size 640 Bytes there is no decrease in the fraction of unidirectional links like on channel 13 but the graphs show a reduced increase.

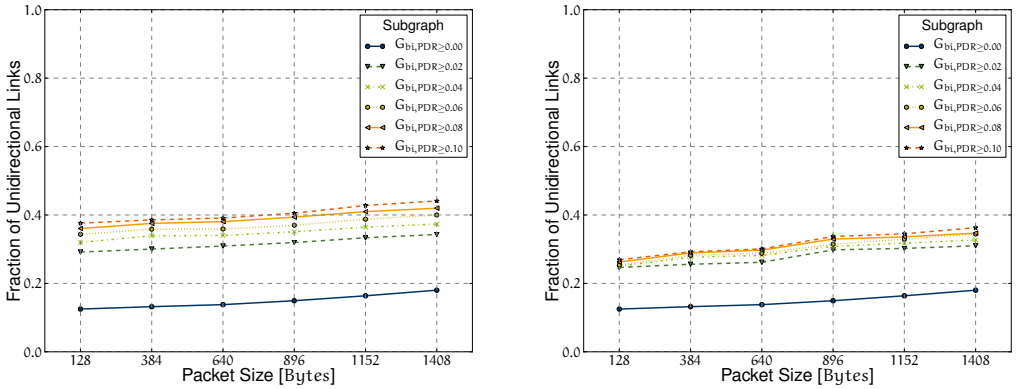

(a) Fraction of unidirectional links including $E_{PDR<t}$

(b) Fraction of unidirectional links excluding $E_{PDR<t}$

Figure B.1.7: Fraction of the unidirectional links in particular subgraphs on channel 1.

B.1.7 Network Fragility

The network is more fragile on channel 1 than on channel 13 (compare Figure B.1.8 and Figure 3.1.10). When all links with PDR < 0.7 are removed, less than 70 of the routers are strongly connected. The same happens on channel 13 but only when all links with PDR < 0.8 to PDR < 0.9 are removed, depending on the packet size.

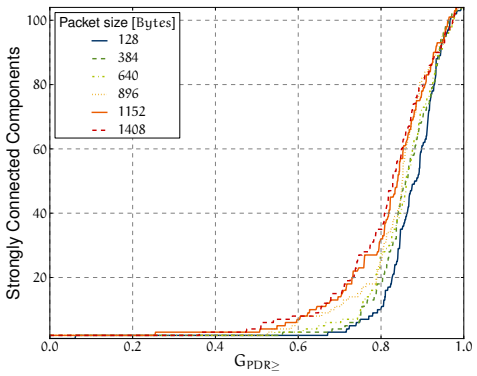

(a) Number of strongly connected components

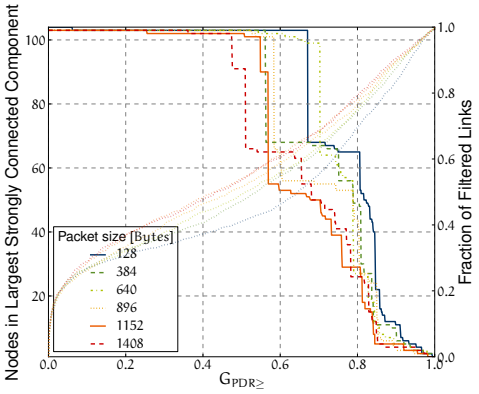

(b) Number of nodes in the largest strongly connected component

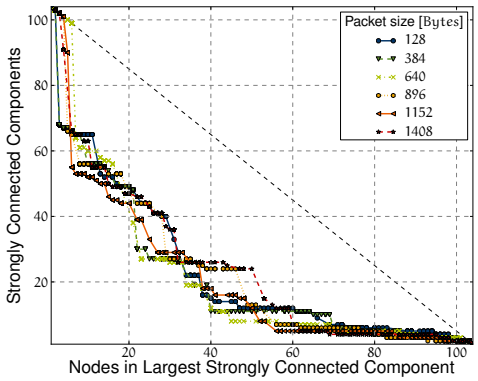

(c) Number of strongly connected components plotted over the number of nodes in the largest strongly connected component

Figure B.1.8: Network fragility on channel 1

B.2 Channel 7

Channel 7 lies in the middle of the 2.4 GHz band and is also exposed to interference of the campus WLAN. We will only briefly comment on the results and the reader should compare the figures for all three channels in the 2.4 GHz band for more details.

B.2.1 Packet Delivery Ratio

The distribution of the packet delivery ratio shows a higher link quality on channel 7 compared with channel 1 (compare Figure B.2.1 and Figure B.1.1). The gradual decrease in quality of a particular subset of links is also observable here, when the packet size increases.

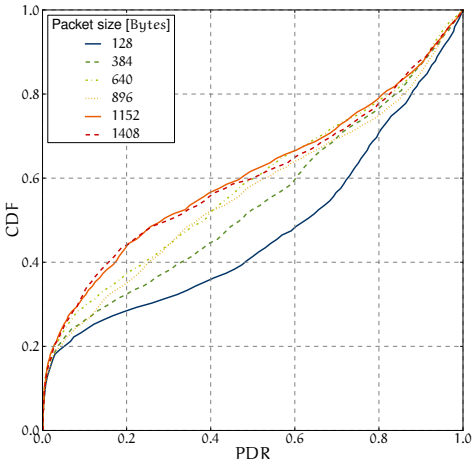

(a) Cumulative distribution function

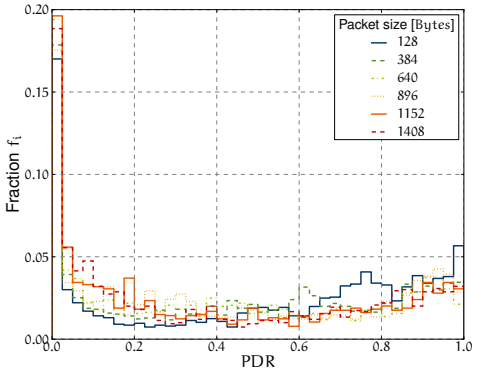

(b) Histogram with 40 bins of equal size

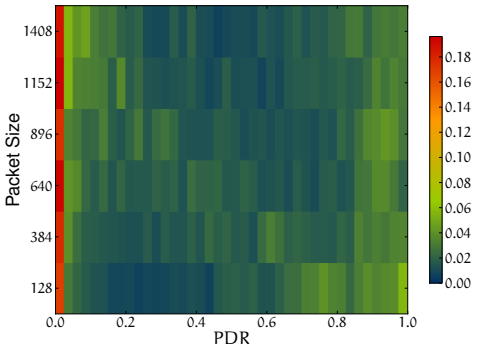

(c) Pseudo-color plot with 40 bins of equal size. The color represents the fraction of links in the bin with a particular PDR.

Figure B.2.1: Distribution of the packet delivery ratio on channel 7

B.2.2 Link Asymmetry

The link asymmetry distribution shows no surprises (compare Figure B.2.1 and Figure B.1.1). The only notable difference is the higher mode and higher kurtosis on channel 7.

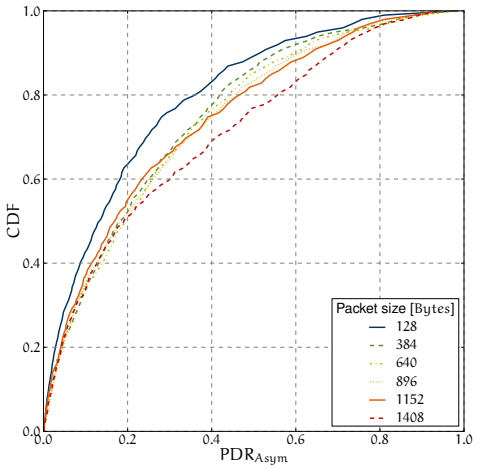

(a) Cumulative distribution

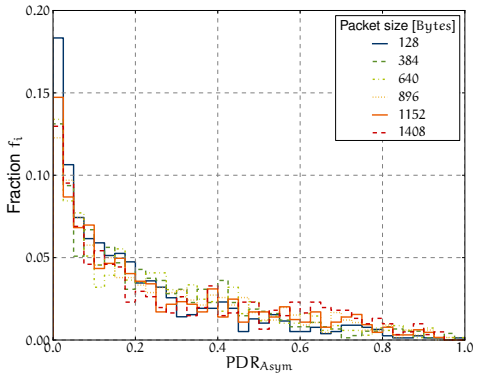

(b) Histogram with 40 bins

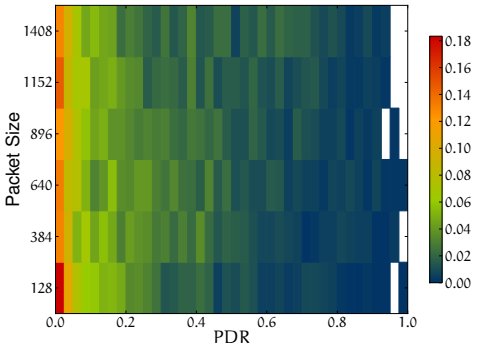

(c) Pseudo-color plot with 40 bins

Figure B.2.2: Link asymmetry on channel 7. The PDR difference of each bidirectional link (PDR_{Asym}) is depicted as measure of the link asymmetry.

B.2.3 Node Degree

The average node degree is on par with channel 7 (compare Figure B.2.3 and Figure B.1.3).

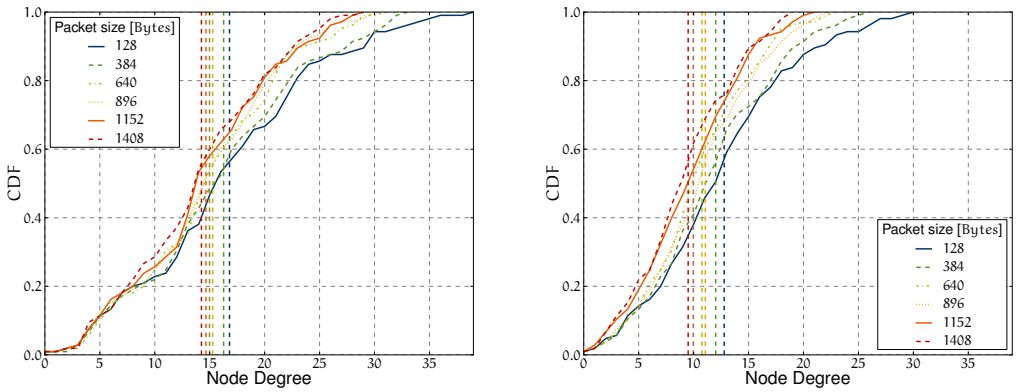

(a) Graph $G_{PDR>0.0}$ (b) Subgraph $G_{PDR\geq 0.10}$

Figure B.2.3: Distribution of the node degree measured on channel 7

B.2.4 Distance

For all considered channels in the 2.4 GHz band, the median and mean ranges of the links are quasi the same. The differences in the median and mean PDR may be caused by the different number of links.

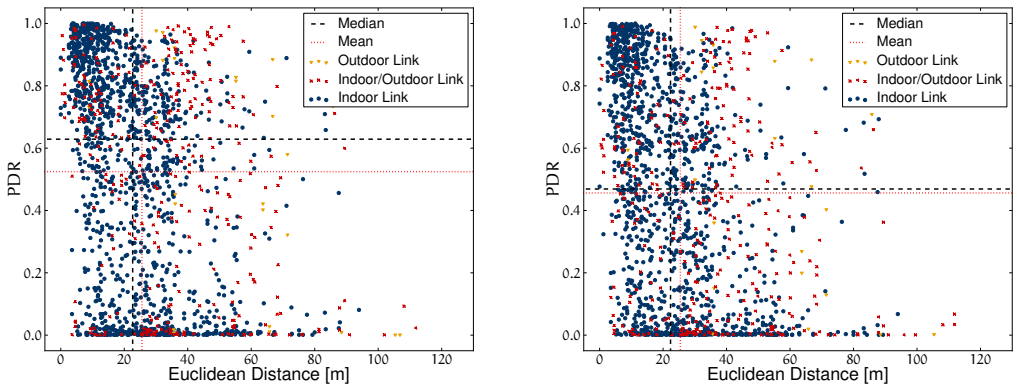

(a) Packet size 128 Bytes

(b) Packet size 384 Bytes

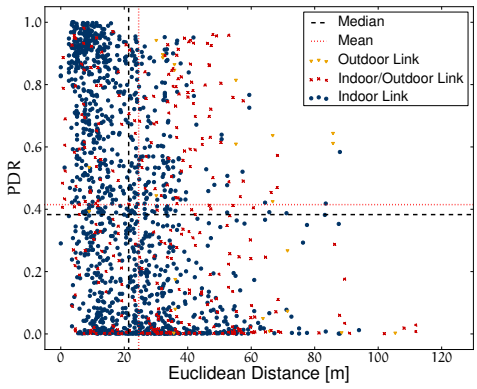

(c) Packet size 640 Bytes

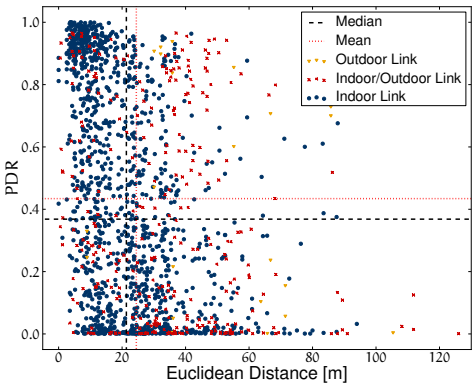

(d) Packet size 896 Bytes

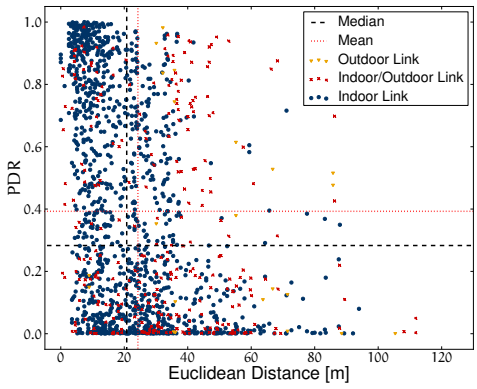

(e) Packet size 1152 Bytes

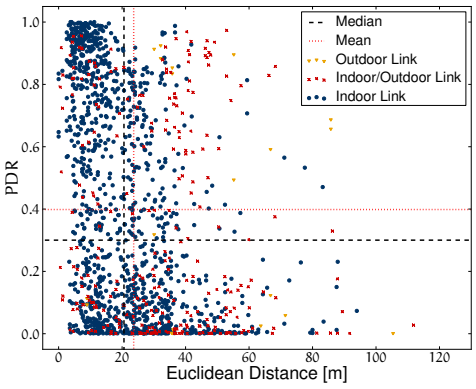

(f) Packet size 1408 Bytes

Figure B.2.4: Scatter plot of the PDR for each link over the distance of the two corresponding mesh routers on channel 7

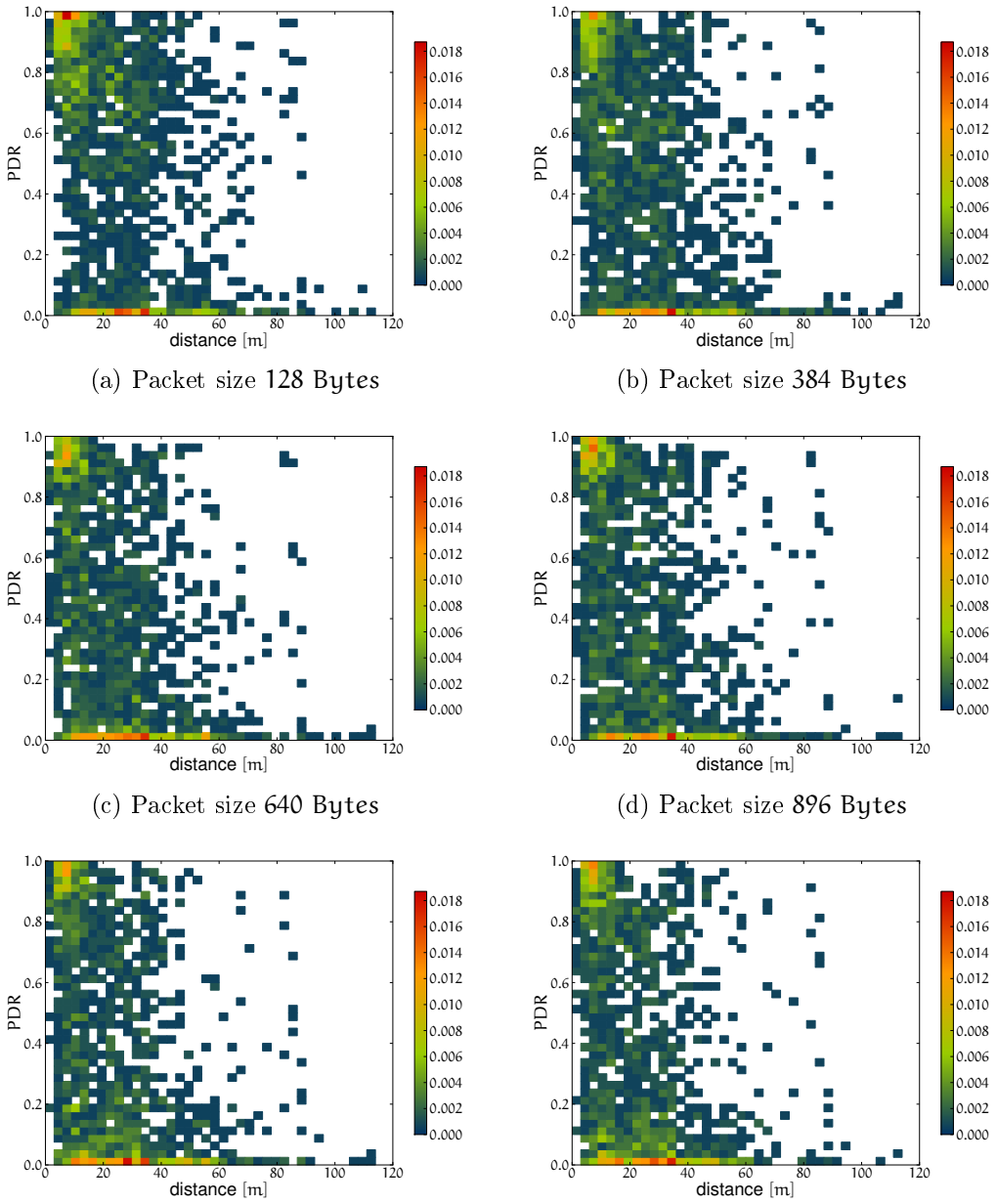

(a) Packet size 128 Bytes

(b) Packet size 384 Bytes

(c) Packet size 640 Bytes

(d) Packet size 896 Bytes

(e) Packet size 1152 Bytes

(f) Packet size 1408 Bytes

Figure B.2.5: Pseudo-color plot of the PDR for each link over the distance of the two corresponding mesh routers on channel 7. The color represents the fraction.

B.2.5 Number of Links

Channel 7 shows the same effect as the other channels: when the packet size is increased some links are not available anymore. Surprisingly, the graphs in Figure B.2.6 are not monotone as for packet size **896 Bytes** there is an increase of the number of links in some of the subgraphs $G_{PDR \geq t}$. This phenomenon is also visible for the fraction of unidirectional links.

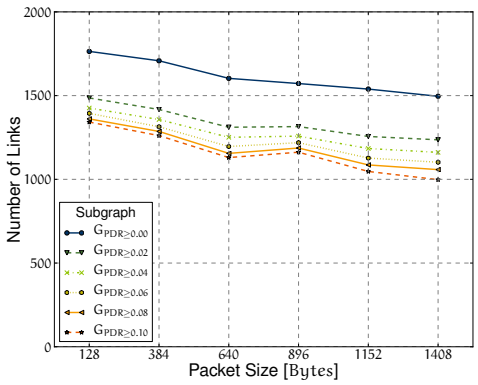

Figure B.2.6: Number of links in the network for different packet sizes on channel 7. The number of links is determined for the denoted subgraphs.

B.2.6 Unidirectional Links

The higher number of links for the packet size **896 Bytes** is caused by an increased fraction of unidirectional links that appeared in the experiment. We suspect that due to changes in the environment, some pairs of nodes where able to communicate (in one direction) over very low quality links at this time.

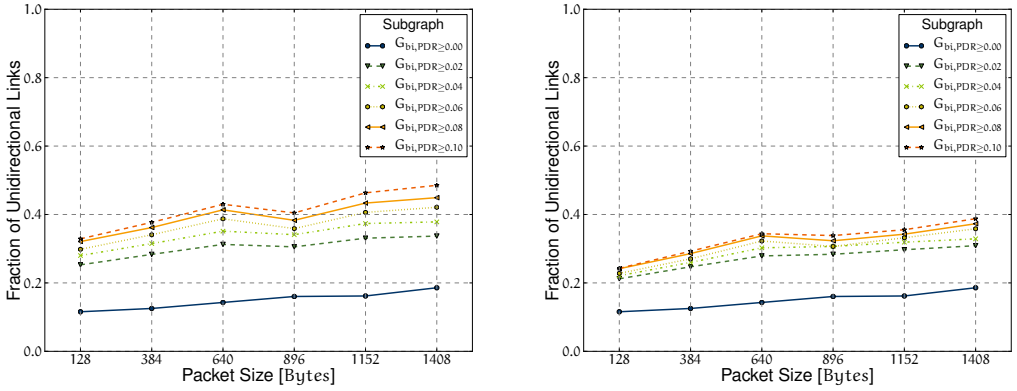

(a) Fraction of unidirectional link including $E_{PDR<t}$

(b) Fraction of unidirectional links without $E_{PDR<t}$

Figure B.2.7: Fraction of the unidirectional links in particular subgraphs on channel 7.

B.2.7 Network Fragility

The network is even less strongly connected on channel 7 than on channel 1 but the decay into partitions is less rapid. As shown in Figure B.2.8c, small subsets of nodes seem to break from the largest component (indicating a gradual decay) which leads leads to a shape that is similar to the one shown in Figure 3.1.10c.

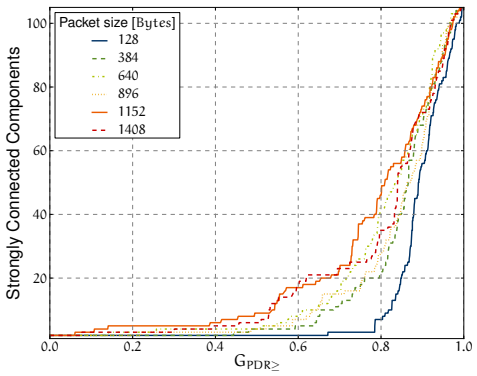

(a) Number of strongly connected components

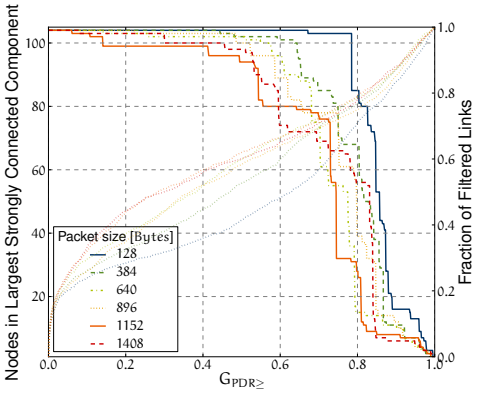

(b) Number of nodes in the largest strongly connected component

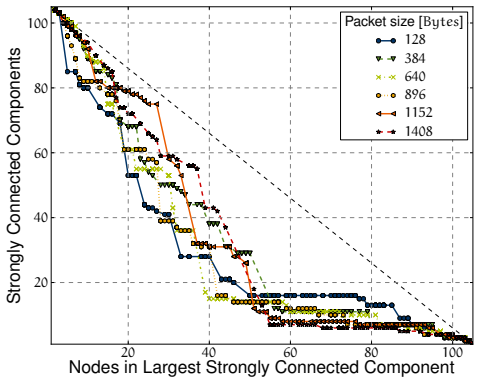

(c) Number of strongly connected components plotted over the number of nodes in the largest strongly connected component

Figure B.2.8: Network fragility on channel 7

Bibliography

[1] S. Shrestha, S. Shrestha, A. Lee, J. Lee, D.-W. Seo, K. Lee, J. Lee, S. Chong, and N. H. Myung, "A group of people acts like a black body in a wireless mesh network," in *Proc. IEEE Global Telecommunications Conference GLOBECOM '07*, A. Lee, Ed., 2007, pp. 4834–4839.

[2] H. van der Heijden and J. van der Mullen, "General treatment of the interplay between fluid and radiative transport phenomena in symmetric plasmas: the sulphur lamp as a case study," *Journal of Physics D: Applied Physics*, vol. 35, no. 17, p. 2112, 2002. [Online]. Available: http://stacks.iop.org/0022-3727/35/i=17/a=307

[3] K. Wehrle, M. Günes, and J. Gross, Eds., *Modeling and Tools for Network Simulation*, 1st ed. Springer, 2010.

[4] M. Günes, B. Blywis, and F. Juraschek, "Concept and Design of the Hybrid Distributed Embedded Systems Testbed," Freie Universität Berlin, Tech. Rep. TR-B-08-10, 2008.

[5] M. Günes, B. Blywis, F. Juraschek, and P. Schmidt, "Practical Issues of Implementing a Hybrid Multi-NIC Wireless Mesh-Network," Freie Universität Berlin, Tech. Rep. TR-B-08-11, 2008.

[6] M. Günes, B. Blywis, F. Juraschek, and O. Watteroth, "Experimentation Made Easy," in *Inproceedings of the First International Conference on Ad Hoc Networks*, ICST, Ed., Ontario, Canada, September 2009.

[7] T. Clausen and P. Jacquet, "Optimized Link State Routing Protocol (OLSR)," RFC 3626 (Experimental), Oct. 2003. [Online]. Available: http://www.ietf.org/rfc/rfc3626.txt

[8] C. Perkins, E. Belding-Royer, and S. Das, "Ad hoc On-Demand Distance Vector (AODV) Routing," RFC 3561 (Experimental), Jul. 2003. [Online]. Available: http://www.ietf.org/rfc/rfc3561.txt

[9] IEEE Std 802.11-2007, "IEEE standard for information technology — Telecommunications and information exchange between systems — Local and metropolitan area networks-specific requirements — Part 11: Wireless LAN medium access control (MAC) and physical layer (PHY) specifications," LAN/MAN Standards Committee, New York, NY, USA, pp. C1–1184, June 2007. [Online]. Available: http://dx.doi.org/10.1109/IEEESTD.2007.373646

[10] B. Blywis, M. Günes, F. Juraschek, and S. Hofmann, "Gossip routing in wireless mesh networks," in *International Symposium on Personal, Indoor and Mobile Radio Communications (PIMRC 2010)*, 2010.

[11] B. Blywis, M. Günes, S. Hofmann, and F. Juraschek, "A study of adaptive gossip routing in wireless mesh networks," in *Ad Hoc Networks*, ser. Lecture Notes of the Institute for Computer Sciences, Social Informatics and Telecommunications Engineering, O. Akan, P. Bellavista, J. Cao, F. Dressler, D. Ferrari, M. Gerla, H. Kobayashi, S. Palazzo, S. Sahni, X. S. Shen, M. Stan, J. Xiaohua, A. Zomaya, G. Coulson, J. Zheng, D. Simplot-Ryl, and V. C. M. Leung, Eds., vol. 49. Springer Berlin Heidelberg, 2010, pp. 98–113. [Online]. Available: http://dx.doi.org/10.1007/978-3-642-17994-5_7

[12] B. Blywis, M. Guenes, F. Juraschek, and J. Schiller, "Trends, advances, and challenges in testbed-based wireless mesh network research," *Mobile Networks and Applications*, vol. 15, pp. 315–329, 2010, 10.1007/s11036-010-0227-9. [Online]. Available: http://dx.doi.org/10.1007/s11036-010-0227-9

[13] B. Blywis, M. Günes, F. Juraschek, P. Schmidt, and P. Kumar, "DES-SERT: A framework for structured routing protocol implementation," in *IFIP Wireless Days conference (WD'09)*, Paris, France, 12 2009.

[14] G. A. Klutke, P. C. Kiessler, and M. A. Wortman, "A critical look at the bathtub curve," vol. 52, no. 1, pp. 125–129, 2003.

[15] D. S. J. De Couto, D. Aguayo, J. Bicket, and R. Morris, "A high-throughput path metric for multi-hop wireless routing," in *MobiCom '03: Proceedings of the 9th annual international conference on Mobile computing and networking*. New York, NY, USA: ACM, 2003, pp. 134–146.

[16] D. B. Johnson and D. A. Maltz, "Dynamic source routing in ad hoc wireless networks," in *Mobile Computing*, T. Imielinski and H. Korth, Eds. Kluwer, 1996, vol. 353.

[17] T. Clausen, C. Dearlove, and J. Dean, "Mobile ad hoc network (manet) neighborhood discovery protocol (nhdp) draft-ietf-manet-nhdp-15," December 2010. [Online]. Available: http://tools.ietf.org/search/draft-ietf-manet-nhdp-15

[18] W. Feller, "On the kolmogorov-smirnov limit theorems for empirical distributions," *Annals of Mathematical Statistics*, vol. 21, no. 2, pp. 301–302, 1950.